LA-UR-16-27110
Approved for public release; distribution is unlimited.

Title: Non-destructive Pre-irradiation Assessment of UN / U-Si “LANL1” ATF formulation

Author(s): Vogel, Sven C.
Bourke, Mark Andrew M.
Losko, Adrian Simon
Pokharel, Reeju
Ickes, Timothy Lee
Hunter, James F.
Brown, Donald William
Voit, Stewart Lancaster
Mcclellan, Kenneth James
Tremsin, Anton

Intended for: Report

Issued: 2016-09-16

Non-destructive Pre-irradiation Assessment of UN / U-Si "LANL1" ATF formulation

Fuel Cycle Research & Development

Prepared for U.S. Department of Energy Campaign or Program

Sven C. Vogel, Adrian S. Losko, Reeju Pokharel, Timothy L Ickes, James Hunter, Donald W. Brown, Stewart L. Voit, Anton S. Tremsin, Mark A.M. Bourke, Kenneth J. McClellan.

Los Alamos National Laboratory

September 15, 2016

LA-UR-16-xxxxx

SUMMARY

The goal of the Advanced Non-destructive Fuel Examination (ANDE) work package is the development and application of non-destructive neutron imaging and scattering techniques to ceramic and metallic nuclear fuels, ultimately also to irradiated fuels. The results of these characterizations provide complete pre- and post-irradiation on length scales ranging from mm to nm, guide destructive examination, and inform modelling efforts. Besides technique development and application to samples to be irradiated, the ANDE work package also examines possible technologies to provide these characterization techniques pool-side, e.g. at the Advanced Test Reactor (ATR) at Idaho National Laboratory (INL) using laser-driven intense pulsed neutron and gamma sources.

Neutron tomography and neutron diffraction characterizations were performed on nine pellets; four UN/ U-Si composite formulations (two enrichment levels), three pure U_3Si_5 reference formulations (two enrichment levels), and two reject pellets with visible flaws (to qualify the technique). The ^{235}U enrichments ranged from 0.2 to 8.8 wt. %. The nitride/silicide composites are candidate compositions for use as Accident Tolerant Fuel (ATF). The monophase U_3Si_5 material was included as a reference. Pellets from the same fabrication batches will be inserted in the Advanced Test Reactor at Idaho during 2016. We have also proposed a data format to build a database for characterization results of individual pellets.

Neutron data reported in this report were collected in the LANSCE run cycle that started in September 2015 and ended in March 2016. This report provides the results for the characterized samples and discussion in the context of ANDE and APIE. We quantified the gamma spectra of several samples in their received state as well as after neutron irradiation to ensure that the neutron irradiation does not add significant activation that would complicate shipment and handling. We demonstrated synchrotron-based 3D X-ray microscopy on the composite fuel materials, providing unparalleled level of detail on the 3D microstructure. Furthermore, we initiated development of shielding containers allowing the characterizations presented herein while allowing handling of irradiated samples.

Key results include:

- Neutron resonance analysis (using Tantalum for normalization) determined isotopic enrichment levels to within 0.1 at% of fabrication values
- Five of seven production pellets were homogeneous to the spatial resolution of the measurements
- One composite pellet shows an inclusion or incipient crack
- One composite pellet shows a density variation of a few % with a maximum on the center plane of the pellet
- 3D characterization of cracks, flaws and isotopic distributions are determined non-destructively in complete pellets to spatial resolutions of at least 100 microns
- 3D characterization of cracks, flaws and density distributions are possible in 6 ATF pellets in 3 to 4 hours of neutron beam time at LANSCE.
- 3D characterization of isotopic distributions are possible in 6 ATF pellets in 3 to 5 days of neutron beam time at LANSCE.
- Diffraction data of crystallographic phase, texture and spatially resolved measurements complements the structural, isotopic, and chemical analysis with microstructural

characterization such as phase composition, texture/grain orientation distribution, and lattice strains.

CONTENTS

FIGURES

TABLES

ACRONYMS

AECL	Atomic Energy of Canada Limited
APS	Advanced Photon Source
AFC	Advanced Fuel Cycle
ANDE	Advanced Non-destructive Evaluation
ATF	Accident Tolerant Fuel
ATR	Advanced Test Reactor
BWR	Boiling Water Reactor
CCD	Charge-Coupled Device
CEA	French Alternative Energies and Atomic Energy Commission
DOE	Department of Energy
DOT	Department of Transportation
EBS	Ethylene bis-stearate
EPMA	Electron Probe Microanalysis
FCCI	Fuel Cladding Chemical Interaction
FCMI	Fuel Cladding Mechanical Interaction
FCRD	Fuel Cycle Research and Development
FOV	Field of View
FR	Fast Reactor
HEU	Highly Enriched Uranium
HFEF	Hot Fuels Examination Facility
HI	High Intensity
HIPPO	High Pressure/Preferred Orientation neutron diffractometer
IAEA	International Atomic Energy Agency
IMCL	Irradiated Materials Characterization Laboratory
INL	Idaho National Laboratory
JAEA	Japan Atomic Energy Agency
LANL	Los Alamos National Laboratory
LANSCE	Los Alamos Neutron Science Center
LEU	Low enriched uranium
LWR	Light Water Reactor
MA	Minor Actinides
MAMOX	Minor Actinide bearing Mixed Oxide Fuels
MOX	Mixed Oxide Fuels

NDE	Non-Destructive Evaluation
ND-PIE	Non-Destructive Post Irradiation Examination
NPDF	Neutron Powder Diffractometer/Neutron Pair Distribution Function
NRC	Nuclear Regulatory Commission
NRC	National Research Council Canada
NSLS	National Synchrotron Light Source
ORNL	Oak Ridge National Laboratory
O/M	Oxygen-to-Metal ratio
PCMI	Pellet Cladding Mechanical Interaction
PIE	Post Irradiation Examination
pRAD	Proton Radiography
PSI	Paul Scherrer Institute
PWR	Pressurized Water Reactor
RE	Rare Earth element
ROI	Region of Interest
SEM	Scanning Electron Microscopy
SMARTS	Spectrometer for Materials Research at Temperature and Stress
TFRE	Transmutation Fuel with Rare earth inclusions
TMRS	Target-Moderator-Reflector System
TEM	Transmission Electron Microscopy
TOF	Time-of-flight
UN	Uranium nitride
U-Si	Uranium silicide (unspecified stoichiometry)
US	United States

1. Introduction

1.1 Science-based Approach to Nuclear Fuel Development

A key enabler for a "science based approach" for accelerated development and certification of new, accident tolerant nuclear fuels is an early and efficient understanding of material behavior at multiple length scales. For new fuel formulations, there is a dearth of irradiation testing experience. When representative irradiation tests take years it is important to extract the maximum insight possible from each test. Post irradiation examination (PIE) of fuels is mature and sophisticated but measurements in hot cells are expensive and typically examine small volumes of irradiated fuels. This leaves the possibility that key failure inducing phenomena will not be observed because of limited PIE. For these reasons there is value in techniques that can quickly and non-destructively characterize properties over volumes consistent with standard fuel geometries. Such techniques can inform models on the initial condition of samples and complement, guide, and leverage destructive post irradiation examination. For example three dimensional characterization of complete fuel pellets within cladding after irradiation could identify regions that are representative of average and atypical response.

Typical in-pile irradiation tests of new fuel types last months or years. Demands on PIE may also impose a delay of years before individual samples can be studied. The resulting levels of radioactivity even for rodlets containing just a handful of pellets require hot cells and remote manipulators to perform destructive PIE. The complexity and cost of such operations limit the PIE possible thus there is a premium on knowing where to measure. This research is focused on developing techniques for non destructive examination of rodlets containing multiple pellets.

The first step in the project is to "benchmark" the initial condition of candidate materials before irradiation. The second step will be to make comparable measurements on irradiated rodlets prior to their destructive examination in INL hot cells. Neutron, proton and (synchrotron) X-ray radiography / tomography techniques all pose opportunities for this endeavor. By virtue of their stand-off capability and ability to probe materials despite an intense gamma field neutrons and protons both offer potential for study of highly radioactive materials. At Los Alamos neutron based techniques are routinely used to evaluate microstructure, phase and composition and protons are widely used for dynamic radiography.

The programmatic emphases for developing advanced non-destructive evaluation (ANDE) techniques applicable to irradiated materials are two-fold. First it will be possible to evaluate fuel rods to guide the destructive post-irradiation examination towards regions of interest that are not obvious with conventional techniques. This will help develop the statistical insight necessary to complement modeling and simulation data. Adding ANDE insight to the standard optical, thermal neutron and gamma ray insights will help identify regions where destructive examination can be focused. This will increase the return from PIE since regions of atypical irradiation performance are more likely to be discovered. A second reason for ANDE lies in the desire to generate data as soon as possible after removal of the test samples from the reactor. This is a key requirement in accelerating the development and time to licensing of new fuel forms. The philosophy is consistent with improving diagnostics to offer faster turnaround and getting "more out of less". Programmatically, the capabilities under development sets the stage for routine pre-irradiation fuel evaluation and potentially for post-irradiation evaluations of Accident Tolerant Fuels (ATF).

The techniques employed at LANSCE use the pulsed neutron source at the Lujan center may. They rely on collocation with the 800MeV proton accelerator. However advances in laser based neutron sources with small-scale accelerators for neutron generation (by D-D fusion) or laser-drive pulsed neutron sources[1] pose interesting opportunities. Although such small scale sources are not currently capable of neutron

production for measurements of the type described here technological advance is ongoing. It is possible that, in the next decade, a “small-scale” accelerator source with sufficient neutron production performance might become available to provide “pool side” implementation of the techniques described in this report.

1.2 Scope and Goals of this activity

One method to enhance accident tolerance of the fuels is to improve the thermal conductivity to reduce the fuel centerline temperature. This increases the time to reach critical temperature in an accident. At LANL a composite of UN with 15-vol% U_3Si_5 is under consideration as a potential ATF forms[2] [3]. In the current work accident tolerant fuels systems based on composites of U_3Si_5 and UN were fabricated, encapsulated in a cladding/capsule configuration and examined with a variety of neutron based techniques to establish their ability to accurately measure chemistry, phase content and isotope distribution, as well as defects and flaws within the ATF pellets. The rodlet geometry matches the configuration that will be used for testing these fuels in the Advanced Test Reactor.

Pre-existing inclusions, density, chemical and isotopic inhomogeneities and cracks as well as microstructural features such as phase composition, texture or residual stresses can affect fuel behavior in an irradiation environment. For science based development initiatives it is hoped that certification of new fuel systems can be achieved by fusing science insight with insights from fewer irradiation tests than has been true in the past. However the goal of accelerated insight from fewer tests places more emphasis on pre-characterizing the condition of test fuel samples prior to irradiation as well as the need for more thorough bulk characterization of the whole irradiated volume to guide destructive examination of irradiated materials. Since neutrons are non destructive, capable of interrogating whole pellets and sensitive to the mesoscale characteristics being implemented in models, they are uniquely suited for the study of prototype nuclear fuels. Non destructive 3D maps of cracks, density, isotopic and geometry variation can be measured using neutrons in pellets prior irradiation. The potential exists for making the same measurements post irradiation. The ultimate goal is to accelerate the time to insight, development and certification of new nuclear fuels.

This initiative is focused on the application of neutrons to draw non-destructive insight on fresh nuclear fuel prior to irradiation and in the future on irradiated fuel. Neutron imaging and scattering techniques easily examine volumes of up to several cubic centimeters, consistent with typical rod assemblies of ceramic fuel pellets. Neutron scattering lengths for high and low atomic number elements are often comparable and allow efficient study of systems consisting of heavy and light elements.

The application of protons and synchrotron X-rays are also under consideration for these studies (though not reported here). Protons like neutrons, have mean free paths in nuclear materials that facilitate characterization of cubic centimeters of material. The interaction of protons with matter is governed by nuclear and Coulomb interactions. They lose energy in the matter because of Coulomb scattering from the atomic electrons, and scatter from the nuclei both because of the strong interaction and the Coulomb interaction with the proton. Proton radiography is performed by illuminating a target object with a beam of protons and focusing the transmitted protons onto a scintillator screen[4]. Magnetic lenses offer different magnification options. Synchrotron X-rays in excess of 50KeV also have applicability to fresh nuclear fuels and have been used in the study of U-Mo fuel. This established their merit for studies of smaller regions of interest than are typically examined in neutron measurements. In future a holistic suite of measurement tools might naturally use neutrons, protons and synchrotron x-rays.

At a pulsed neutron sources time of flight energy sorting allows examination of samples by setting the contrast on isotopes or crystal structures. Neutron detector technology has been revolutionized by the use of micro-channel plates (MCPs) for radiographic applications and proved a catalyst for these studies. The

micro-channels are coated with neutron absorbing materials such as boron. They currently offer a spatial resolution of 55μm at count rates of 10^8 $cm^{-2}s^{-1}$. Spatial resolution of 15μm has been demonstrated at lower count rates [5].

At a LANL/INL workshop held in December of 2012 a plan was conceived to use the advanced non-destructive evaluation techniques including neutron and proton radiography available at LANL and INL for analysis of irradiated fuel rodlets from the AFC-2C irradiation at the ATR in Idaho[6]. In the first phase a set of mock-up rodlets were examined containing pellets of depleted uranium dioxide (dUO_2) with defects similar to that seen in irradiated fuel rodlets. After these first measurements over the last few years, measurements have demonstrated the applicability of neutrons, protons and synchrotron X-rays to a range of ceramic and metallic fuels. Several terabytes of imaging and scattering data have been collected. The ability to observe cladding dimensions, cracks, phase and isotopic species nondestructively and in three dimensions has been demonstrated. Development in data analysis and instrumentation is ongoing.

Tomographic analysis of typical fuel clad geometries using only thermal neutrons can elucidate three dimensional heterogeneities in a few hours. Whereas determination of isotopic species requires measurements of resonances in the epithermal range and measurements on typical clad/pellet geometries typically require a few days of beam time for between 3 and 6 pellets. Diffraction characterization in slices through the sample provides valuable additional information at beam times of about 0.5 days. Although early work focused on UO_2 recent initiatives have focused on developing fuels with enhanced accident tolerance, increased burn-up and reduced waste.

2. Neutron Analysis

2.1 Neutrons

Neutrons offer excellent characterization capabilities for nuclear fuels and provide non-destructive insight on mechanical integrity, microstructure, chemistry and crystallographic phase. Measurements are possible at reactors or pulsed sources, but the energy resolution is implicit at pulsed sources and offers capability not efficiently pursued at reactor sources. Recent advances in 2D neutron detection enable improved opportunities for imaging and tomography of nuclear materials. Moreover, time-of-flight (TOF) neutron measurements enable isotope specific tomography. Isotopic densities are deduced from transmission spectra exhibiting neutron resonances, which are recorded for each pixel. Tomographic algorithms allow 3D reconstructions of the spatial distribution of isotopes as well as density and feature heterogeneities. Energy resolved neutron radiography above 1eV is an effective approach for studying samples with compositions that impede measurements with thermal neutrons. By using epithermal neutron energies and assuming known total neutron cross sections of constituents, isotopic enrichment levels can be determined.

Neutrons interact with the nucleus rather than the atomic shell. Thus, their interaction characteristics differ markedly from X-rays. Figure 1: Penetration depth vs element atomic number; neutrons (red), X-rays (blue), and electrons (yellow). Circles highlight Silicon (number 14) and Uranium (number 92).

illustrates this by showing penetration depths as a measure of interaction potential for all elements with neutrons, X-rays, and electrons. The data explain why neutron measurements are more sensitive to light elements in the presence of uranium than X-ray measurements. Since the scattering lengths of neutrons for high and low Z-number elements are comparable in many cases they are more effective in resolving the elemental contribution of for example uranium and silicon. By contrast in X-rays diffraction the scattered intensity is biased towards the heavier element. Indeed, for structural analyses of uania determined by diffraction techniques reported and collected in the Inorganic Crystal Structure Database,

of the 66 experimental structure records for urania, UO_{2+x}, 55% were measured using neutron diffraction. Neutron measurements routinely characterize samples as small as a few mm^3 or as large as cm^3. For this report, both energy-resolved neutron imaging and neutron diffraction were employed. While neutron diffraction was developed and applied for over half a century, energy-resolved neutron imaging became possible with the recent availability of pixilated neutron time-of-flight detectors. We describe this technique therefore in more detail below. Besides LANSCE, only three other pulsed neutron sources are operational world-wide at this time that would allow the development and application of energy-resolved neutron imaging: SNS at ORNL, J-PARC in Japan, and ISIS in England. SNS at this time does not have a suitable imaging beam line (the VENUS beamline is under funding negotiations), J-PARC's authorization basis prevents characterization of actinides at that facility, including depleted uranium compounds, and at ISIS the technique is developed with a focus on Bragg-edges rather than absorption resonances with applications in archeology. Thus, the development reported here is world-leading in application of neutron absorption resonance analysis for materials characterization and the only one in the world applying it to nuclear energy problems. Our group is represented at annual meetings of the comparably small community developing and applying energy-resolved neutron imaging techniques, most recently the 8th Workshop on Neutron Wavelength Dependent Imaging (NEUWAVE- 8), held in June 2016 in Abingdon, England.

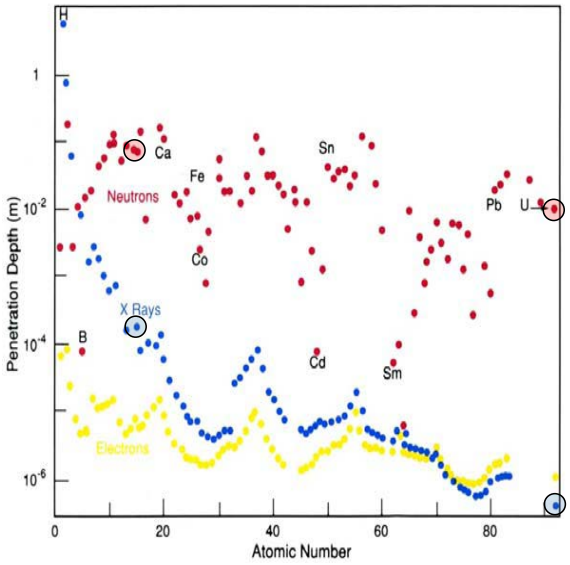

Figure 1: Penetration depth vs element atomic number; neutrons (red), X-rays (blue), and electrons (yellow). Circles highlight Silicon (number 14) and Uranium (number 92).

2.2 Neutron radiography

Imaging with neutrons, protons and X-rays has been applied at LANL to demonstration nuclear fuels since 2010 [7] [8]. The primary research focus is on neutrons because of their isotopic sensitivity, their applicability to cm^3 size samples and their potential application to irradiated material. At a pulsed neutron source neutron absorption resonances provide a unique finger-print for many isotopes. Energy-resolved neutron imaging, enabled by time-of-flight (TOF) neutrons, can used different energy ranges. For example, Lehmann et al. described energy-selective neutron imaging using thermal and cold neutrons [9]. "Energy-dependent neutron imaging with a double crystal monochromator at the ANTARES facility at FRM II" is described by Schulz et al with neutron wavelengths ranging from 2.7 to 6.5 Å [10]. Strobl et al. describe advances in energy-selective imaging in detail in their review "Advances in neutron radiography and tomography" [11], however mostly focused on thermal neutrons and not neutron absorption resonances in the

epithermal energy range. New detector technology has expanded the opportunities into the energy regime >1eV as described below. With sufficient penetration and resolution, tomographic methods provide nondestructive measurements of voids, cracks, density variations. By collecting a series of two-dimensional radiographs, tomographic reconstruction software can routinely produce three representations from attenuation-based features.

2.3 Tomographic reconstruction

2.3.1 Data Processing

The detector employed for the energy-resolved neutron imaging and tomography stores ~3,000 frames corresponding to defined neutron time-of-flight or energy values. Subsequent handling and manipulating the data for tomographic reconstruction is challenging. A significant challenge in developing the routine application of this capability lies in provision of facile user access to the breadth of interpretive opportunity. A few examples are listed below each of which requires considerable data manipulation.

- Integration over a thermal energy window offers maximum spatial resolution in minimum time (due to spectral characteristics of the pulsed Lujan neutron source)
- Integration over a broad epithermal energy range may offer good spatial resolution if resonances from one or more isotopes dominates.
- Integration across one or more discrete energy windows may offer isotopic sensitivity.
- Spectral fitting can be applied to pixel average data or single detector pixels

After raw radiographs are produced for any of the options above, tomographic reconstructions are possible provided multiple projections were collected. The tool used for the 3D- reconstruction in these measurements was TomoJ which is a plugin for the image analysis tool ImageJ. It is a free software package that was originally designed for electron tomography. In our experience it compared well with commercial reconstruction tools, such as Octopus or VGStudio. To prepare transmission vs. energy spectra for fitting the raw data was background corrected and divided by open-beam. Scaling factors (determined from an open beam measurement) were included for individual detector pixels.

Tomographic projections are prone to ring artifacts and when they were observed a ring-filter was applied. This process first required a polar transform of the reconstructed images (normal to the cylinder axis of the pellets and the rotation axis for the tomography). A minimum value for the corrected data was set to 60% of the maximum. Then a one-dimensional median filter was applied with a length of 30 pixels along the stripes. The polar-transformed image was divided by the resultant median-filtered-polar-transformed image to remove the ring artifacts. Finally the images were transformed back into Cartesian coordinates and the filtered slices were normalized to the original grey-values. An example of the ring-filter is shown in Figure 2:.

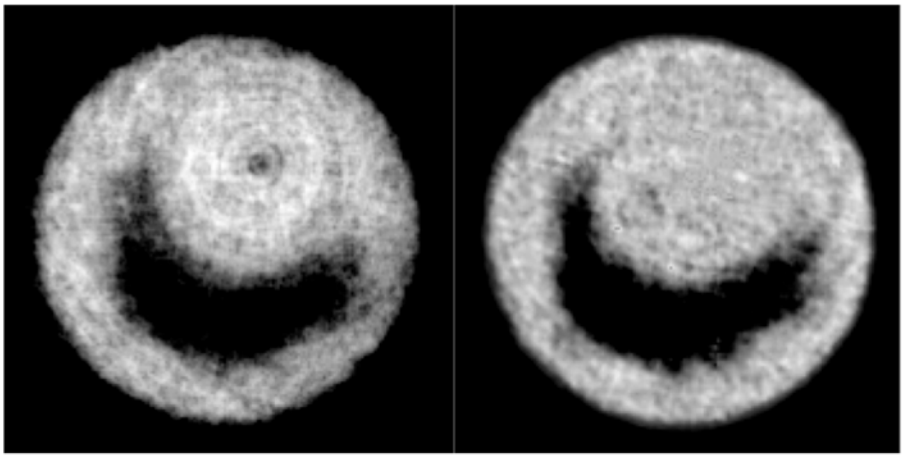

Figure 2: The effect of the "Ring filter" is shown above on a single slice for pellet 4; Before (left) and after (Right).

The ring filter improves the quality of the CT reconstruction and is entirely implemented in software. While developing quantitative analysis of aerial densities from the transmission spectra, it became clear that the energy-dependent neutron background poses a significant problem for reliable determination of the number of nuclei in the beam path. The use of a standard foil with neutron absorption resonances during the data collection allows more reliable determination of neutron energy-dependent background levels, normalization for the isotopic measurements, and enables e.g. reliable determination of enrichment levels. For reasons described below tantalum proved best suited for this purpose. It has several narrow resonances in the 1 to 200eV energy range and a foil of known thickness was measured simultaneously with the rodlets. By including a known aerial density for the tantalum, the SAMMY resonance fit (described below) can more accurately fit the energy dependent background. Figure 3 shows the background observed at flightpath 5.

Besides modelling the background properly in the analysis, our group also pursues identification of background sources. The majority of the background observed for these measurements appears to originate in the LANSCE neutron source, consisting of neutrons arriving at a time-of-flight not consistent with their neutron energy. Shielding or other modifications of the beamline and experimental setup therefore are not useful in reducing the background.

In 2016, materials and nuclear physics users of the LANSCE target 1, used for the measurements described here, was charged with designing a new target to be deployed around 2021. For our projects, this provides opportunity to optimize the new target for the applications described herein as well as simulations providing insight into the background sources observed today.

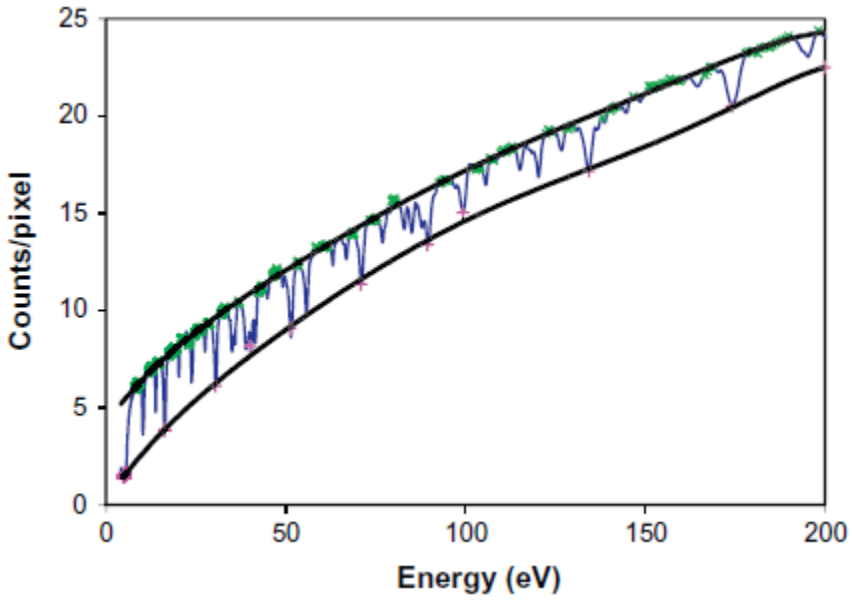

Figure 3: Background observed at flightpath 5 as a function of neutron energy. The resonances connected by the lower line in the graph should show zero transmission due to the thickness of the foils used. Correct modelling of the background is of paramount importance to reliably measure the aerial density of nuclei present in the sample (from [7]).

2.3.2 Thermal and Epithermal neutron spectrum

The neutron beam on flight path 5 at the Lujan provides thermal and epithermal neutrons with each pulse, see Figure 4. The moderator is optimized for the thermal spectrum (<0.4 eV, with a maximum at ~25 meV). In this energy region, individual projections can take as little as one minute to acquire sufficient counting statistics. Measurements of neutron resonances are typically performed at >1eV for which count-times per projection typically require between 30 and 180 minutes for sufficient statistics to allow the fits shown in Figure 21 thru Figure 25. This is due to the 2-3 orders of magnitude weaker incident flux in this energy range combined with the two order of magnitude lower detector efficiency due decreased cross-section (Figure 4). Above ~100 eV, the incident neutron flux and the detector efficiency of the presently used borated glass detector are too weak to allow meaningful analysis. Developing detector technology that also moderates neutrons, e.g. with hydrogen containing liquids or plastic, may allow to mitigate this problem in the future and allow utilization of neutron energies higher than 100 eV for energy-resolved imaging. In general, moderation by inelastic collision blurs the obtained radiographs. Thicker MCPs than the present ~2mm thick plates may also improve the cross-section. ^{10}B, 6Li, and 3He are the only isotopes that provide a continuous cross-section without resonances over a large energy range. Resonances in detector materials are undesirable as the background signal also shows spikes, limiting the available choices.

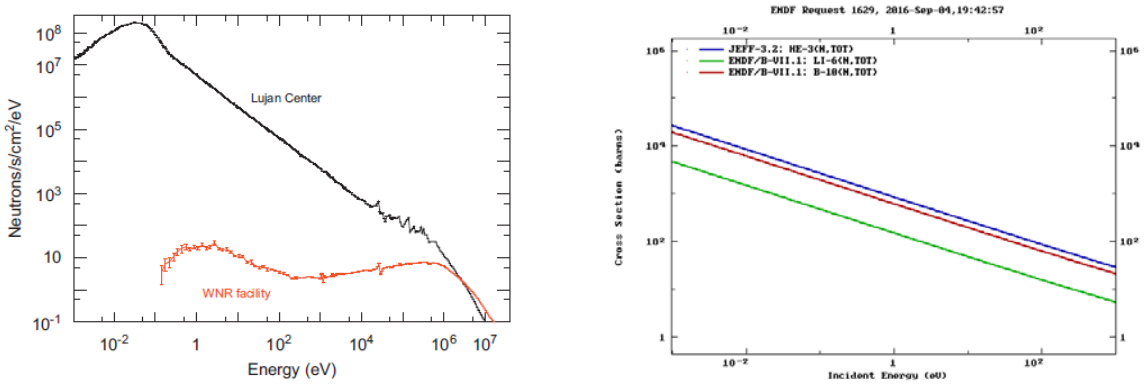

Figure 4, Left: The total neutron energy spectra produced by the LANSCE target 1 (Lujan Center) and target 4 (WNR). These neutron fluxes are calculated for maximum proton currents provided by the LANSCE accelerator, 125 μA for target 1, 5 μA for target 4 (after [16]). Right: Cross-sections of the most common detector materials. The decrease of both result in the limitation to neutron energies below ~100 eV with the present setup.

Thus thermal imaging is an effective and "quick" way to identify the presence of cracks, whereas epithermal imaging of resonances requires longer acquisition times but provides isotope specific insight. Since data for both energy regions are collected simultaneously, the long count times for resonance imaging also provide high quality thermal radiographs. The energy resolution ΔE/E of a measurement dictates the ability to resolve individual neutron absorption resonances. This results in a tradeoff between the source to sample distance and the energy resolution.

2.3.3 Resonance Cross sections from ENDF

The energy dependent neutron cross sections associated with isotope specific nuclear absorption resonances provide a material signature necessary for imaging. An enabling capability for these measurements are the tabulated nuclear cross sections in the Evaluated Nuclear Data File (ENDF) database[12]. This provides cross sections, determined by standardized experimental measurements such as neutron transmission measurements, for individual isotopes. In general, neutron resonances are measurable in a regime of 1ev to 0.1 MeV. Below 1eV cross sections are typically inversely proportional to the velocity of the neutron and do not exhibit "sharp" resonances.

2.3.4 Resonance fitting by SAMMY

Resonance spectra recorded in this study were fit using the SAMMY code (SAMMY, Multilevel R-Matrix Fits to Neutron and Charged-Particle Cross Section Data)[13]. This code was developed by Oak Ridge National Laboratory. It can analyze time-of-flight, cross section data from meV to MeV, where the incident particle is either a neutron or a charged particle. For energies up to several KeV, cross sections are generated using the Reich-Moore approximation to R-matrix theory[14]. The code includes a variety of mechanisms to account for normalization, background, and sample thickness as well as options to account for measurement resolution and Doppler broadening. Corrections for self-shielding and multiple-scattering are also available.

Resolved resonance parameters can be output in the ENDF format for inclusion in the evaluated nuclear data files. Bayes' Theorem of generalized least squares is used to find "best fit" values of parameters and the associated parameter covariance matrix. After data are normalized they are fit with SAMMY. The data input consists of an ENDF database input file with pre-determined resonance parameters (literature values of energies, capture and partial widths and spin numbers as well as the sample element's name, atomic weight and energy range for the data set). Background parameters (constant, linear in energy and time) are varied to account for the efficiency and response of each individual pixel.

When the sample thickness is large compared with respect to the cross section of the resonance for a given energy, the sample can absorb all incident neutrons in a discrete energy range. This causes the transmission to drop to zero and the resonances are described as "black". For attenuation based imaging, a fully absorbed beam will appear as an opaque feature in the transmission image, making tomographic reconstruction impossible since the depth information is lost. However, for resonance imaging, reconstruction with black resonances remains possible by considering energy regions around the resonance. Indeed in that case they provide an accurate energy specific measurement of the background.

2.4 Calculating enrichment levels from resonance data

To interpret transmission data correctly, it is essential that an accurate background is included. This is essential if absolute values of areal densities are desired. If the background is not correctly accounted for, deviations in the measured transmitted intensity introduce errors in the absolute areal density. For this work a scaled open-beam profile was used as a "baseline" background. The normalized data were then treated with the SAMMY code[15]. The resonance parameters provided by the ENDF database were treated as constants. Background parameters (constant, linear in energy and linear in time) were varied to account for the efficiency and response of individual detector pixels. Then the areal density of different constituents were varied, from which absolute isotopic densities were determined.

2.5 Neutron diffraction

Imaging is complemented by diffraction, which provides insight on crystal structure (space group, lattice parameters, atomic positions, thermal motion etc.), phase volume fractions, lattice strains (mechanical strain, chemical strain from e.g. interstitial atoms, etc.) and texture (orientation distribution of crystals). For neutron powder diffraction data analysis, typically full pattern "Rietveld" refinements are performed. From these crystal structure (lattice parameters, atomic positions etc.), microstructure (sample induced peak broadening, phase fractions, texture etc.), and instrument (background, instrument contributions to peak broadening etc.) can be determined.

3. Instrumentation

3.1 Flight Path 5 (for imaging)

Imaging measurements described in this report were performed using Flight-Path-5 (FP5) at the Lujan Neutron Scattering Center (for a description see M. Mocko et al.[16]). It provides a thermal neutron flux of ~ $2.4\,10^{7} n \cdot cm^{-2} s^{-1}$ at ~8.8m from the moderator with a peak at ~25meV. The beam is collimated using borated polyethylene and steel disks with a circular exit collimator. For the measurements reported here the detector was positioned ~ 8.2 m from the source. The fuel rodlets were placed as close as possible to the detector to maximize the collimation ratio, L/D. A collimator to sample distance L of about 2m and beam diameter of 2 cm gave a collimation ratio of approximately 100. Samples are mounted on a rotation stage with a linear motion stage, allowing translation of the sample in multiple directions (Figure 6:).

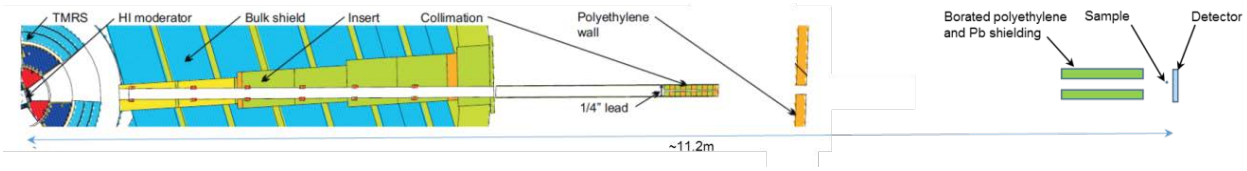

Figure 5: Flight Path 5 Schematic

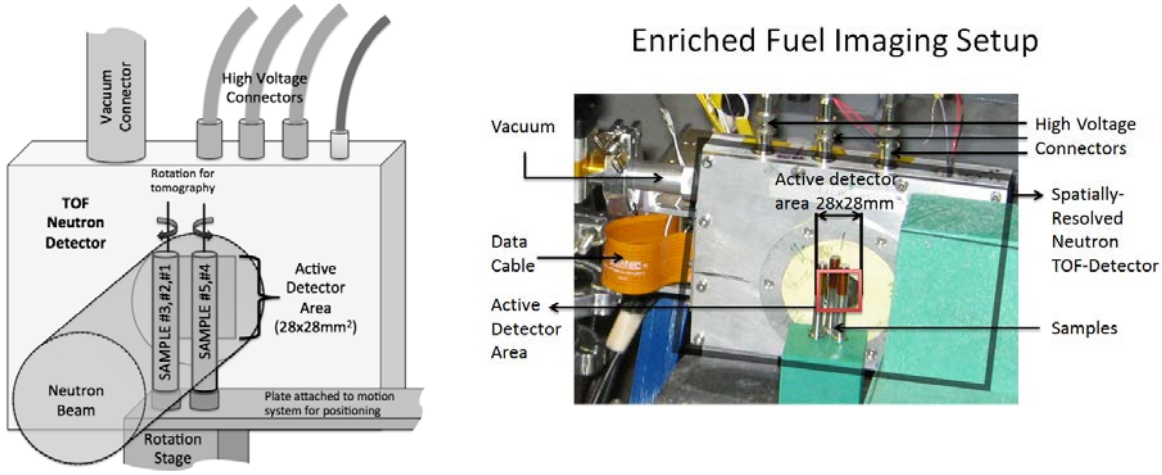

Figure 6: Rodlets in front of detector; schematic (left), photograph (Right).

The pixilated neutron time-of-flight imaging detector used at LANL is custom-designed and manufactured by Dr. A. Tremsin (Space Science Laboratory, UC Berkeley). It consists of a Gd/B doped multi-channel plate and MediPix read-out chip[17]. To account for differences in the individual pixel response of the detector, an open-beam measurement was recorded over the entire energy range (0.5 to 200eV). Individual TOF images are divided by the normalized open-beam image. The pixel size of the detector is 55μm with an active area of 512x512 pixels i.e. ~ 28 x28 mm^2.

3.2 HIPPO and SMARTS (for diffraction)

Two instruments were used for diffraction studies on the ATF fuels; HIPPO and SMARTS (for spatially resolved measurements). The HIPPO instrument is a general purpose neutron time-of-flight powder diffractometer. Its key characteristics are large detector coverage (1200 ^{3}He detector tubes distributed on 53 panels arranged on five rings around the incident beam) and proximity to the neutron source (~8.9 meters between moderator and sample). The short flight path and detector coverage and allow count times as short as one minute and efficient texture characterization. The resolution ($\Delta d/d$) in the back scattering geometry is ~ 0.0037 and the 20Hz repetition rate of the Lujan Center source accesses a d-spacing range from 0.12 to 22°A. A robotic arm is available for sample changes.

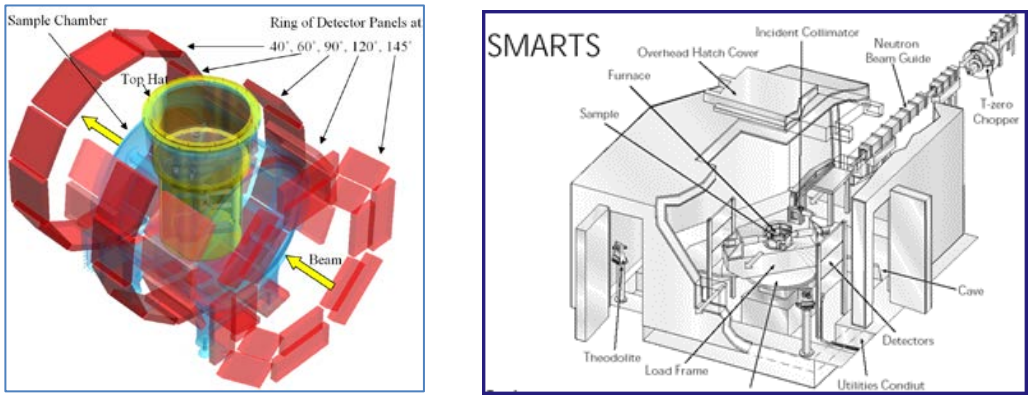

Figure 7, left: Schematic of general purpose neutron powder diffractometer HIPPO. Red areas are 3He detector panels, the blue volume is the sample chamber, and the yellow volume is a sample environment containing the sample. Right: Schematic of the principal components of the engineering neutron diffractometer SMARTS.

4. FY15 measurements on ATF and Transmutation fuels

4.1 Crystal Structure, Composition and Texture in UN / U-Si

In FY15 studies of crystal structure were performed on samples of ATF fuels fabricated with depleted uranium. Rietveld refinement provided spatially resolved characterization in slices along the pellet/rodlet axis of various crystallographic and microstructural parameters. The results indicated variations in chemistry between pellets. Texture evaluation indicated no preferred orientation in the UN phase, but showed a strong preferred orientation in the U_3Si_5.

A UN 15vol% U_3Si_5 pellet was scanned in 2mm steps along the length of the rodlet with 2mm vertical spatial resolution slit. A typical data set is shown in Figure 8. Data (red), Rietveld fit (green) and difference curve (magenta) are displayed. The data were collected with the HIPPO 144° detector panels, data collected in the other detectors was analyzed simultaneously (i.e. the structural parameters are a fit to data from several detectors) but is not shown here. The phases for the Rietveld fit were γ-Fe (stainless steel of the rodlet), cubic UN, and hexagonal U_3Si_5. Refined parameters included; weight fractions of the three phases, lattice parameters/unit cell volume of the three phases, peak width of the steel and UN/U_3Si_5, thermal motion parameters of the Fe, U, and Si/N atoms (the latter were constrained to a single thermal motion parameter for numerical stability of the analysis).

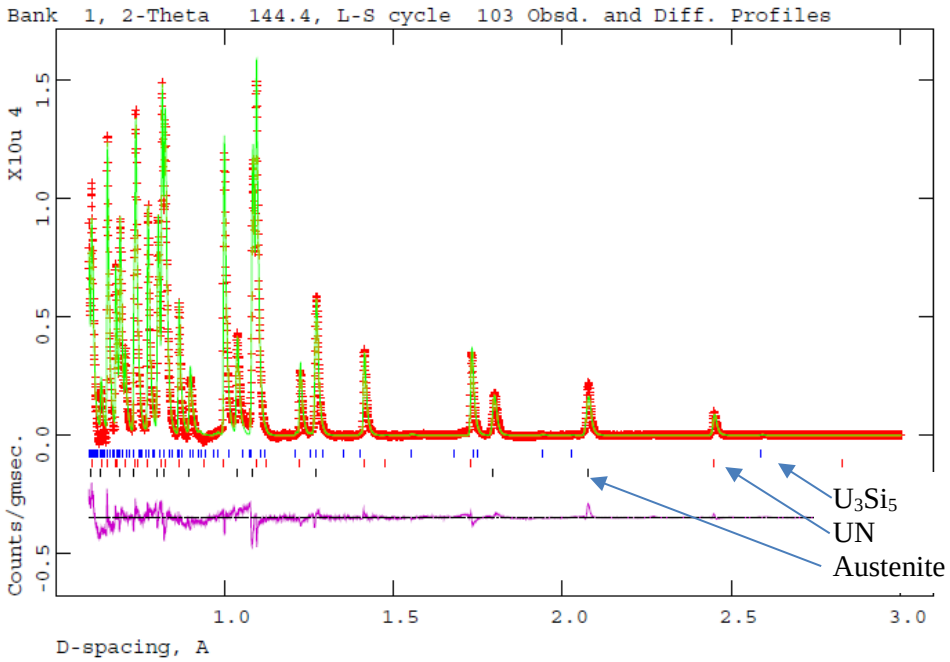

Figure 8: Diffraction from a 2mm slice of the ATF. Ticks mark calculated peak positions for austenite (black), UN (red), and U_3Si_5 (blue).

A series of 2mm high scans were executed across 5 pellets. Figure 9shows the variation of the UN lattice parameter and U_3Si_5 unit cell volume as a function of sample height (the first two data points were only partially illuminated, resulting in larger scatter). For the third to seventh data point a significant difference in lattice parameter is noted. This is consistent with a difference in chemistry of the bottom pellet compared to the remaining pellets.

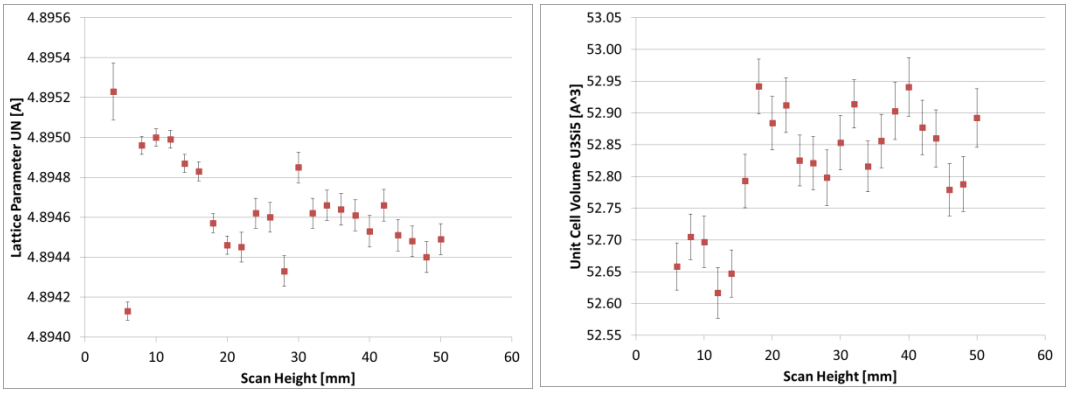

Figure 9: UN lattice parameter as function of height (left) and U_3Si_5 unit cell volume (2mm scan height over 5 ATF pellets).

Texture measurements through the same slices indicated that the UN phase, for these samples, exhibited a preferred orientation that is close to random whereas the U_3Si_5 phase exhibited either substantial preferred orientation – or large grains (i.e. the probed volume consists of few U_3Si_5 grains). Figure 10 shows the pole figures from a full texture refinement of a single slice. Each U_3Si_5 grain has one c-axis (002) and three a-axis poles (200). The U_3Si_5 pole figures therefore indicate that the probed volume consists of ~3 grains as there are three maxima present in the 002 pole figure. The UN pole figures confirm the absence of preferred orientation qualitatively derived from the raw diffraction data. The cylinder axis of the pellets and the

rodlet is perpendicular to the paper. These findings are consistent with a melting of the U_3Si_5 phase in this pellet during sintering, which indeed was done at temperature close to the melting point of U_3Si_5, but below the melting point of UN (see also section 5.1). The U_3Si_5 then likely mixed with the UN, leading to the differences in lattice parameters as silicon atoms diffused into UN (leading to an increase of the UN lattice parameter) and some nitrogen diffused into the U_3Si_5 (leading to a decrease in the U_3Si_5 unit cell volume). The melt than re-solidified in large, interconnected volumes, resulting in the observed strong texture consistent with large volumes in the probed slice being a single crystal. Since the hexagonal U_3Si_5 crystal structure has anisotropic thermal expansion along the crystallographic *a* and *c* axes, such strong preferred orientation is likely to cause substantial mechanical stresses in the pellet, which may ultimately lead to failure.

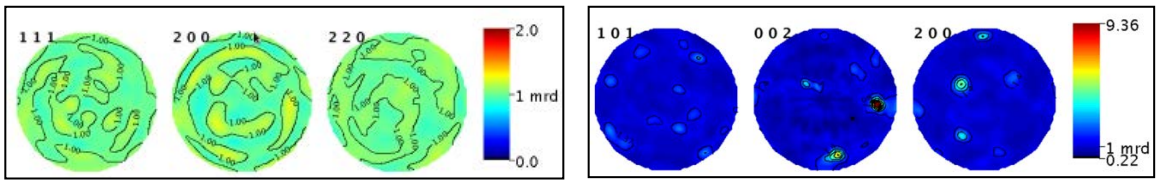

UN U_3Si_5

Figure 10: Pole figures, UN (left) and U_3Si_5 (right).

4.2 Rare earth inclusions in transmutation fuel

U-10Zr slugs were fabricated at INL with three levels of rare earth (RE) additions; 0, 1, and 5 at%. The composition of the RE lanthanide mix was reported in the previous milestone report. The RE mix was added to the U-10Zr and cast into a slug. At INL, the U-10Zr samples were placed inside HT-9 rodlets and sealed with sodium (to aid in thermal transport). The rodlets were then welded inside a secondary capsule. Figure 11 shows the welded rodlets. These rodlets were made for demonstration purposes and approximated irradiation geometries, but were not fabricated to meet engineering tolerances necessary for ATR insertion.

Neutron tomography identified regions of rare earth inclusions. Tomographic features noted in thermal radiography were related to the increase or absence of ^{238}U and Nd in resonance tomographs. Discrete rare earth inclusions are resolved with resonance reconstructions. An example of a tomographic reconstruction is included in Figure 12. The metallic slug is double encapsulated in 316L stainless steel capsule and HT-9 rodlet. The image shows the thermal neutron reconstruction (left), Nd resonance energy reconstruction (center, slug dimensions indicated by dashed red line), and the ^{238}U resonance energy reconstruction (right).

Figure 11: U-10Zr- 5% RE slug (left) and Rodlets containing metallic fuel slugs (right).

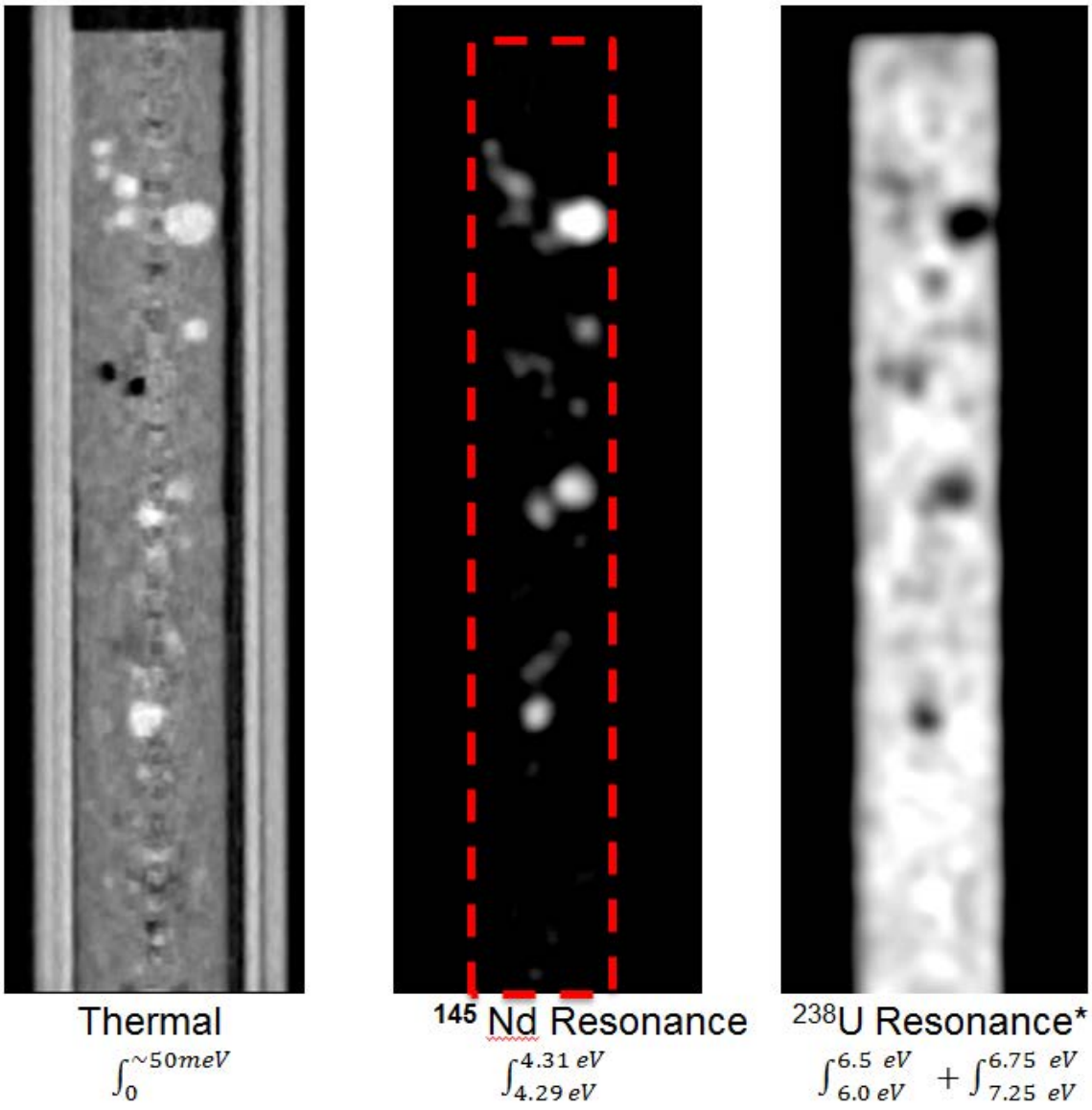

Figure 12: Thermal and epithermal imaging of U-10Zr transmutation fuel with 5% rare earth (lanthanide mix) inclusion.

Based on the U-Nd phase diagram shown in Figure 13, there is very little solubility for Nd atoms in the uranium matrix. This explains the large agglomerations of rare earth elements and illustrates and application of energy-resolved neutron imaging to metallic fuels, where such larger features are more likely than in ceramic fuels.

Utilizing diffraction on HIPPO, the inclusions can be further characterized. While tomography provides location and size, diffraction data provides the crystal structure and information on the microstructure. Figure 14 shows diffraction data of the region with the largest inclusion. While several other phases are present from container and U-10Zr matrix, a phase based on pure neodymium (hexagonal crystal structure) shows excellent agreement with the otherwise un-accounted diffraction peaks at 2.8 to 3.0 Å. The good agreement of the modelled peak intensity, assuming a powder average with random crystal orientations, with the measured intensity indicates that the inclusion is a polycrystalline aggregate without strong preferred orientation, i.e. not larger single crystals.

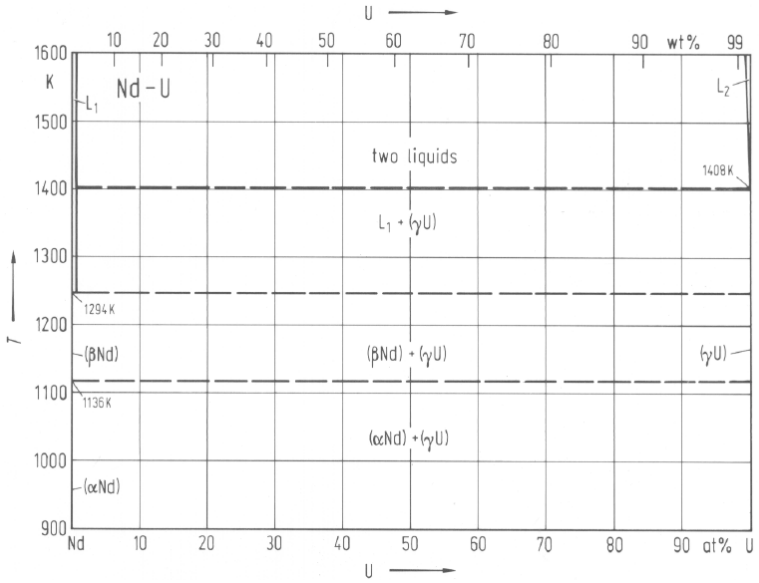

Figure 13: U-Nd phase diagram[18].

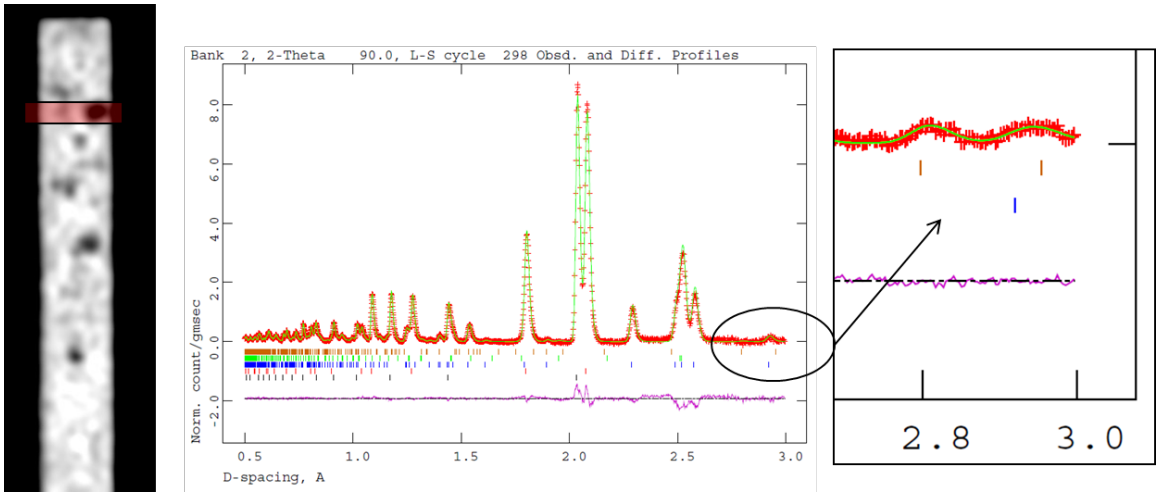

Figure 14: Diffraction scan of the volume shaded in red in the tomography slice shown on the left. Diffraction data was collected using HIPPO. The diffraction pattern in the center shows tick marks indicating the calculated peak positions for steel and sodium (two bottom rows), uranium (center row), a trial phase, and neodymium. The agreement of the observed peak positions in the zoomed region on the left with the neodymium phase shows that the inclusions have the crystal structure of metallic neodymium.

5. Pellet fabrication and Rodlet assembly

5.1 Synthesis

U_3Si_5 and UN-15v%U_3Si_5 fuel pellets were prepared using conventional powder metallurgical methods as outlined in the flow diagrams shown in Figure 15. The feedstock for the U_3Si_5 pellets was prepared by arc-melting stoichiometric amounts of uranium (8.84% enriched in ^{235}U) and silicon metals followed by a heat treatment to homogenize the phase content. The silicide was then crushed, ground, and the powder sieved to -44µm.

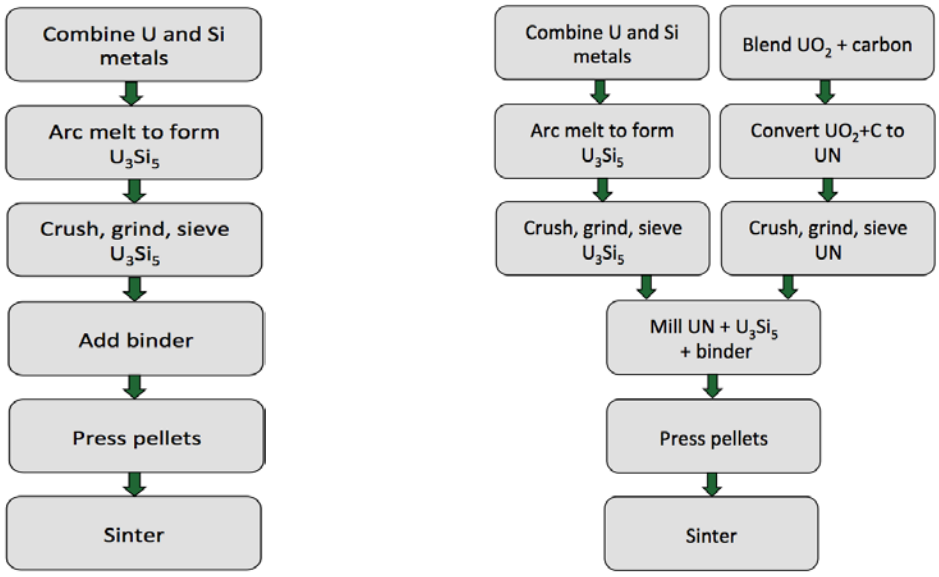

Figure 15: Pellet fabrication flow diagrams; U_3Si_5 (Left), UN-15v%U_3Si_5 (Right))

The powder binder EBS (ethylene bis stearamide) was blended with sieved U_3Si_5 powder. Individual powder charges were loaded into a die then pressed at 100 MPa into simple right cylinders. Green pellets were then sintered for 12 hours at 1515°C under flowing argon to a theoretical density of >90%. The UN-15v%U_3Si_5 pellets were fabricated by first synthesizing the UN and U_3Si_5 feedstock materials then subsequently milling the feedstock powders, pressing the powder into pellets at 100MPa, and sintering for 12 hours at 1775°C under flowing argon to achieve high density pellets.

Two different uranium enrichment schemes were used in the fabrication of UN-15 vol. % U_3Si_5 pellets. In one batch of pellets, the ^{235}U enrichment of the UN was fixed at a nominal LWR (Light Water Reactor) fuel value of 4.9%. The enrichment of the corresponding U_3Si_5 phase was 8.84% to give an overall uniform ^{235}U density across the fuel. In the second batch of UN-15v%U_3Si_5 pellets, the ^{235}U enrichment was set to 2.7% in both the UN and U_3Si_5 and given the difference in material densities the UN phase has a higher ^{235}U density than the U_3Si_5 phase.

5.2 Pellets

During the 2015/2016 LANSCE run cycle measurements were performed on nine pellets:

- Four UN/ U_3Si_5 pellets (3 of one enrichment level and one of a second).
- Two UN/ U_3Si_2 pellets (of a single enrichment level).
- Three monolithic U_3Si_5 pellets (with two enrichment levels).

The UN/U-Si composite compositions reflect candidate accident tolerant fuel compositions. The U_3Si_5 is studied as a reference to complement the studies on the composites. Pellets for study were selected in varying conditions with and without end cap defects to help understand the capability.

The composition, phase fraction and ^{235}U enrichments for the nine pellets are listed in Table 1below. The four UN U_3Si_5 pellets weighed approximately 6.5g. The two UN U_3Si_2 pellets weighed approximately 5.6 g. The three U_3Si_5 pellets weighed between 4 and 4.6g. All pellets were approximately 9mm in length and 8mm in diameter.

		U Enrichment (wt. %)						
Composition	**Pellet ID**	**UN**	**U_3Si_5**	**U_3Si_2**	**Rodlet #**	**Position in rodlet**	**Batch ID (Voit)**	**Lujan - Pellet ID**
UN (15 Vol% U_3Si_5)	1	2.70	2.70	N/A	1	(1 of 3, Cap up -Top)	Lujan LANL-1-27-27	UN-U3Si5 (2.7,2.7) Rod 1, Pel 1/3 t
	9				3	(1 of 2, Cap down -Top)	COMP1-Lujan3	UN-U3Si5 (2.7,2.7) Rod 3 Pel 1/2 t
	8				3	(2 of 2, Cap down Bottom)	COMP1-Lujan3	UN-U3Si5 (2.7,2.7) Rod 3 Pel 2/2 b
UN (15 Vol% U_3Si_5)	7	4.95	8.84	N/A	4	(1 of 2, Cap down-Top)	COMP2-Lujan4	UN-U3Si5 (4.95,8.84) Rod 4 Pel 1/2 t
UN (30 *Wt* % U_3Si_2)	4	4.1	N/A	4.9	2	(1 of 2, Cap up Top)	Lujan WEC-1	UN-U3Si2 (4.1,4.9) Rod 2 Pel 1/2 t (WEC)
	5				2	(2 of 2, Cap up Bottom)	Lujan WEC-2	UN-U3Si2 (4.1,4.9) Rod 2 Pel 2/2 b (WEC)
U_3Si_5 (100 Vol %)	2	N/A	8.84	N/A	1	(2 of 3, Cap up Middle)	Lujan LEU3SI5	U3Si5-LEU (8.8) Rod 1 Pel 2/3 m
	6				4	(2 of 2, Cap down Bottom)	LEU3SI5-Lujan4	U3Si5-LEU (8.8) Rod 4 Pel 2/2 b
U_3Si_5 (100 Vol %)	3	N/A	0.20	N/A	1	(3 of 3, Cap up Bottom)	Lujan DU3SI5	U3Si5-DU (0.2) Rod 1 Pel 3/3 b

Table 1: As fabricated enrichment levels ; ATF pellets

5.3 Rodlet / Pellet Assembly

The pellets listed in Table 1 were assembled in four rodlets as described in Table 2 and shown schematically in Figure 16. The rodlets for these examinations were made of aluminum though previous measurements demonstrated capability on representative cladding. Aluminum spacers were inserted between the pellets to facilitate visualization. A spring and aluminum spacers were also included to reduce the potential for pellet rotation. The designation “cap up” and “cap down” in the table describes (an arbitrary) change in can orientation for the measurements. (For rodlets 1 & 2 the cap was “up” and for rodlets 3&4 the cap was “down”).

				U Enrichment (wt. %)				
Rodlet #	**Position in rodlet**	**Pellet ID (Losko)**	**Composition**	**UN**	**U3Si5**	**U3Si2**	**Batch ID (Voit)**	**Lujan - Pellet ID**
1	(1 of 3, Cap up -Top)	1	UN - 15 Vol% U3Si5	2.70	2.70	N/A	Lujan LANL-1-27-27	UN-U3Si5 (2.7,2.7) Rod 1, Pel 1/3 t
	(2 of 3, Cap up Middle)	2	100 % U3Si5 (LEU)	N/A	8.84	N/A	Lujan LEU3SI5	U3Si5-LEU (8.8) Rod 1 Pel 2/3 m
	(3 of 3, Cap up Bottom)	3	100 % U3Si5 (DU)	N/A	0.20	N/A	Lujan DU3SI5	U3Si5-DU (0.2) Rod 1 Pel 3/3 b
2	(1 of 2, Cap up Top)	4	UN 30 Wt % U3Si2	4.1	N/A	4.9	Lujan WEC-1	UN-U3Si2 (4.1,4.9) Rod 2 Pel 1/2 t (WEC)
	(2 of 2, Cap up Bottom)	5	UN 30 Wt % U3Si2	4.1	N/A	4.9	Lujan WEC-2	UN-U3Si2 (4.1,4.9) Rod 2 Pel 2/2 b (WEC)
3	(1 of 2, Cap down -Top)	9	UN 15 Vol% U3Si5	2.70	2.70	N/A	COMP1-Lujan3	UN-U3Si5 (2.7,2.7) Rod 3 Pel 1/2 t
	(2 of 2, Cap down Bottom)	8	UN 15 Vol% U3Si5	2.70	2.70	N/A	COMP1-Lujan3	UN-U3Si5 (2.7,2.7) Rod 3 Pel 2/2 b
4	(1 of 2, Cap down-Top)	7	UN 15 Vol% U3Si5	4.95	8.84	N/A	COMP2-Lujan4	UN-U3Si5 (4.95,8.84) Rod 4 Pel 1/2 t
	(2 of 2, Cap down Bottom)	6	100 % U3Si5 (LEU)	N/A	8.84	N/A	LEU3SI5-Lujan4	U3Si5-LEU (8.8) Rod 4 Pel 2/2 b

Table 2: Rodlet/pellet Assembly position

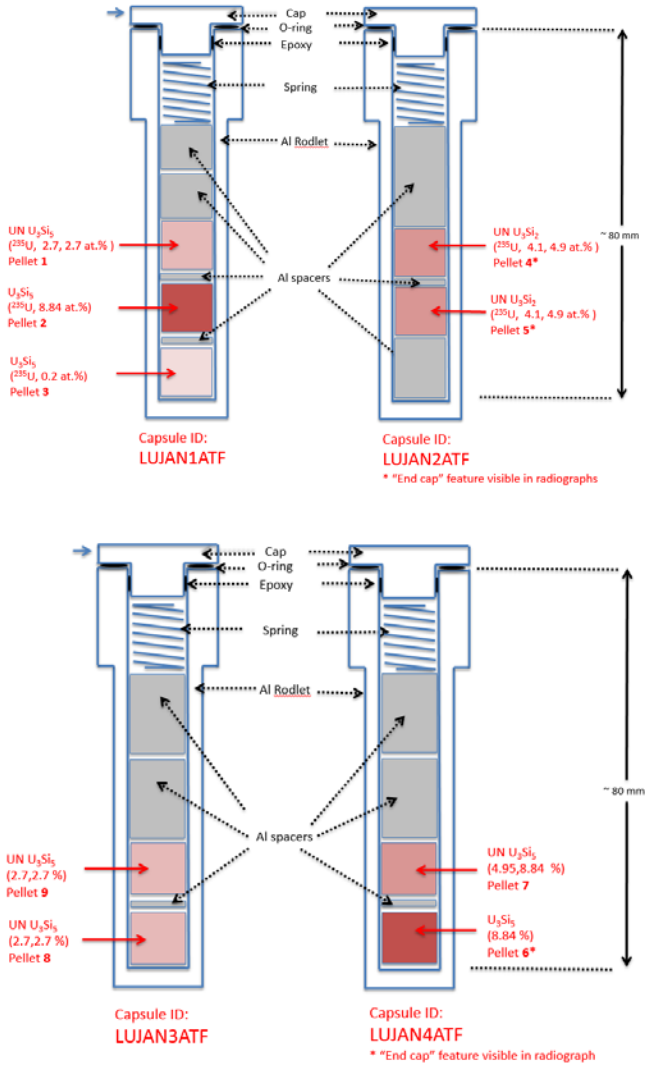

Figure 16: Rodlet/Pellet assembly schematics.

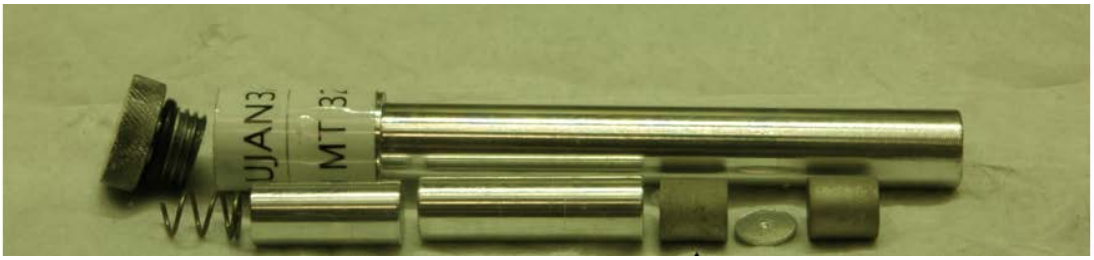

Figure 17: Rodlet 3 loading assembly configuration. From left to right; threaded cap, spring, two aluminum spacers, pellet, aluminum spacer and pellet.

6. UN/U-Si Results

6.1 Experiment Summary

Between October 2015 and February 2016, spatially resolved sliced neutron diffraction data collection on rodlet LUJAN1ATF as well as LUJAN3ATF and tomographic data collections were acquired on rodlets 1 thru 4 listed in section 5 (Table 3). Data acquisition of 5 minute per projection were sufficient for tomographic reconstructions using thermal neutrons and for simultaneous reconstruction in the epithermal region data acquisition greater than 20 minutes was required. Diffraction measurements were performed spatially resolved in slices on HIPPO and spatially resolved diffraction in cube-shape gage volumes using SMARTS.

Utilizing the pulsed neutron beam at the Lujan Neutron Scattering Center, tomographic data-sets were recorded for the rodlets described in section 5. Typical data-sets consisted of 51 projections with an angular step-size of 3.6 degree per projection and 20 minutes integration time per projection. Transmission images were acquired in TOF-mode with a time-bin-width used to record the time of flight neutron data was set to 320ns. For measurement in the epithermal region, data were recorded from 40 to 800μs in equal spaced time bins corresponding to an energy-range approximately from 207 to 0.6 eV**.** Diffraction data collection on SMARTS and HIPPO covered the d-spacing range from ~0.3 Å to up to 22 Å on the lowest diffraction angle bank of HIPPO, thus allowing to use the majority of diffraction peaks occurring in typical fuel materials, even if the unit cell is large.

	Rods	Date	Detector to source [m]	L/D	Acquisition/ Projection [min]	Cd-Filter	Total# Projections	Angular Step [degree]
FP-5	1&2	10/21/2015	11.20	260	20	Yes	100	1.8
FP-5	1&2	10/23/2015	8.26	113	45	Yes	50	3.6
FP-5	1&2	12/03/2015	8.50	125	20	Yes	200	0.9
FP-5	3&4	22/01/2016	11.20	260	60	Yes	50	3.6
FP-5	3&4	26/02/2016	11.20	260	5	No	100	1.8
FP-5	1&2	26/02/2016	11.20	260	5	No	100	1.8

Table 3: Summary of neutron tomographic data collected during the 2015/2016 LANSCE run cycle

6.2 Measurements of isotopic enrichment.

Both ^{235}U and ^{238}U have neutron absorption resonances in the1 to 100 eV range that is accessible on FP5. In Figure 18, the four strongest resonances are for ^{238}U while many ^{235}U resonances are also apparent with cross sections up to 1000 barns. With calibration by a foil of known thickness and SAMMY fitting, an absolute determination of the isotopic composition of any isotopes with resolved resonances is possible. To demonstrate this, ^{235}U enrichment levels were determined for all pellets.

To calculate absolute atomic concentrations, a calibrant is required to define the background levels over the whole energy range. In the first test with rodlets 1 and 2, cadmium was tried. Due to the large thermal absorption cross-section, cadmium is an effective mask for thermal neutrons and thus reduces the activation of the enriched fuel. However for reasons discussed below, tantalum was used for rodlets 3 and 4. Figure 19 shows that tantalum is better suited to define interpolation points for the background due to its preponderance of resonances in the 1 to 50eV regime compared with a single Cd resonance in the same region.

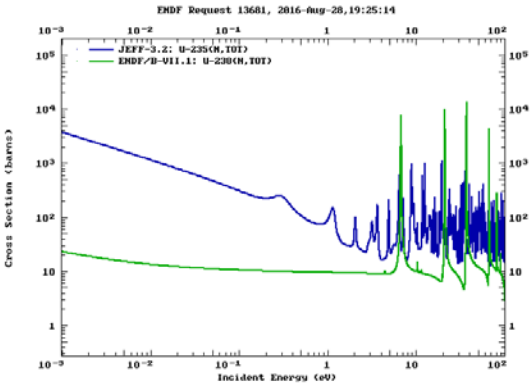

Figure 18: ^{235}U, ^{238}U cross-section (ENDF).

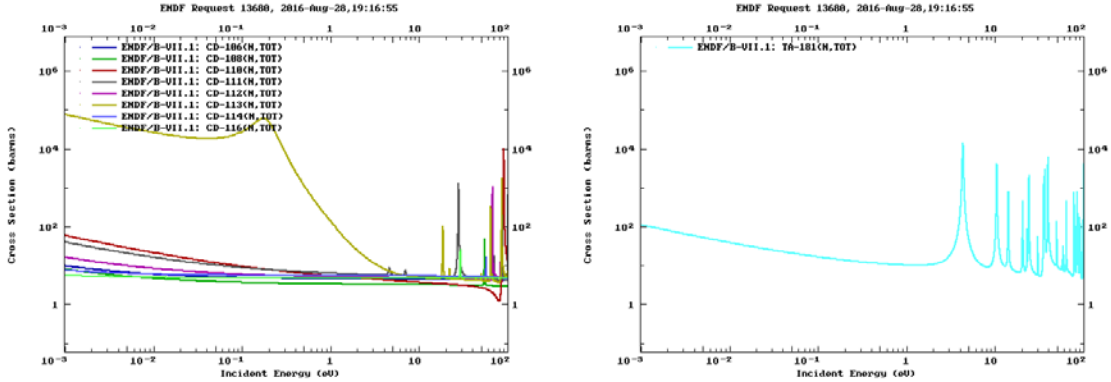

Figure 19: ^{106}Cd (1.25 at%), ^{108}Cd (0.89 at%), ^{110}Cd (12.47 at%), ^{111}Cd (12.80 at%), ^{112}Cd (24.11 at%), ^{113}Cd (12.23 at%), ^{114}Cd (28.75 at%), ^{116}Cd (7.51 at%), ^{181}Ta (99.98at%) cross-sections (ENDF, all atom percent are for natural composition).

For each pellet a region in the center of each pellet (see marked regions in Figure 20) was integrated from which an average enrichment value was determined. In Figure 21 thru Figure 25 the SAMMY fits for the region between 1eV and 50eV are shown for each pellet. SAMMY calculated enrichment levels are shown in Table 4. For Rodlets 3 and 4, tantalum was used as a standard and the neutron measurement of the average enrichment was within 0.1 at % of the nominal fabrication values. For rodlets 1 and 2 which used cadmium as a standard, the calculated ^{235}U enrichment levels showed a systematic underestimation when compared to the fabrication values. It is currently assumed that this disparity resulted from the weak presence of cadmium resonances in the key region of 1 to 50eV. Ta works better because it has multiple strong and sharp resonances in the 1 to 50eV energy range providing a better determination of background. The nominal and measured ^{238}U areal density showed agreement within uncertainties for the runs using Ta as a standard.

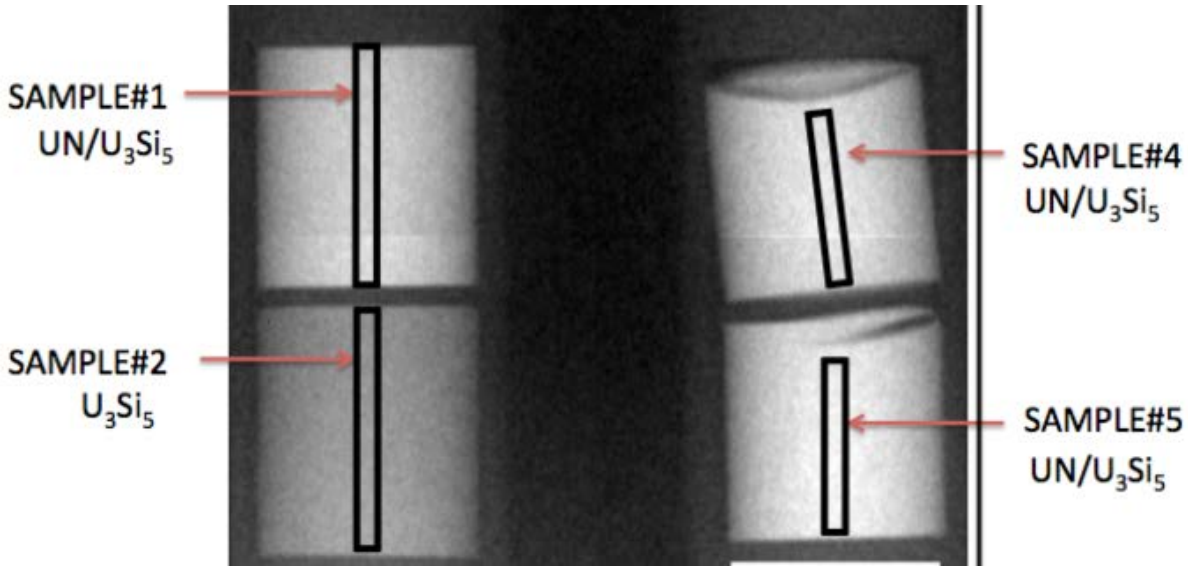

Figure 20: Attenuation image Rodlets 1 and 2 (integrated from 0.5 to200 eV). The black rectangles indicate region used for SAMMY fits.

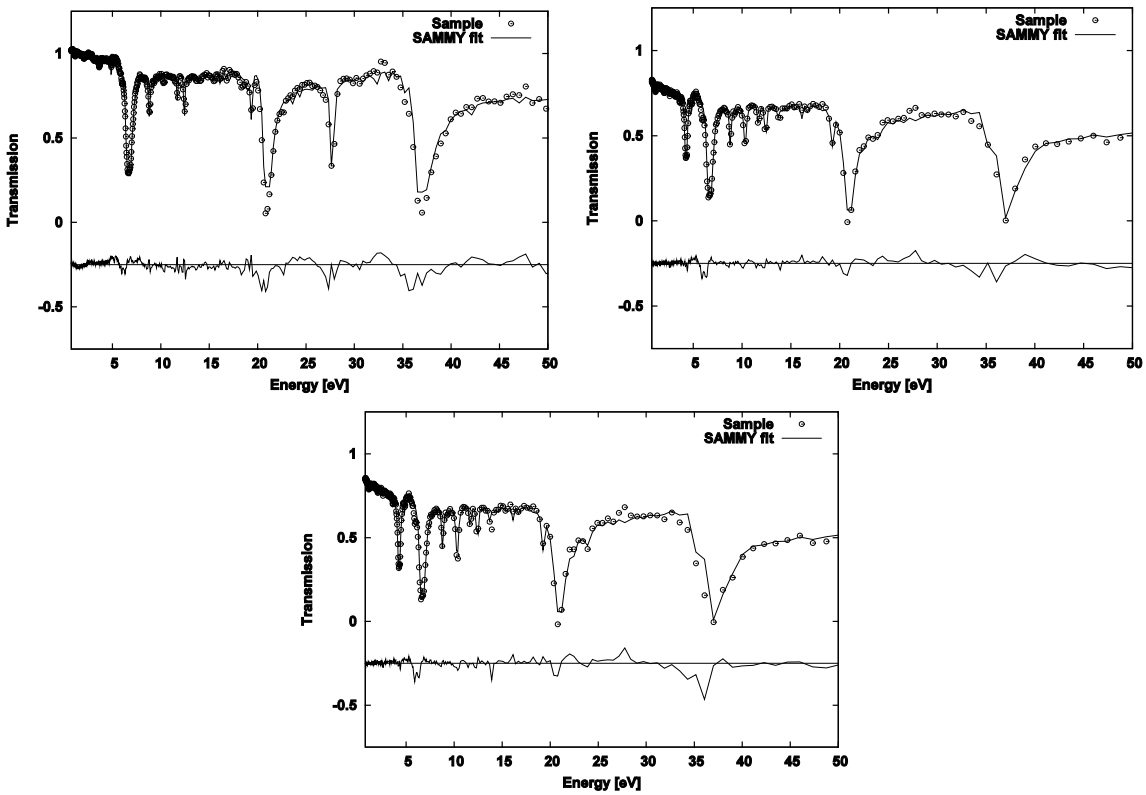

Figure 21: UN 15 vol.% U_3Si_5 (2.7, 2.7% enrichment) Pellet 1 (top left) , Pellet 9 (top right) , Pellet 8 (bottom). [Pellet 1 Cd standard, Pellets 8 and 9 Ta standard.]

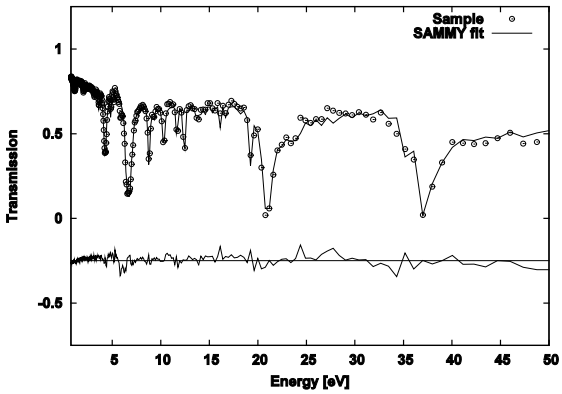

Figure 22: UN 15 vol.% U_3Si_5 (4.95, 8.84 % enrichment) Pellet 7 (Ta standard)

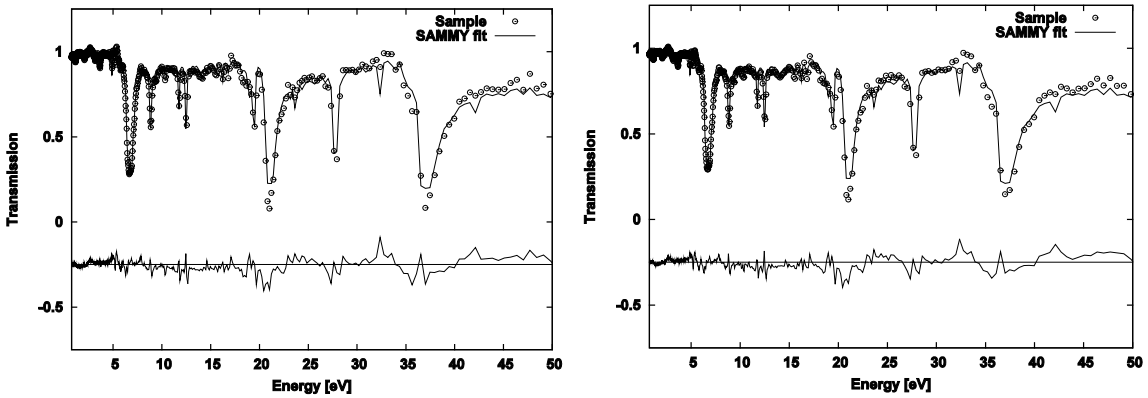

Figure 23: UN 30 wt.% U_3Si_2 (4.1, 4.9 % enrichment) Pellets 4 (left) Pellet 5 (right) (Cd standard)

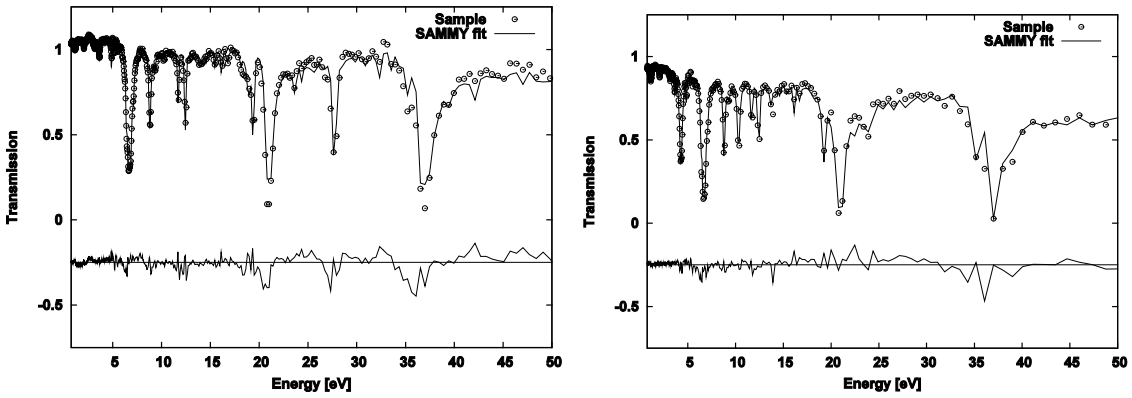

Figure 24: U_3Si_5 (8.84 % enrichment) Pellet 2 (left), pellet 6 (right) [Pellet 2 Cd standard, Pellet 6 Ta standard]

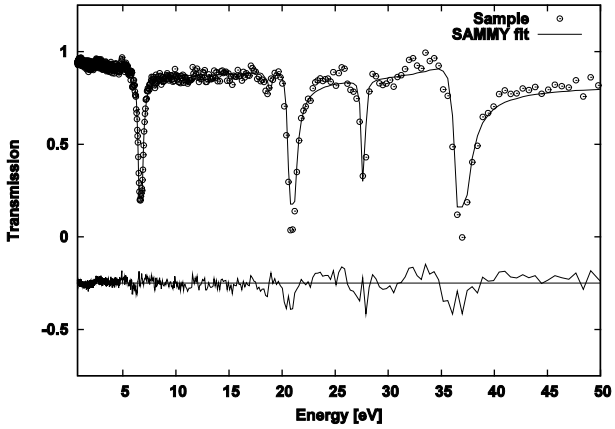

Figure 25: U_3Si_5 (0.2 % enrichment) Pellet 3 (Cd standard)

				235-U enrichment (wt %)		
Pellet #	Rod #	Normalization	Composition	Fabrication target	SAMMY measurement	Comment
2	1	Cd	U_3Si_5 (100 Vol %)	8.84%	6.97%	Poor Background fit
4	2	Cd	UN U_3Si_2 (30 Wt%)	4.34%	3.72%	Poor Background fit
5	2	Cd	UN U_3Si_2 (30 Wt%)	4.34%	3.79%	Poor Background fit
1	1	Cd	UN U_3Si_5 (15 Vol%)	2.70%	2.27%	Poor Background fit
3	1	Cd	U_3Si_5 (100 Vol %)	0.20%	0.14%	Poor Background fit
6	4	Ta	U_3Si_5 (100 Vol %)	8.84%	8.68%	Good Background fit
7	4	Ta	UN U_3Si_5 (15 Vol%)	5.53%	5.58%	Good Background fit
8	3	Ta	UN U_3Si_5 (15 Vol%)	2.70%	2.65%	Good Background fit
9	3	Ta	UN U_3Si_5 (15 Vol%)	2.70%	2.65%	Good Background fit

Table 4: ^{235}U enrichment. As fabricated and Neutron resonance determination (SAMMY).

6.3 Features observed in tomographic reconstructions

The limiting spatial resolution of the tomographic characterization in the current measurement suite is dictated by the 55 micron pixel size in the detector. (The potential for improving this spatial resolution is discussed in section 8. Here, observations of the current data set are presented focusing on the anomalies.

Attenuation image of all nine pellets: Figure 26 shows an attenuation image of all nine pellets (pellet 3 is truncated). A summary of the density heterogeneities is provided in Table 5. The overall homogeneity of density and pellet uniformity was within the current limiting spatial resolution of 55 microns of the technique with two exceptions (not including the reject pellets).

				U Enrichment (wt. %)		
Composition	**Pellet ID**	**Crack**	**Comment**	**UN**	**U_3Si_5**	**U_3Si_2**
UN (15 Vol% U_3Si_5)	1	Homogeneous to < 100 microns	Possible density variation?	2.70	2.70	N/A
	9	Oblate inclusion ~ 100 microns	Incipient crack?			
	8	Homogeneous to < 100 microns				
UN (15 Vol% U_3Si_5)	7	Homogeneous to < 100 microns		4.95	8.84	N/A
UN (30 *Wt* % U_3Si_2)	4	End cap 50% penetration End cap 20% penetration	Reject pellet	4.1	N/A	4.9
	5	End cap 90% penetration	Reject pellet			
U_3Si_5 (100 Vol %)	2	Homogeneous to < 100 microns	Reference pellet	N/A	8.84	N/A
	6	Homogeneous to < 100 microns Divot off one end	Reference pellet			
U_3Si_5 (100 Vol %)	3	Divot off one end	Reference pellet	N/A	0.20	N/A

Table 5: Summary of observations from tomographic characterization

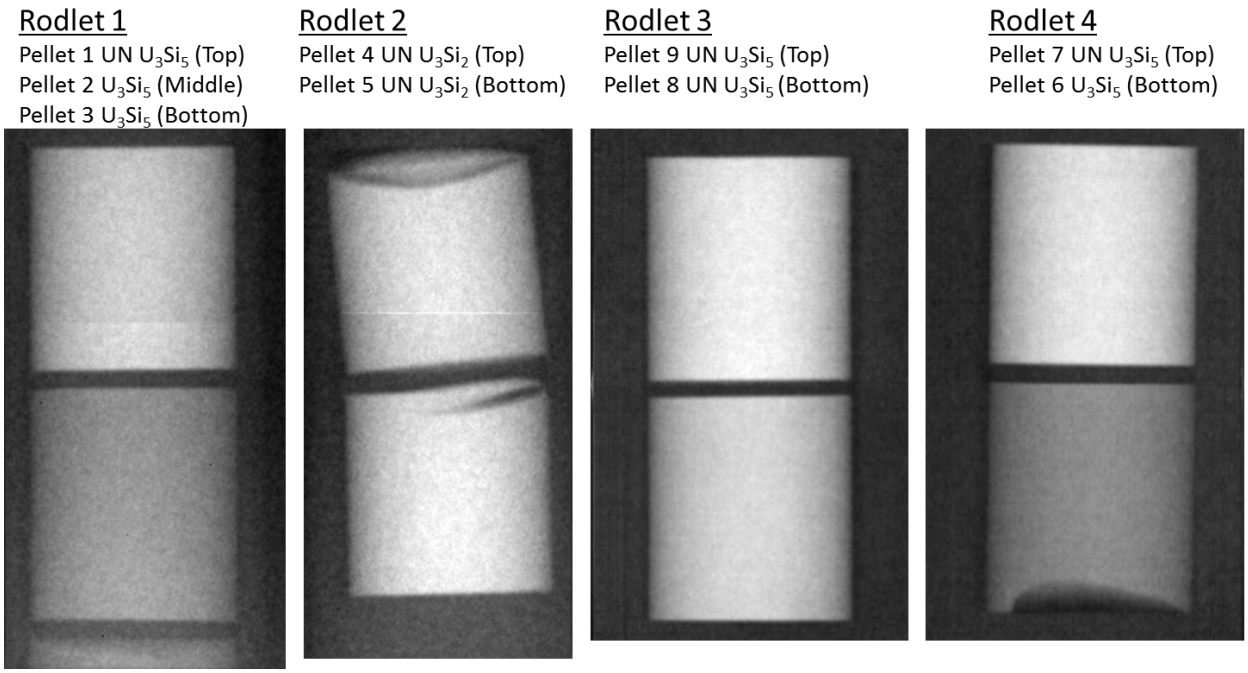

Figure 26: Radiographic images of four rodlets (The cap is oriented at the top of the page for all images).

Oblate feature Pellet 9 (UN-U_3Si_5) shows an oblate feature ~100 microns in dimension that is visible in both thermal (dominated by ^{235}U) and epithermal (dominated by ^{238}U) tomographic reconstructions (Figure 27). The rotation of the pellet was not maintained between the thermal and epithermal data, thus, the feature appears at slightly different locations in the figure. Figure 28 includes a profile plot through the inclusion. The dimension of the inclusion in the vertical orientation is close to the spatial resolution of the technique. The dip in intensity observed in Figure 28 is consistent with absence of uranium, but higher than the intensity observed for the aluminum spacers above and below the pellet. However, this is not inconsistent with a void since material may partially fill the voxels forming this feature, leading to a higher

average density assigned to that voxel. At a minimum, our technique provides evidence that this particular feature was present pre-irradiation. Our observation could also guide destructive examination.

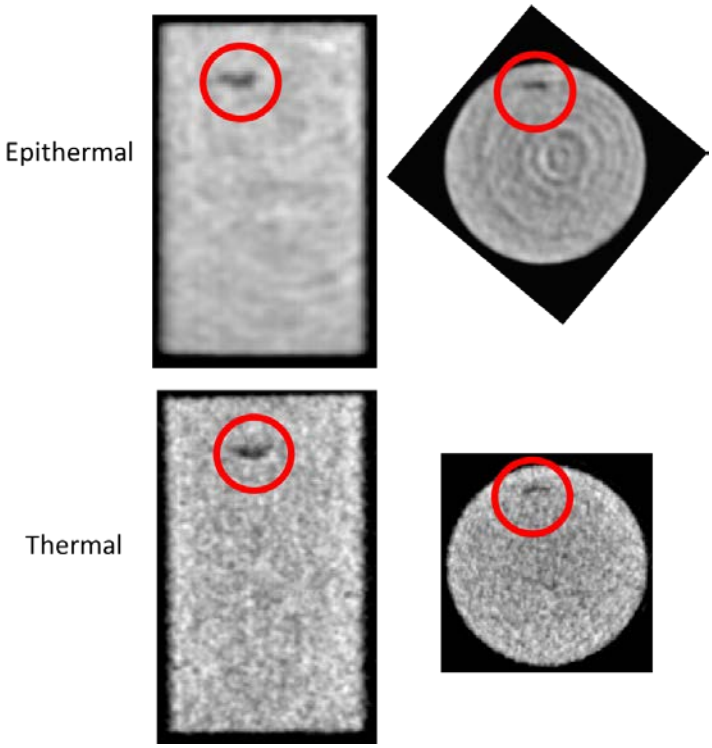

Figure 27: Pellet 9; Slices through side and plan view reconstructions showing a feature that is present in both the epithermal (top) and thermal reconstructions (bottom).

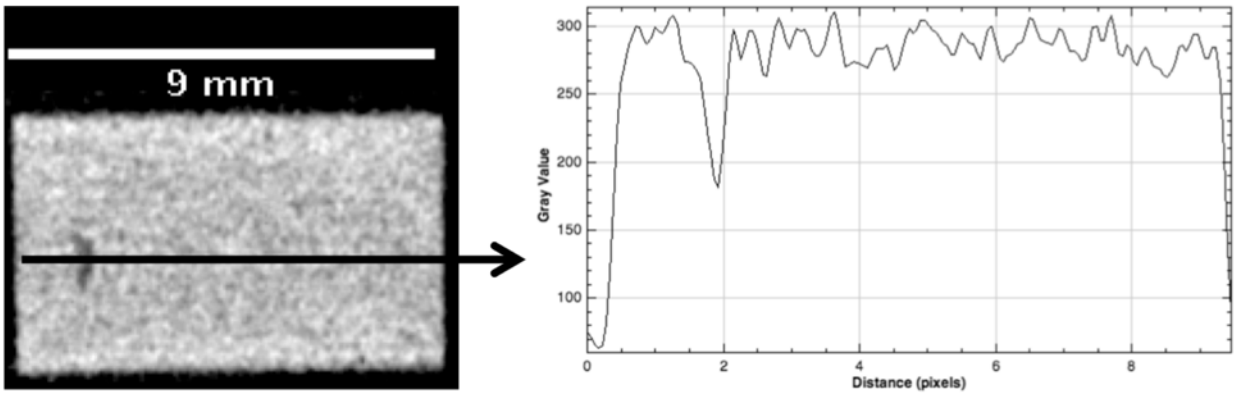

Figure 28: Pellet 9. Profile plot of reconstructed slice (thermal neutrons) through the feature shown in Figure 23...

Density Variation: Pellet 1 (UN-U_3Si_5) suggests a long range density variation along the axis of the pellet that is a maximum on the center plane of the pellet and diminishes to either end. The effect is small but appears to exceed experimental error and is under examination (Figure 29).

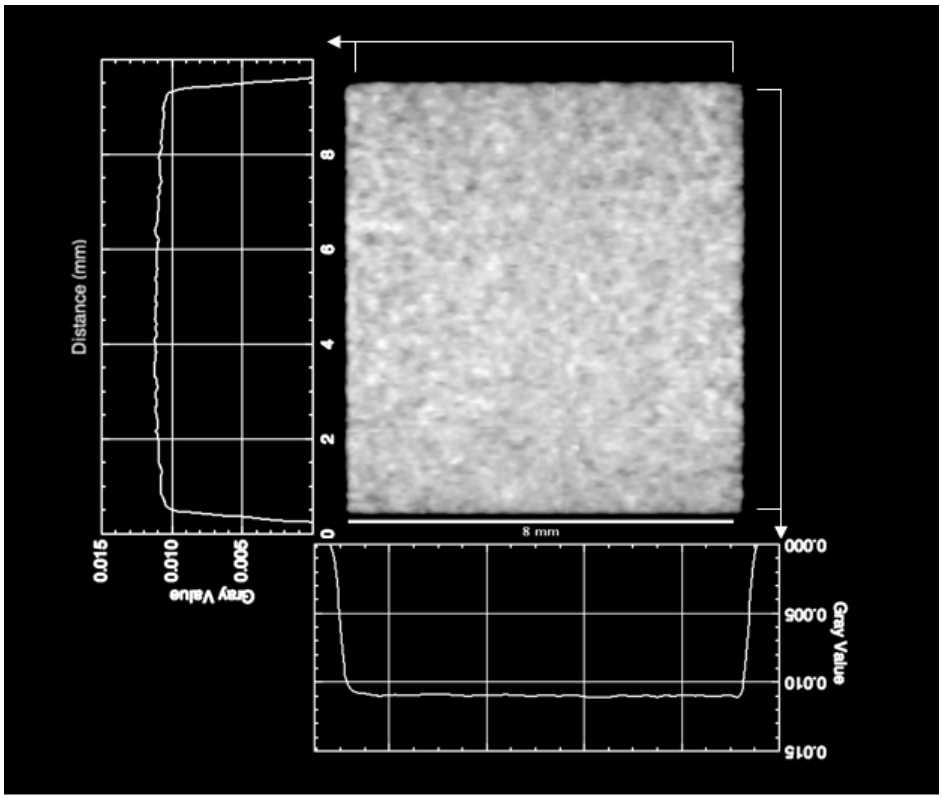

Figure 29: Pellet 1 Sections through thermal reconstruction. The profile on the left of the pellet is consistent with a density variation that is maximum on the center horizontal plane of the pellet and diminishes to top and bottom.

End cap cracks in reject pellets. Pellets 4 and 5 (UN-U_3Si_2) were both reject pellets. They were rejected because of visible end caps that extended across >50% of the pellet cross section. Sections through tomographic reconstructions are included in Figure 30. Pellet 4 shows an incipient crack at one end that only weakly penetrated the surface and would likely have been hard to identify visually if it had been less well developed.

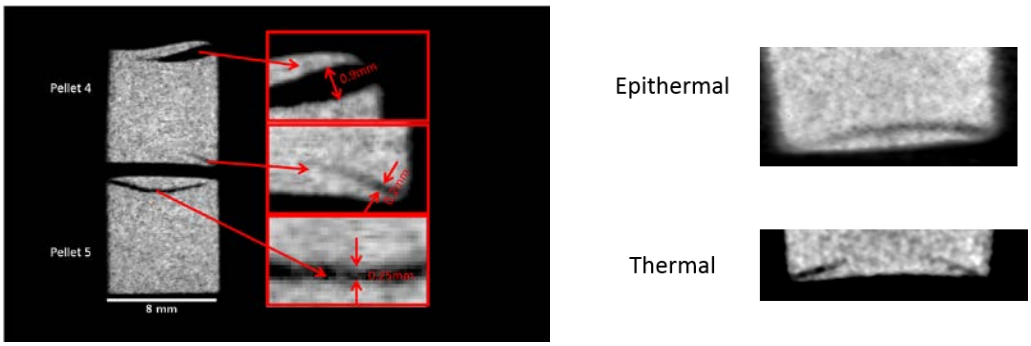

Figure 30: (Reject) Pellets 4 (top) and 5 (bottom) (Left). Pellet 4 lower region (Right)

Contrast variation. One advantage of energy-resolved tomographic reconstructions is the ability to alter the contrast of the reconstructions after the data collection to highlight different aspects of the reconstruction. This can place the focus on features of interest (though it also means that the data needs to be interpreted by a skilled operator familiar with the materials science features of interest). In Figure 31, two contrast settings are selected for rodlet 4.

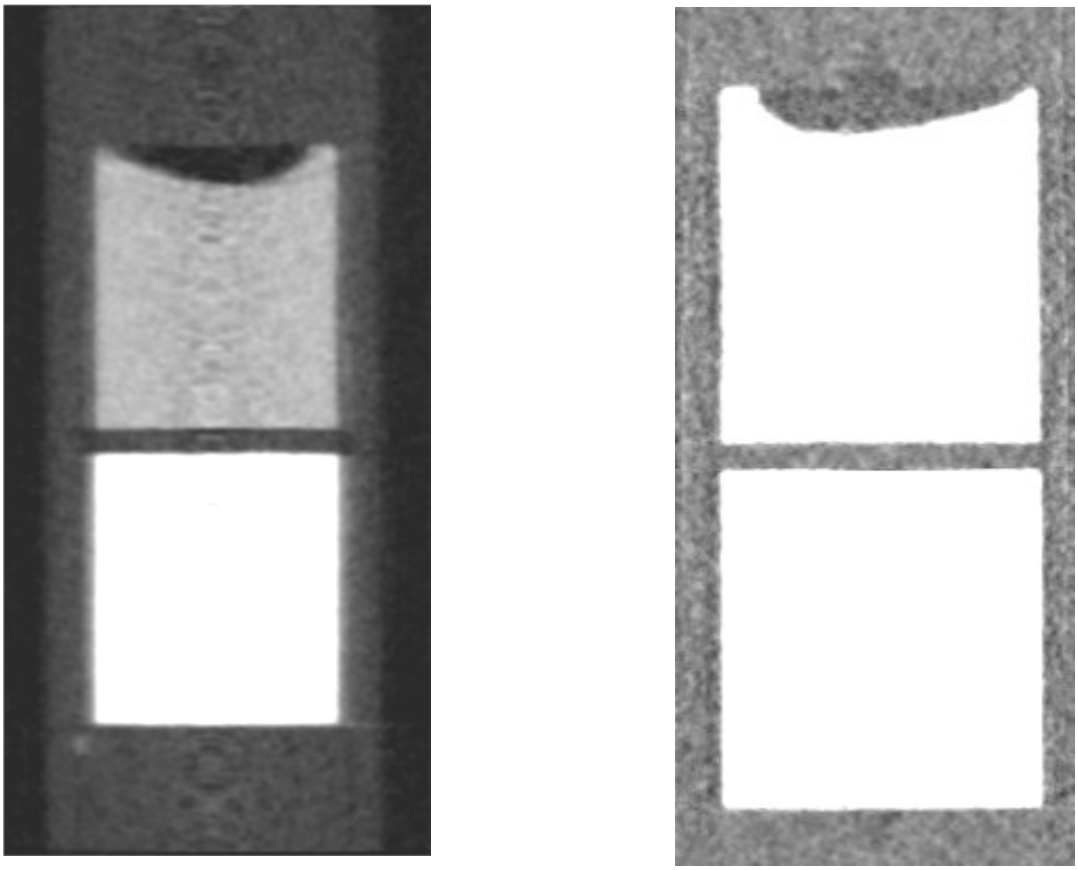

Figure 31: Rodlet 4, contrast set to highlight divot in pellet 6 (left). Rodlet 4 contrast set to highlight Aluminum can (right)

6.4 Diffraction characterization

Diffraction data was collected on the HIPPO instrument. A 2mm high cadmium slit allowed to probe each rodlet in 2mm slices. Data was collected for texture analysis, i.e. the sample was rotated in each position along the pellet axis by 0°, 67.5°, and 90° around the vertical axis. Count time for each orientation was 90 minutes or 4.5 hours per slice. This comparably long integration time was chosen due to the expected absorption by ^{235}U.

The data was analyzed for lattice parameter and phase fractions using GSAS. For this purpose, the data from detector panels on each ring were integrated and the summed for all three rotations, thus, randomizing any preferred orientation that might be present. For texture analysis, for each rotation 44 histograms from individual detector panels were analyzed, resulting in a simultaneous Rietveld refinement against 132 histograms. In both cases, the lattice parameter of aluminum was fixed at a value of 4.05Å, providing an internal standard for the lattice parameters of the two other phases. An overview of the diffractions scans along the pellet axis for LUJANATF1 is shown in Figure 32.

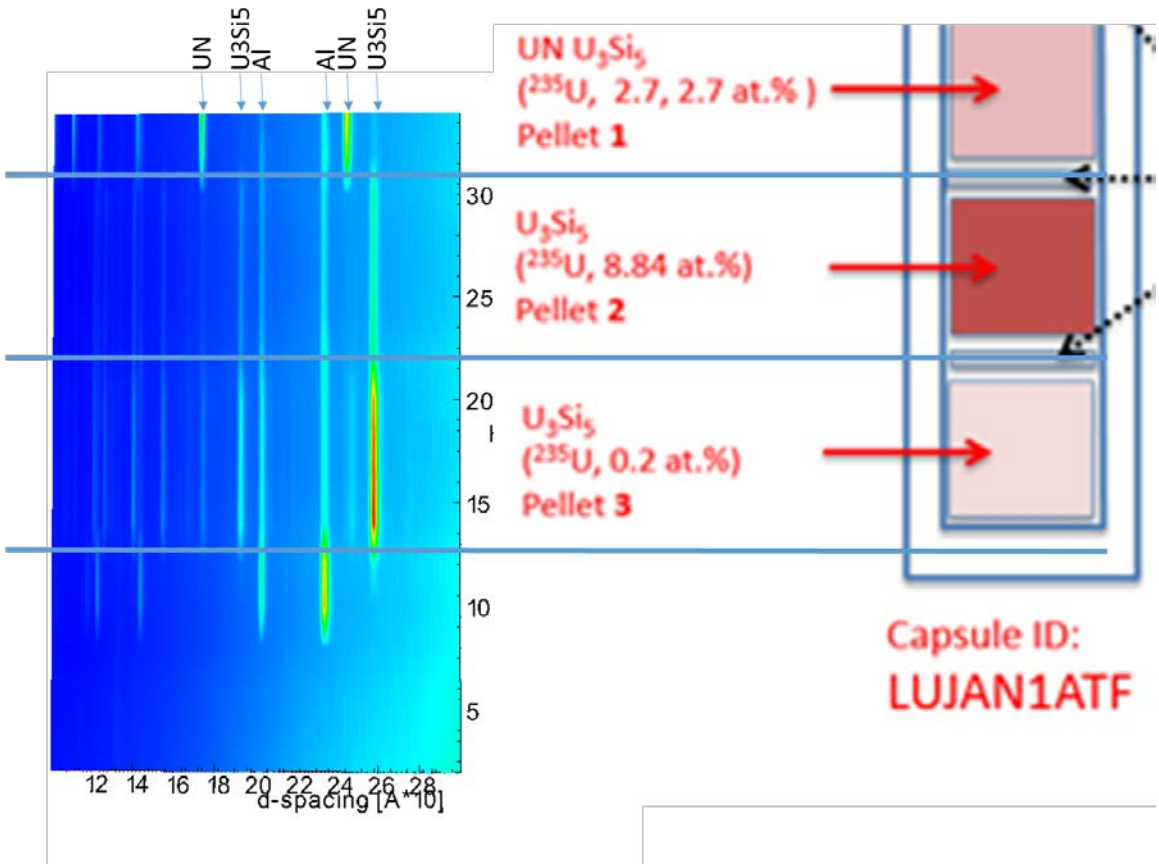

Figure 32: Overview of the diffraction data collected for LUJAN1ATF on HIPPO with normalized diffraction intensity shown as contour (left). Phases corresponding to diffraction peaks are indicated on top. The vertical scale is in millimeters. Left: Schematic of the rodlet with nominal phase composition scaled to the same dimensions. Horizontal lines are guides to the eye.

The overview plot in Figure 32 shows aluminum peaks in all slices since the container material was in the beam for all measurements. For pellet #3, the aluminum intensity gets relatively weaker compared to the slice before since more neutrons are diffracted by U_3Si_5. Diffraction lines corresponding to UN are also clearly visible at ~2.5Å and 1.75Å. This is remarkable since nominally, see e.g. the composition shown in the schematic in the right of Figure 32, no UN should be present. The individual diffraction pattern for the 90° detector bank in Figure 33 also clearly shows a peak at ~2.5Å between Al and U_3Si_5 peaks.

In pellet #2, only U_3Si_5 is visible as expected by the nominal composition. Especially in Figure 32, it is evident that this pellet has the weakest diffraction signal owing to the highest enrichment level which attenuates thermal neutrons utilized for the diffraction. As expected for the composition of UN-15 wt% U_3Si_5 with an enrichment level of 2.7 at%, the strongest diffraction peaks visible for pellet #1 are those corresponding to the UN phase.

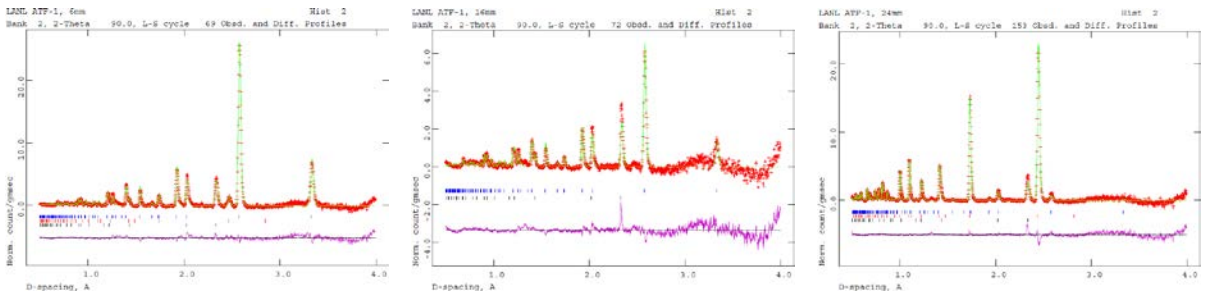

Figure 33: Diffraction patterns from the HIPPO 90° detector bank for pellet #3 (left), pellet #2 (center), and pellet #1 (right). The tick marks indicate calculated diffraction peak positions for aluminum (bottom row), UN (center row, missing in #2), and U_3Si_5 (top row). Measured intensity is shown as crosses with the curve being the Rietveld fit through all data points. Difference curve between experimental data and fit is shown below.

Figure 34 shows the pole figures for the 002 (c axes) and 200 (a axes) of U_3Si_5 in pellets #3, #2, and #1 together with the 111, 200, and 220 pole figures of the UN phase in pellet #1. The U_3Si_5 pole figures all show a moderate preference of the c axes to be aligned radially. This could be due to the sintering close to the melting point of U_3Si_5 introducing recrystallization along the presumably radial thermal gradients. The only case where the UN phase was present to allow reliable texture analysis, pellet #1, indicates no preferred orientation for the UN crystals.

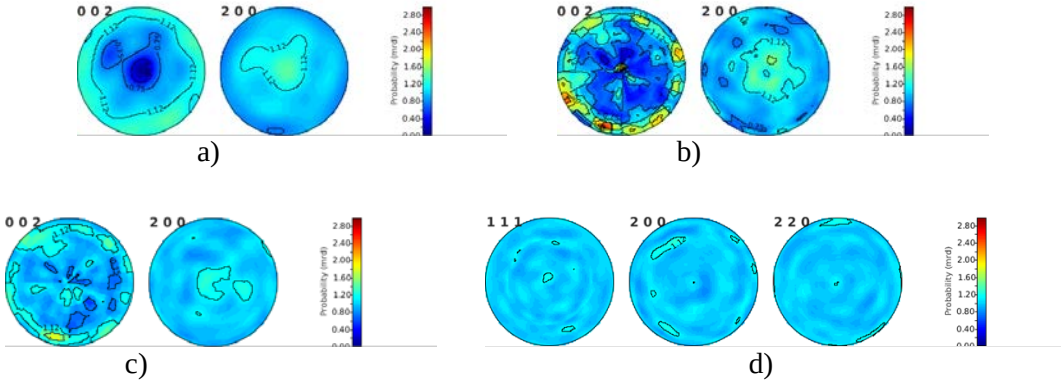

Figure 34: Pole figures representing the preferred orientation of a) U_3Si_5 in pellet #3, b) U_3Si_5 in pellet #2, c) U_3Si_5 in pellet #1 and d) UN in pellet #1. In all cases the pellet axis is in the center of the pole figures.

Results of the Rietveld refinement against full patterns is shown in Figure 35. The weight fractions, consistent with the occurrence of UN peaks, show 3 to 4 wt.% UN in pellet #3 for the data points corresponding to sample heights between 12 and 18 mm. No UN is observed in pellet #2. Despite the nominal composition of 15 wt% U_3Si_5 in pellet #1, the Rietveld analysis yields only ~5 wt. % U_3Si_5. Whether this is an artefact of the analysis or actual reaction between UN and U_3Si_5 during sintering in unclear at this point. Also shown in Figure 35 are the unit cell volumes of UN and U_3Si_5. While unit cell volumes for data points originating from the same pellet are fairly consistent, we observe for U_3Si_5 a slight increase from pellet #3 to pellet #2 and a substantially increased unit cell volume in pellet #1. This could be due to exchange of N and Si atoms between the two phases during the sintering (so-called chemical lattice strain). This is consistent with a decrease in the unit cell volume of UN for pellet #1 relative to pellet #3.

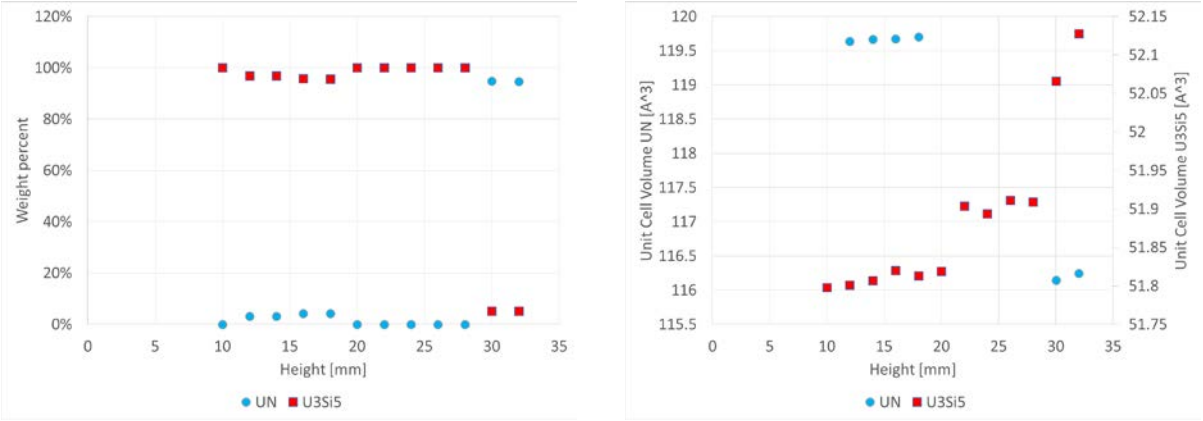

Figure 35: Weight fractions of UN and U_3Si_5 (left) and unit cell volumes (right) resulting from the Rietveld refinement as a function of height.

7. High-energy X ray investigation of 3D microstructure of UN-U_3Si_5

7.1 Introduction

Depending on processing temperature, many possible stoichiometries of the U-Si system exist[19,20,21]. This section addresses high resolution X-ray measurements performed on a flake of UN/U_3Si_5. Their purpose is to examine the microstructure at the micron spatial resolution to complement the neutron measurements of bulk pellets. In particular since it is essential to know everything we can about both the initial state and the evolved state after the sample has been heat treated and ultimately after it has been exposed to a radiation environment. Whereas neutrons offer nondestructive examination of whole pellets X-rays are complementary by virtue of their higher spatial resolution at the cost of reduced penetration depth. In particular High-energy X-ray diffraction microscopy (HEDM) in concert with micro-tomography (Micro-CT) are state-of-the-art techniques that are demonstrated for the first time to a high Z material system. Previous work has been reported on low Z materials, where 3D microstructure evolution in a single sample subjected to variety of stressors is measured under ex-situ as well as in-situ conditions [22,23]. Recently, HEDM and Micro-CT techniques have been extended to study high-z materials with application to nuclear fuels, where small regions of as-received or irradiated fuels have been probed at unprecedented resolution [24,25].

7.2 Method

A single flake of UN/U_3Si_5 approximately 1×0.4×0.1 mm^3 in dimension was used for this examination. HEDM and Micro-CT measurements were performed at the Advanced Photon Source (APS) beamline 1-ID at Argonne National Lab (ANL). For the experimental results reported here, calibrated high-energy X-rays with E = 88.005 KeV (Pb edge) were used. Diffraction measurements were performed in a layer by layer basis, where a cross-section of the sample µm was illuminated by a planar focused high-energy X ray beam. The data were collected on a two-dimensional CCD detector. Each diffraction image was acquired at 1° integration, while the sample was rotated, and 180 such images were collected. For the multiple angle measurements of each layer, the detector was moved to a second sample-to-detector distance and the measurements were repeated. The sample was then translated vertically and measurements were repeated to map the entire volumetric region of the sample. In this case, a total of 40 layers (160 microns along z) were measured, where the distance between two layers was 4 µm in the z-direction, to ensure that each

illuminated cross-section was an entirely new region in the sample. For µ-CT, volumetric measurements were performed with a box beam illuminating a full 3D region of the sample. 1800 images were collected at 0.2° rotation interval by rotating the sample through 360°. For full 3D measurements, HEDM and µ-CT required 12 hours and 0.5 hours of beam time, respectively. Details of the experimental setup and measurement methods are described elsewhere [22,23,26].

The raw diffraction images are background subtracted and diffraction spots are extracted. The IceNine software is then used for orientation field reconstruction[27]. For a given vertical slice of the sample, z_i and any location within the slice, x, given a guess orientation g, the forward model produces multiple simulated diffraction images $P_{s;x;di}$ $(j_x; j_y)$, giving a value for the simulated diffraction (1 or 0) at each detector location $(j_x; j_y)$ and detector to sample distances d_i. The simulated diffraction image is then compared to the actual experiment-based detector images $P_{e;di}$ $(j_x; j_y)$, and an overall count of the number of overlapping peaks, divided by the total number of simulated peaks, gives an estimate of the reconstruction accuracy, which is termed as the confidence index. The reconstruction algorithm proceeds by an iterative Monte-Carlo method, maximizing the confidence index of reconstruction throughout the sample. The method has been validated against electron backscattering diffraction microscopy (EBSD) and with multiple reconstructions of a single sample. With the current set-up, limited by the available scintillators and detectors, a spatial resolution of up to 1.5 µm and orientation resolution of 0.1° is typically achieved.

Tomographic reconstruction is performed using the RECON software, which was developed at LANL. RECON can perform reconstructions using several X-ray beam geometries and algorithms. Beam geometries include parallel beam, fan beam, and cone beam. Algorithms include direct FFT inversion, filtered back projection, and the Feldkamp method, a modification of filtered back projection, for cone beams having vertical angles. A filtered back projection method was used for this data. In addition to reconstruction, RECON performs numerous image processing tasks that assist in the reconstruction. These include detector raw data calibration, converting calibrated radiographs to attenuation images, generating sinograms, automatic centering of sinograms, low pass filtering, median filtering, ring removal, resizing, and attenuation correction for beam hardening.

7.3 Data Analysis

7.3.1 High-energy X-ray diffraction microscopy (HEDM)

If multiple phases are present in a single sample, orientation field reconstruction requires prior knowledge of the crystal structures of all phases. The two main phases are known to be cubic UN as a primary phase of the matrix and hexagonal U_3Si_5 as a secondary phase. For the analysis, the UN phase was considered to have a face centered cubic structure with lattice parameter a = 4.888 Å and the U_3Si_5 phase was reconstructed assuming hexagonal symmetry with lattice parameters a = 3.843 Å and c = 4.069 Å. Layer by layer reconstruction was performed separately for each phase to determine the orientation field of the 3D measured volume. First the orientation field of the UN phase was reconstructed. The already identified spatially resolved orientations were then masked from the sample space to only have regions whose orientations were yet to be determined. This limited search space was utilized to reconstruct the orientation field of the second phase. The mask was created with a confidence threshold of 0.85, where each pixel with lower than the threshold confidence was considered unidentified in the first phase reconstruction. This masking was performed to accelerate the reconstruction process by limiting the sample search space during U_3Si_5 phase reconstruction. Single layer reconstructions of the two phases are shown in Figure 36 (a) and Figure 36 (b) and the combined map is shown in Figure 36 (c). The colors correspond to Rodriguez vectors mapped to RGB colors, where clusters of similar orientations have same colors and

are identified as a single grain. After the two phase reconstructions, there were still unfilled regions in the sample, which were speculated to be either pores or an undetermined third phase that was not reconstructed.

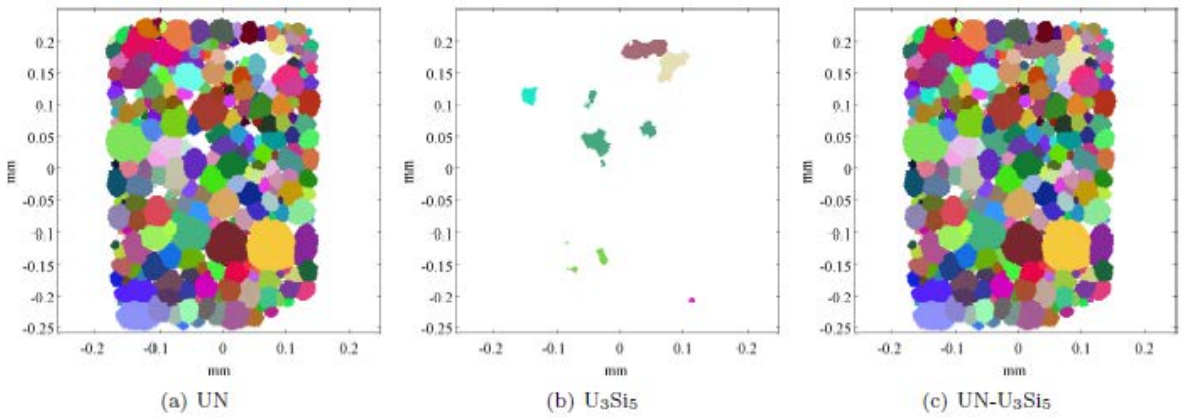

Figure 36: A single layer orientation map of two phases obtained from high-energy X-ray diffraction microscopy measurements. (The white regions in (c) in the sample interior are either pore or a third phase material).

Phase	# of processors	Time (hrs)	Resolution (μm)
UN	600	4.5	2.5
U_3Si_5	600	8.5	2.5

Table 6: Average data processing summary per layer.

The reconstructions were performed in LANL on Darwin cluster in CCS-7. Table 6 shows the summary of average processing time for each layer reconstruction. The hexagonal phase structure took longer time for reconstruction, which could be due to lower crystal symmetry compared to cubic phase. Using the masked sample space for U_3Si_5 phase reconstruction, also reduced the total reconstruction time.

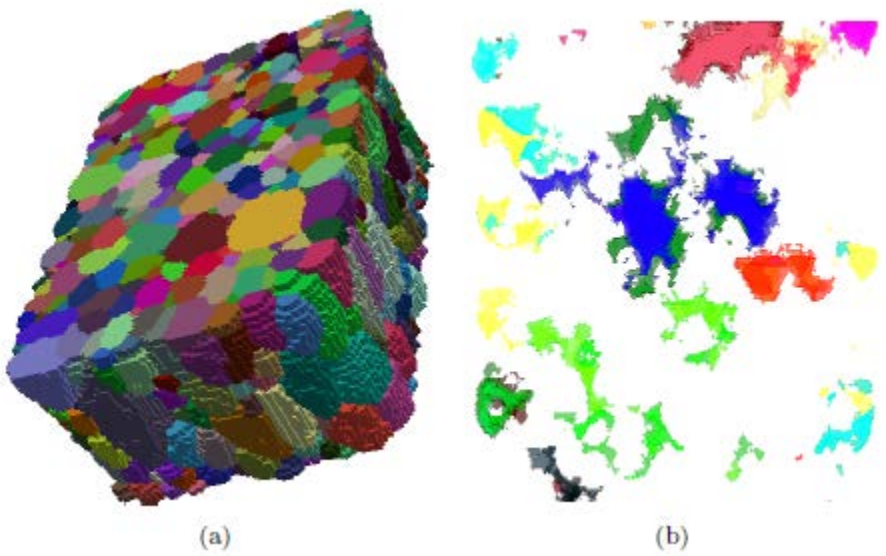

Figure 37: (a) A 3D reconstruction of the orientation field of the UN phase. (b)U_3Si_5 orientation field, where 10 layers are projected onto a 2D plane.

Out of the measured 40 layers, 30 layers of UN phase and 10 layers of U_3Si_5 reconstructions have been completed thus far. As the sample was not touched during the layer by layer measurements, the 3D reconstruction was obtained by stacking the 2D cross-sections; thus, eliminating the need for registration between layers. Figure 37 (a) shows the 3D reconstructions of the UN phase with 30 layers corresponding to a volume of 320×450×120 μm^3 and Figure 37 (b) shows the 3D clusters of regions in the sample from 10 layers reconstructions that belonged to the U_3Si_5 phase. The remaining unfilled regions had diameters ranging from sub micrometer up to 50 µm. The limited resolution of the HEDM reconstructions of the current orientation field maps would miss small features that are below ~ 5 µm. Higher resolution reconstructions to 1.5 µm can be achieved, but would require longer processing time (up to 24 hours per layer given the same number of processors).

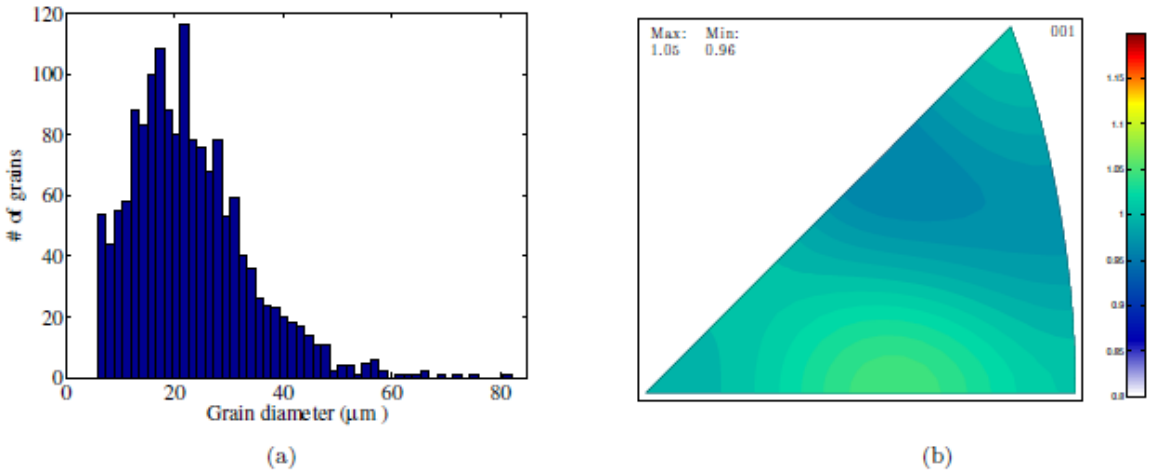

Figure 38: (a) Grain size distribution for 1559 bulk UN grains. (b) Inverse pole figure map for 1559 grains indicates random texture.

Phase	Average (µm)	Std (µm)	Max (µm)	Total # of grains
UN	600	4.5	2.5	1559

Table 7: Grain size distribution of the UN phase

Grain size distribution was calculated for the UN phase from the 3D image in Figure 37 (a). Figure 38 (a) shows the distribution for 1559 grains with average grain diameter of 22.8 µm and standard deviation of 10.8 µm. Only grains with at least 4 voxels were considered in this analysis. The largest grain using the spherical estimation was found to have 82 µm diameter. The above distribution indicates heterogeneous grain growth resulting in some grains having greater than twice the diameter of the average grain size. Figure 38 (b) shows the inverse pole figure map generated from the reconstructed orientation fields of 1559 grains belonging to the UN phase. The intensity ranged from 0.96 to 1.05, which corresponds to a random texture, which is as expected for ceramics materials. Figure 39 (a) shows the 3D projection of the 30 layers onto a 2D plane, where the white region corresponds to the UN phase and rest of the pixels in the sample interior are either materials or pores. Figure 39 (b) shows a 2D projection of the 3D center of mass (COM) positions of UN grains in the measured volume. The COM position is represented by a circle, where its size and color are based on the corresponding grain size. This map was plotted to determine if there was heterogeneous distribution of grain sizes based on their spatial location on the sample. From visual inspection, it seems that the bottom region has higher likelihood of finding larger grains than the top region. Visually, it is also observed that the location of the small UN grains corresponds to the region with large

clusters of secondary phases in Figure 4(a). A possible reason for this could be either the presence of large pores and second phase hinders grain growth in UN or there is a temperature gradient resulting in this spatial heterogeneity. However, further speculation would require information on the direct connection between the reconstructed region and the corresponding location in the rodlet from where the sample was extracted.

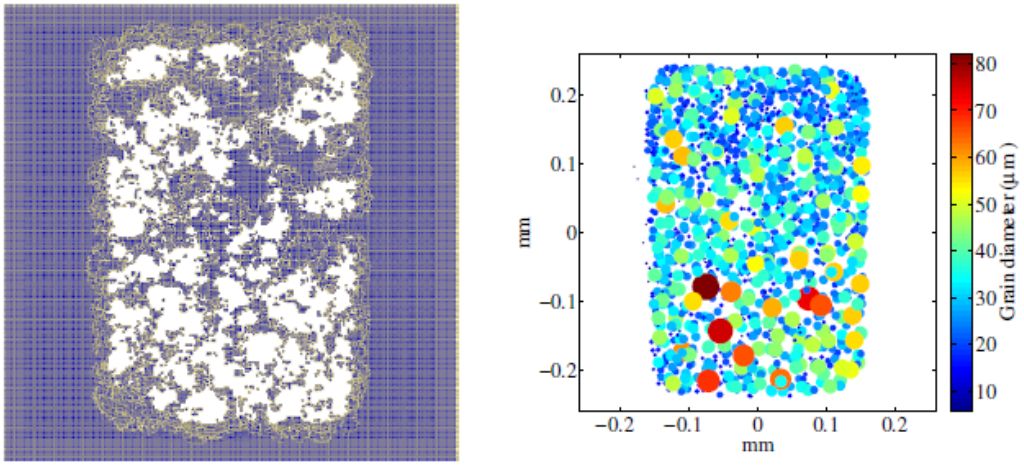

(a) (b)

Figure 39: (a) Unfilled region in the sample interior after removing the UN phase. (b) Spatial distribution of the center of mass of individual grains projected onto a 2D plane where each marker size and color represents the corresponding grain size.

7.3.2 Computed micro-tomography (μ-CT)

Tomographic reconstructions from the transmission data revealed the presence of four different densities in the UN/U_3Si_5 sample. Figure 40 shows a cross-section of the 3D image, along with a line profile from a region in the sample. P1 with the lowest absorption was the porous region while P4 with the highest density was the matrix corresponding to the UN phase. The other two phases, P2 and P3 have densities in between P1 and P4. From the diffraction data, it was determined that P3 was the U_3Si_5 phase and earlier SEM/EDS analysis confirmed that the unknown third phase was U(Si,N), which had higher X ray absorption cross-section than U_3Si_5.

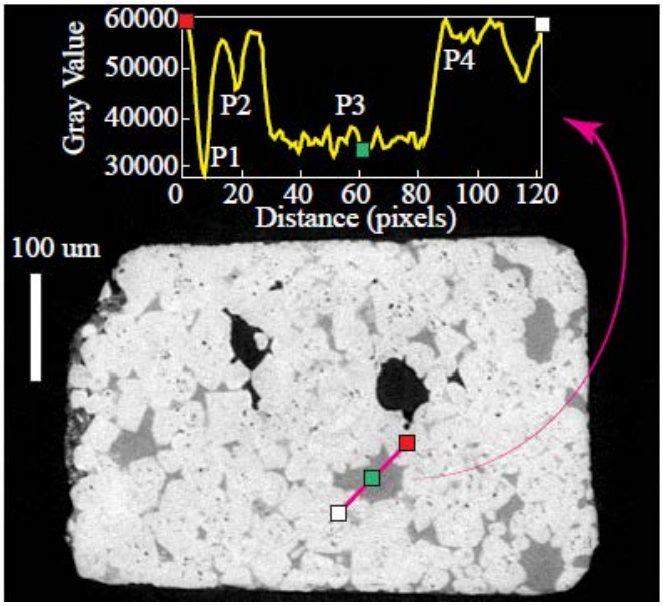

Figure 40: Absorption profile obtained from the tomographic density map indicated the presence of four different phases in the sample, where the highest absorption corresponded to UN or the matrix phase with the highest density, and the lowest absorption regions corresponded to pores. The other two phases were lower in density in comparison to the UN phase.

Figure 41 shows the 3D reconstruction of the measured sample along with a rectangular region of interest, from where different phases were segmented for calculating phase fractions. Figure 41 (a)-(d) show the spatial distribution of the UN matrix, U_3Si_5, U(Si,N), and pores, respectively. Table 8 shows the corresponding phase contents for all four phases. The major phase comprised ~85% of the sample, where the other two phases were more or less in equal amount accounting for ~13% of the measured volume, and the rest of the region was found to be porous. The volumetric density data indicated that the sample was greater than 98% dense.

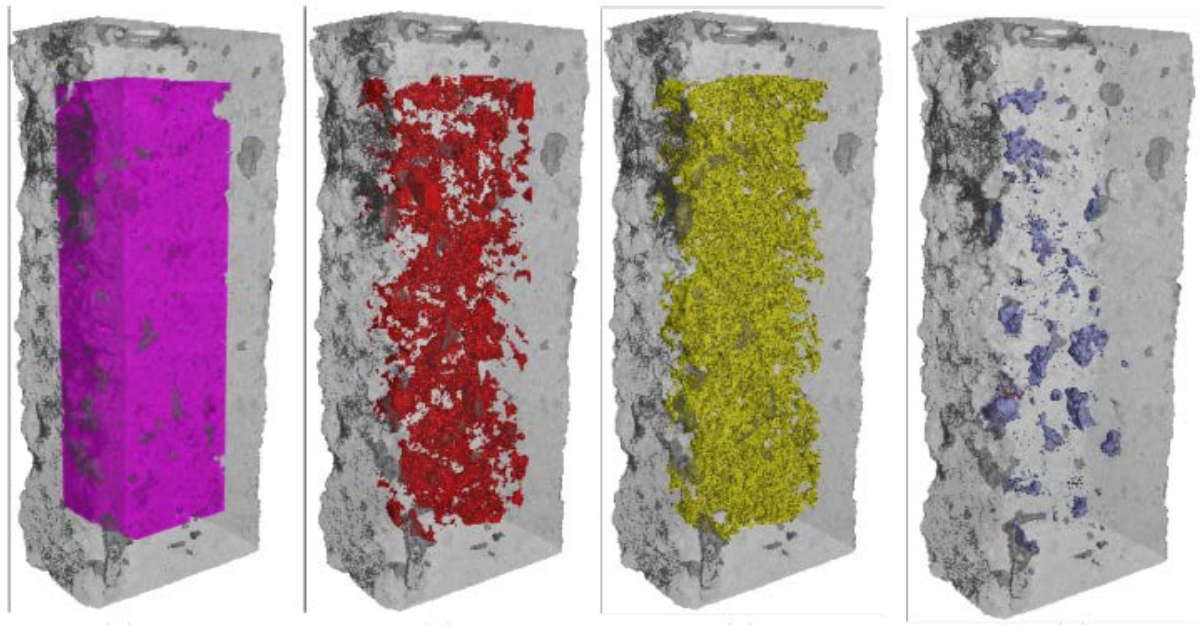

(a) (b) (c) (d)

Figure 41: Four phases segmented from a rectangular region of interest selected from a 3D tomographic reconstruction of the measured UN-U_3Si_5 sample. (a) UN, (b) U_3Si_5, (c) U(Si,N), and (d) pores).

Phase	**UN**	**U_3Si_5**	**U(Si,N)**	**Porosity**
Volume [mm^3]	0.125	0.009	0.011	0.002
Fraction (vol. %)	84.9	6.2	7.5	1.4

Table 8: Volume and volume fraction extracted for the four identified phases.

Figure 42 shows the vertical and horizontal 2D cross-sections extracted from the 3D volume. The four phases are indicated by different colors. From visual inspection, large clusters of U_3Si_5 and pores were seen to be heterogeneously distributed, whereas smaller voids were uniformly distributed throughout the sample. The U(Si,N) phase seems to be decorating the interfaces of either the secondary phase and the matrix or the matrix and the large voids around which traces of U_3Si_5 were also observed. In case of U_3Si_5 and pores, feature sizes ranged anywhere from submicron up to ~ 50 microns, while the U(Si,N) phase was seen to be 2-3 pixels wide; hence, most features of this phase were below 5 µm.

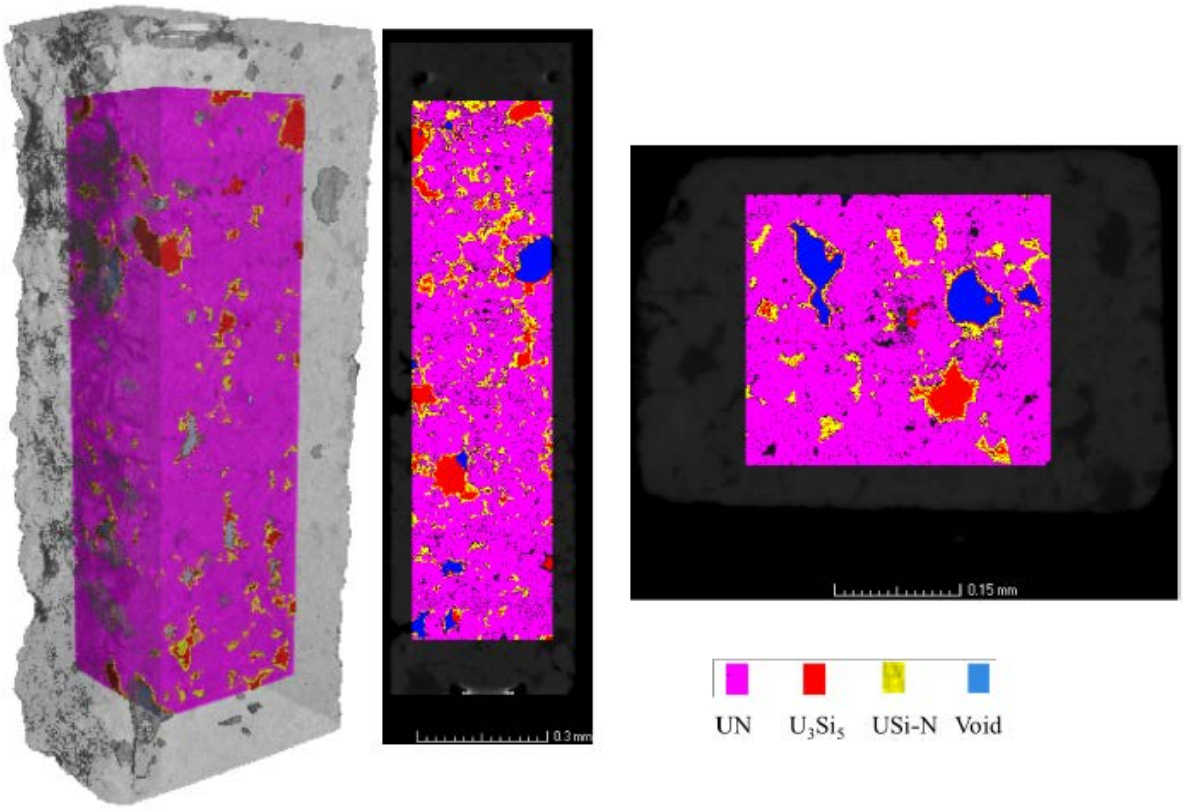

Figure 42: Color coded representation of three materials phases and one void phase shown in vertical and a horizontal cross-sections of the 3D sample.

7.4 Summary of APS measurements

This complementary X-Ray activity demonstrates for the utilization of high-energy X-rays to non-destructively map 3D microstructures of UN/U_3Si_5. The use of the advanced photon source has great potential to provide microstructural information at micron length scales that can complement the neutron measurements which naturally interrogate on length scales of full size pellets. Diffraction and transmission X-ray data provide distinct insights. Initial experimental data were processed and analyzed to extract information on spatially resolved information on orientations, grain sizes and shapes, phases, and porosity and their distributions. This data analysis of UN/U_3Si_5 suggests it would be valuable to understand mechanisms that led to:

1. Heterogeneous grain growth in UN.
2. Grain boundaries and interfaces being decorated by the U(Si,N) phase.
3. Broad size distribution in both U_3Si_5 and pores, ranging from sub-micron to ~50 µm in diameter.

3D data gathered by HEDM and µ-CT techniques is crucial to inform and validate microstructurally aware models. By fully, non-destructively characterizing a single sample at multiple states, these techniques both provide a way to calibrate models with uncertainties and enable a true test of model accuracy, by using the initial state as input and comparing the modeled predictions to actual intermediate and final state measurements. Unlike destructive techniques such as EBSD, NDE characterization using high-energy X-

rays provides a detailed view, at sub-grain resolution, of a single sample as it evolves through various states, allowing comparison with models at a level of detail that is otherwise impossible.

Initial work towards these goals includes initial and heat-treated characterizations of UO_2 samples, data which was used to calibrate a Potts model, which was then used to predict the evolution of similarly heat treated, but varying stoichiometry UO_{2+x} samples, allowing for a study of grain growth dependence on various material properties such as Oxygen content, sintering time, and average initial grain size[25]. We could take a similar approach with the UN/U_3Si_5 sample initially characterized in this work, which could be re-characterized if the same sample is subjected to any environment or placed in a reactor. The before and after data will be highly valuable in development and improvement of models for accurate prediction of fuel structure evolution under variety of conditions. NDE techniques along with predictive models would enable and advance the study of the relationship between microstructures and fuel properties such as thermal conductivity, ductility, mechanical strength, and resistance to oxidation, and aid in ATF design.

8. Discussion

Between October 2015 and March 2016, tomographic and diffraction data were recorded for nine ATF pellets. The pellets were removed from batches fabricated for irradiation and exemplified materials that both passed and failed quality control assessment for irradiation testing. Tomographic reconstruction is complex and inspecting the images and reconstructions takes experience so the data analysis reported here is preliminary. In fact a key aspect of making the techniques accessible will be facilitating the data processing and viewing and reporting of the results to identify relevant features in an efficient manner.

A significant step forward has been the quantitative determination of isotopic composition. When using Tantalum the ^{235}U atomic enrichment was in agreement with nominal fabrication values to within +- 0.1 atomic %. When using Cadmium the systematic underestimate of the enrichment values was ascribed to the paucity of cadmium resonances in the 1 to 50eV range and thus a poor background fit.

Potentially the shape and features of cracks can be related to stress distributions and fabrication conditions and have the potential to inform and guide synthesis parameters. The limiting spatial resolution of the detector used in these studies is 55 microns. Improved spatial resolution is clearly desirable to approach the grain size and length scales consistent with the individual phases of the composite phases in the ATF fuels. Detector developments are underway to improve the spatial resolution. Precedent at NIST and PSI suggest that spatial resolution approaching 10 microns is possible.

Neutron diffraction characterization provides complementing information on length scales of crystallographic unit cells (e.g. lattice strains) and grains (e.g. texture and phase composition). Both texture and unit cell volumes show indications of rearrangement of atoms: The U_3Si_5 phase for all three examined pellets shows a preference of the crystallographic c-axes to be aligned radially. If this not due to a shape effect occurring during compaction, this could be due to recrystallization during sintering with a growth direction along the thermal gradients. Consistent with this, we observe lattice parameter changes in UN and U_3Si_5 in pellet #1 relative to lattice parameters observed in pellet #2 and #3. This can be explained by exchange of Si and N atoms between the two phases, changing the unit cell volumes due to the difference in ionic radius. In situ studies of the sintering would allow to study this problem.

Synchrotron-based X-ray diffraction allows a complete mapping of grains with their phase and orientation. Detailed 3D maps can be created for these parameters that can be used for models. Penetration of even hard X-rays into uranium bearing phases is low compared to neutrons, such that only sub-millimeter sized samples can be characterized and containers, e.g. for shielding purposes, are not possible. However, single effect studies, e.g. changes during sintering, can be studied.

All three characterization methods, neutron tomography, neutron diffraction, and synchrotron diffraction, provide data suitable for models on various length scales.

The national capacity for destructive PIE of irradiated fuels is limited. The cost is large and the schedule constrained. For these reasons there is merit in exploring the opportunity to non-destructively examine irradiated fuels. At the current point in development of the neutron based techniques they have the potential to contribute mechanical integrity, phase, isotopic distribution and pellet clad interactions data for many cubic centimeters of irradiated fuel that is integral to validation of mesoscale/engineering scale models. Improved spatial resolution is a key development goal. However the shipping cost for moving irradiated fuels between INL and LANL remains an impediment. One exciting possibility that is under consideration concerns the availability of nascent neutron production technologies using small scale accelerator and laser based sources that might be realized to enable poolside characterization at INL or industrial facilities.

9. Future Work

Diffraction analyses

Diffraction measurements of stoichiometry and phase were performed using the HIPPO instrument on rodlets 1 and 3 and spatially resolved diffraction measurements were performed on Rodlet 1 using the SMARTS instrument. These data will be addressed over the next 6 months with analysis of complementary gamma ray spectroscopy activation measurements and gamma ray sensitivity measurements of the detector.

Instrument improvements

Resonances measured in these studies have been measured up to 200eV. However our collaborator Anton Tremsin collected data using the same detector at the J-PARC pulsed neutron source in Japan and observed resonances up to keV. Thus control of the instrument background on FP5 is a key goal to expand the energy range over which isotopic resonances can be measured.

An MCNP model of flight path 5 indicated that some, though not all, of the background originates from the moderator on the opposite side of the target/moderator/reflector assembly. This produces a delayed spectrum and resonances that should have exhibited 0% transmission were observed with transmissions of 10-20% of the incident intensity. Unfortunately this cannot be addressed without a redesign of the target.

We have moved the sample position for the 2016/17 run cycle to the closest position possible on FP5, right behind the exit of the incident beam pipe. The gain in flux should be about a factor of 2. This pipe is evacuated to reduce air scatter between moderator and sample position. We will re-arrange collimator pieces to provide acceptable L/D by having the smallest diameter the furthest away from the source. We have proposed to run for a short time with the opposite side moderator filled with He instead of liquid H_2, thus being transparent. If this test eliminates substantial background, the involvement of our team in the design of the new target will possibly allow optimizations for this particular background source.

We will also replace the current steel collimation with borated steel (NEUTRONIT from Boehler, Austria). Entrance and exit collimation will be modified to square, to match the moderator and detector and will follow an approach demonstrated at FRM-2 in Europe. The square entrance and exit cross-sections adapt better to the original moderator shape as well as the detector shape and promise to provide a gain of ~40% in flux.

A separate effort will explore the option of a boron only MCP for the detector. The detector currently employs a boron and gadolinium-doped MCP and was developed for use in the thermal regime for which the Gd epithermal resonances response were irrelevant but which complicate measurements in the 1 to 200eV range. Exploring possible other detector materials, including downscatter of incident neutrons to increase detector efficiency, are also explored in discussions with our colleagues.

Multiple characterizations

We have three HIPPO detector panels that could be installed in FP5 to allow simultaneous imaging and diffraction characterization. We are following the iMAT instrument development at ISIS[28], which has pioneered this technique. While iMAT is a general purpose instrument, we would strive to optimize our setup for nuclear fuels, i.e. with respect to shielding and sample handling. For the combination of imaging and diffraction, it is likely advantageous to collimate the beam to only have a smaller probed volume for diffraction. With a collimation that is efficient also for higher energy neutrons, the neutron transmission analysis could be combined with prompt time-of-flight gamma analysis (PGA). This was recently demonstrated at the ANNRI beam line at J-PARC[29], where neutron induced prompt gammas were recorded as a function of time-of-flight of the incident neutron (see Figure 43). With this technique, a higher sensitivity and utilization of neutron resonances that are too high in energy for measuring the neutron transmission with our setup could be achieved.

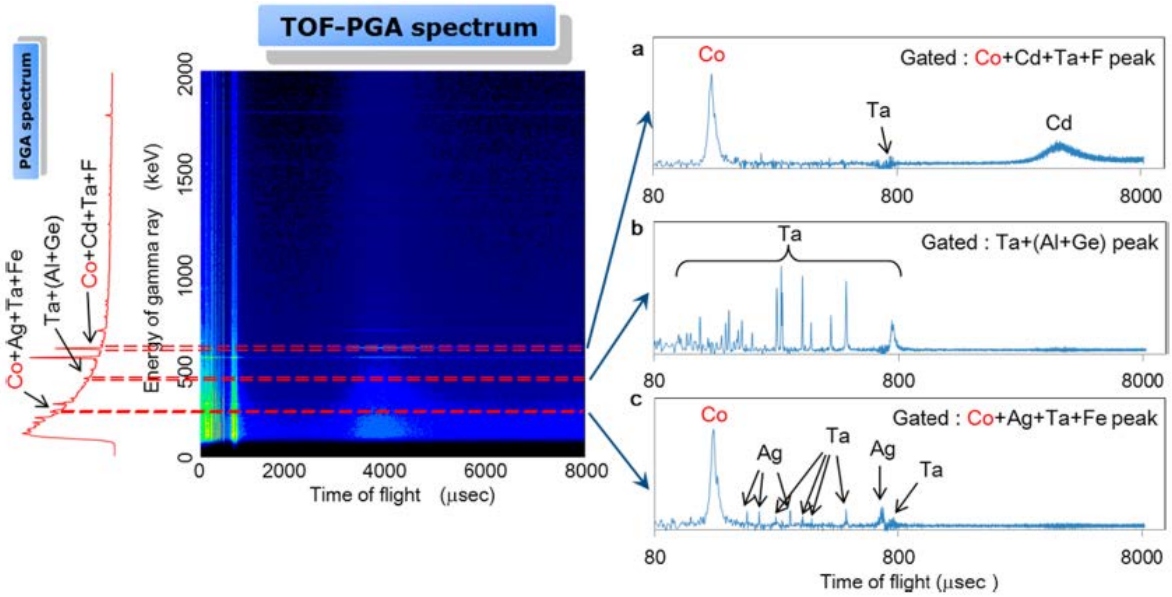

Figure 43: Illustration of the time-of-flight prompt gamma analysis technique (TOF PGA). While the overall gamma spectrum measured without a neutron beam only shows gammas emitted from radioactive nuclei, the pulsed neutron beam may also cause prompt gamma emission which can be correlated with the neutron time of flight to unambiguously identify the emitting nucleus (from [29]).

Receipt of Transuranic fuels

In the next run cycle we will examine two U-20Pu-10Zr fuel rodlets containing transuranics. Shipment and receipt of these samples to LANL by Randy Fielding is scheduled for this fiscal year. The samples are cast and scheduled for encapsulation in April 2016. Their nominal dimensions are 0.168" OD and 1.5" long. When chemical analysis and isotopic estimates are available, the Authorization basis calculations will be completed to execute transfer of the samples from INL to LANL. The possibility of repackaging archive MOX or MA-MOX pellets for examination remains of interest.

Continued assessment of potential for study of irradiated fuels

The measurements on the pre-irradiated material are valuable in their own right but a huge "payoff for this work would be to perform measurements on irradiated fuel rodlets. A key milestone test to demonstrate the viability of measurements on irradiated fuel will be a detector test to be performed by Anton Tremsin at INL in May when he will test the detector performance in the vicinity of irradiated fuel. This will demonstrate the ability of the detector to resolve the neutron measurements from the gamma induced signal from real irradiated fuels. Appendix A section 11 of this report includes a conceptual cask

for handling rodlets of LANL ATF in the beam line. Discussion about handling irradiated fuel rodlets and hot cell utilization at LANL are ongoing.

10. Conclusions

The application of non-destructive neutron based evaluation for the analysis of as-fabricated nuclear fuels has the potential to provide critical enabling data to realize science based fuels development. For R&D research on small batches of prototype material it maximizes the scientific merit of irradiations by establishing the initial condition of the material as well as serving a Quality Assurance role. By characterizing fuels before irradiation it can identify features that are invisible to visual inspection which may or may not be a cause for rejecting a pellet. Non destructive characterization of irradiated material has the potential to ensure that destructive evaluation in hot cells is used to maximum cost efficiency by directing focus to regions in samples that represent average and or atypical behavior.

Neutron tomographic imaging and scattering measurements on nuclear fuels of fabrication geometries provide non destructive measurement of cracks, flaws, chemistry, phase, texture, and fission gas pressure. The data for fresh fuel contributes data that establishes the benchmark for the initial condition of the fuel. Measurements on irradiated fuel could add substantial data sets for validating the modeling and simulation of irradiation effects that are integral to improved fuel performance codes.

This work was funded by the Fuel Cycle R&D program with the support of Kenneth J. McClellan (LANL), Heather Chichester (INL), and Jon Carmack (INL).

11. References

[1] M.D. Roth et al. "Bright laser-driven neutron source based on the relativistic transparency of solids." Physical review letters 110, no. 4 (2013): 044802.
[2] Brown, A., and J. J. Norreys. "Beta-Polymorphs of Uranium and Thorium Disilicides." (1959): 673-673
[3] Dwight, A. E. Study of the uranium-aluminum-silicon system. Argonne National Lab., IL (USA), 1982.
[4] M. B. Aufderheide III, H.-S. Park, E. P. Hartouni, P. D. Barnes, D. M. Wright, R. M. Bionta, J. D. Zumbro, C. L. Morris, "Proton radiography as a means of material characterization", AIP Conference Proceedings, **497** (1999) 706.
[5] AS Tremsin, JB McPhate, JV Vallerga, OHW Siegmund, JS Hull, WB Feller, and E Lehmann. High-resolution neutron radiography with microchannel plates: Proof-of-principle experiments at psi. Nuclear Instruments and Methods in Physics Research Section A: Accelerators, Spectrometers, Detectors and Associated Equipment, 605(1):103–106, 2009.
[6] Vogel et al., "Assessment of advanced NDE techniques and the path forward to evaluating an AFC-2 irradiated fuel pin", LA-UR 13-2167.
[7] A. Tremsin, S. Vogel, M. Mocko, M. Bourke, V. Yuan, R. Nelson, D. Brown, B. Feller, "Non-destructive studies of fuel rodlets by neutron resonance absorption radiography and thermal neutron radiography", Journal of Nuclear Materials, **440** (2013) 633–646.
[8] C. Morris, M. Bourke, D. Byler, C. Chen, G. Hogan, J. Hunter, K. Kwiatkowski, F. Mariam, K. McClellan, F. Merrill, et al., "Qualitative comparison of bremsstrahlung X-rays and 800 MeV protons for tomography of urania fuel pellets", Review of Scientific Instruments **84** (2013) 023902.
[9] EH Lehmann, G Frei, P Vontobel, L Josic, N Kardjilov, A Hilger, W Kockelmann,and Axel Steuwer. The energy-selective option in neutron imaging. Nuclear Instruments and Methods in Physics Research Section A: Accelerators, Spectrometers, Detectors and Associated Equipment, 603(3):429–438, 2009.
[10] Michael Schulz, Peter B¨oni, Elbio Calzada, Martin M¨uhlbauer, and Burkhard Schillinger. Energy-dependent neutron imaging with a double crystal monochromator at the antares facility at frm ii. Nuclear Instruments and Methods in Physics Research Section A: Accelerators, Spectrometers, Detectors and Associated Equipment, 605(1):33–35, 2009.
[11] M Strobl, I Manke, N Kardjilov, A Hilger, M Dawson, and J Banhart. Advances in neutron radiography and tomography. Journal of Physics D: Applied Physics, 42(24):243001, 2009.
[12] MB Chadwick, M Herman, P Oblo˘zinsk`y, Michael E Dunn, Y Danon, AC Kahler, Donald L Smith, B Pritychenko, Goran Arbanas, R Arcilla, et al. Endf/b-vii. 1 nuclear data for science and technology: cross sections, covariances, fission product yields and decay data. Nuclear Data Sheets, 112(12):2887–2996, 2011.
[13] http://web.ornl.gov/sci/nuclear_science_technology/nuclear_data/sammy/
[14] Philip G Burke and Keith A Berrington. Atomic and molecular processes: an r-matrix approach. 1993.
[15] N. LARSON, "Updated user's guide for SAMMY: multilevel R-matrix fits to neutron data using Baye's equations." No. ORNL/TM-9179. Oak Ridge National Lab., TN (USA), 1984.
[16] M. MOCKO *et al.*, "Advantages and limitations of nuclear physics experiments at an ISIS-class spallation neutron source." Nuclear Instruments and Methods in Physics Research Section A: Accelerators, Spectrometers, Detectors and Associated Equipment 589.3 (2008): 455-464.
[17] A. Tremsin *et al.*, "High-resolution neutron radiography with microchannel plates: Proof-of-principle experiments at PSI." Nuclear Instruments and Methods in Physics Research Section A: Accelerators, Spectrometers, Detectors and Associated Equipment 605.1 (2009): 103-106.
[18] B. Predel, Editor: O. Madelung, Nd-U (Neodymium-Uranium), Landolt-Börnstein, Physical Chemistry, IV/5H, 1997
[19] Brian J Jaques, Jennifer Watkins, Joseph R Croteau, Gordon A Alanko, Beata Tyburska-Puschel, Mitch Meyer, Peng Xu, Edward J Lahoda, and Darryl P Butt. Synthesis and Sintering of UN-UO_2 fuel composites. Journal of Nuclear Materials, 466:745-754, 2015.

[20] Jason M Harp, Paul A Lessing, and Rita E Hoggan. Uranium silicide pellet fabrication by powder metallurgy for accident tolerant fuel evaluation and irradiation. Journal of Nuclear Materials, 466:728 738, 2015.

[21] KJ McClellan, DD Byler, EP Luther, JT White, and P Medvedev. 5.1 ATF-1 UN-U_3Si_5 Composite Fuel Development and Irradiation Test Design. FY2014 CERAMIC FUELS DEVELOPMENT ANNUAL HIGH- LIGHTS, 2014.

[22] Reeju Pokharel, Jonathan Lind, Anand K Kanjarla, Ricardo A Lebensohn, Shiu Fai Li, Peter Kenesei, Robert M Suter, and Anthony D Rollett. Polycrystal plasticity: comparison between grain-scale observations of deformation and simulations. Annu. Rev. Condens. Matter Phys., 5(1):317-346, 2014.

[23] J Lind, SF Li, R Pokharel, U Lienert, AD Rollett, and RM Suter. Tensile twin nucleation events coupled to neighboring slip observed in three dimensions. Acta Materialia, 76:213-220, 2014.

[24] Donald W Brown, Levente Balogh, Darrin Byler, Chris M Hefferan, James F Hunter, Peter Kenesei, Shiu Fai Li, John Lind, Stephen R Niezgoda, and Robert M Suter. Demonstration of near field high energy x-ray diffraction microscopy on high-z ceramic nuclear fuel material. In Materials Science Forum, volume 777, pages 112{117. Trans Tech Publ, 2014.

[25] R Pokharel, Donald W Brown, Darrin Byler, James F Hunter, and Peter Kenesei. Non-destructive 3d microstructural characterization of as sintered UO_{2+x}. To be submitted to Journal of Nuclear Materials, 2016.

[26] Reeju Pokharel, Jonathan Lind, Shiu Fai Li, Peter Kenesei, Ricardo A Lebensohn, Robert M Suter, and Anthony D Rollett. In-situ observation of bulk 3D grain evolution during plastic deformation in polycrystalline Cu. International Journal of Plasticity, 67:217-234, 2015.

[27] SF Li and RM Suter. Adaptive reconstruction method for three-dimensional orientation imaging. Journal of Applied Crystallography, 46(2):512-524, 2013.

[28] Kockelmann, W., Zhang, S. Y., Kelleher, J. F., Nightingale, J. B., Burca, G., & James, J. A. (2013). IMAT–a new imaging and diffraction instrument at ISIS. Physics Procedia, 43, 100-110.

[29] Toh, Y., Ebihara, M., Kimura, A., Nakamura, S., Harada, H., Hara, K. Y., ... & Furutaka, K. (2014). Synergistic Effect of Combining Two Nondestructive Analytical Methods for Multielemental Analysis. Analytical chemistry, 86(24), 12030-12036.

12. Appendix A: Irradiated Fuel Manipulation Container

A limiting factor for applying these types of characterization to irradiated fuel, is the necessity for shielding and remote alignment capabilities for such samples at the beam line. This proposal addresses this limitation by combining a motion control suitable for neutron/proton imaging & tomography and neutron diffraction with containment designed for irradiated fuel rodlets. Our design concept is shown in Fig. 1.

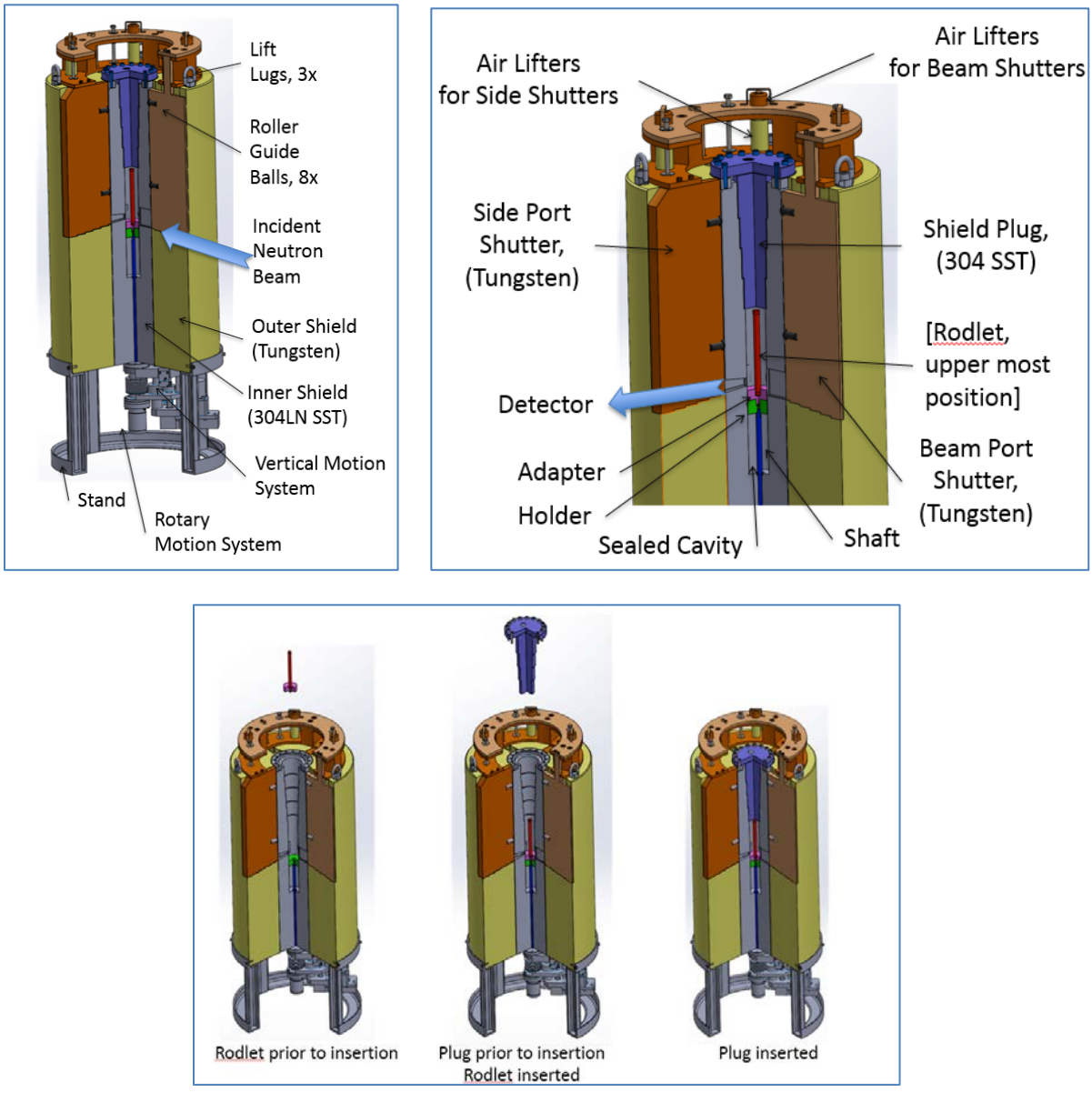

Fig. 1: Irradiated Fuel Manipulation Container for in situ examination (Design concept).

With this container any beam line at any facility capable of accommodating this assembly would be able to contribute to the characterization of irradiated materials. At LANSCE, this would include the imaging beam line on flight path 5 (for tomographic characterization and isotopic densities); the SMARTS engineering diffractometer (e.g. for residual stress measurements or profile analysis to characterize e.g. dislocation densities), the HIPPO general purpose diffractometer (to assess phase composition and texture). Besides

the neutron characterization, LANSCE offers characterization by proton radiography and tomography. With the proposed container/motion control combination, radioactive materials could be transferred between beam lines without exposing personnel to radiation, and then be characterized utilizing the shutters integrated into the container for incident, transmitted, and diffracted beams and the motion control to align, rotate, and scan them in the beam lines.

Existing shielding of experimental hutches would protect personnel when the shutters are open. The integrated rotation and translation of the sample, enabled by remote controlled motors allow one to sample rotation for tomography while probing different sections along the sample axis (e.g. for diffraction probing slices or imaging techniques with smaller field of view than the whole sample). Irradiated rodlets (or other radioactive samples) would be loaded into the container in hot cells available at LANL. The combination of all these techniques would provide unprecedented characterization of e.g. irradiated materials and thus advance the field of nuclear engineering.

13. Appendix B: Detailed Results for all Pellets

In this appendix we list detailed tomography results for each pellet. For each pellet, the following information is provided:

1. A table with nominal phase composition and enrichment level, details of the data acquisition for thermal and epithermal data collection, and a summary of the findings.
2. A table with the ^{235}U enrichment levels as well as ^{238}U and ^{235}U gravimetric densities as derived from the SAMMY refined aerial densities.
3. A table with refined aerial densities for each isotope in the SAMMY fit
4. A graph with the SAMMY fit, showing experimental measured transmission as a function of neutron energy, the difference curve between fit and experimental data, and tick marks for resonance positions.
5. Slices of the tomographic reconstruction from thermal and epithermal data
6. Slices of the tomographic reconstruction for ^{238}U and ^{235}U densities

We propose this as a standard format for data sets describing pellets and have created a database with web interface for easy access to this data. We are engaging in discussion with collaborators in fuel synthesis as well as in modelling to optimize the data collected.

Pellet #1 Rodlet #1

Composition	UN (15 vol% U3Si5)
Enrichment	^{235}U in UN: 2.7 wt%; ^{235}U in U_3Si_5: 2.7 wt%
Pellet #	1
Rodlet #	1
Measurement date	10/23/2015
Background stabilization	1mm Cd sheet on collimator
Projections #	51
Time/ projection	45 mins
Angular separation	3.6 degrees
L/D	100
Source to detector	8.36 m
Summary	No features > xmm No density ^{238}U variation noted to 2.3% [SAMMY analysis showed background dependent anomaly at boundary of detector quadrants]

SAMMY Fit

^{235}U enrichment	2.27 wt%
^{238}U density	11.854 g/cc
^{235}U density	0.254 g /cc

ISOTOPE	MOLAR MASS	AREAL DENSITY [ATOMS/BARN]	AREAL DENSITY REL. ERROR
^{238}U	238.051	2.35E-02	0.61%
^{235}U	235.044	5.47E-04	1.73%
^{184}W	183.951	2.24E-05	6.60%
^{186}W	185.954	1.73E-06	5.71%

Pellet 1 Rodlet 1

Fitted energy profile of pellet 1 from detector area indicated above:

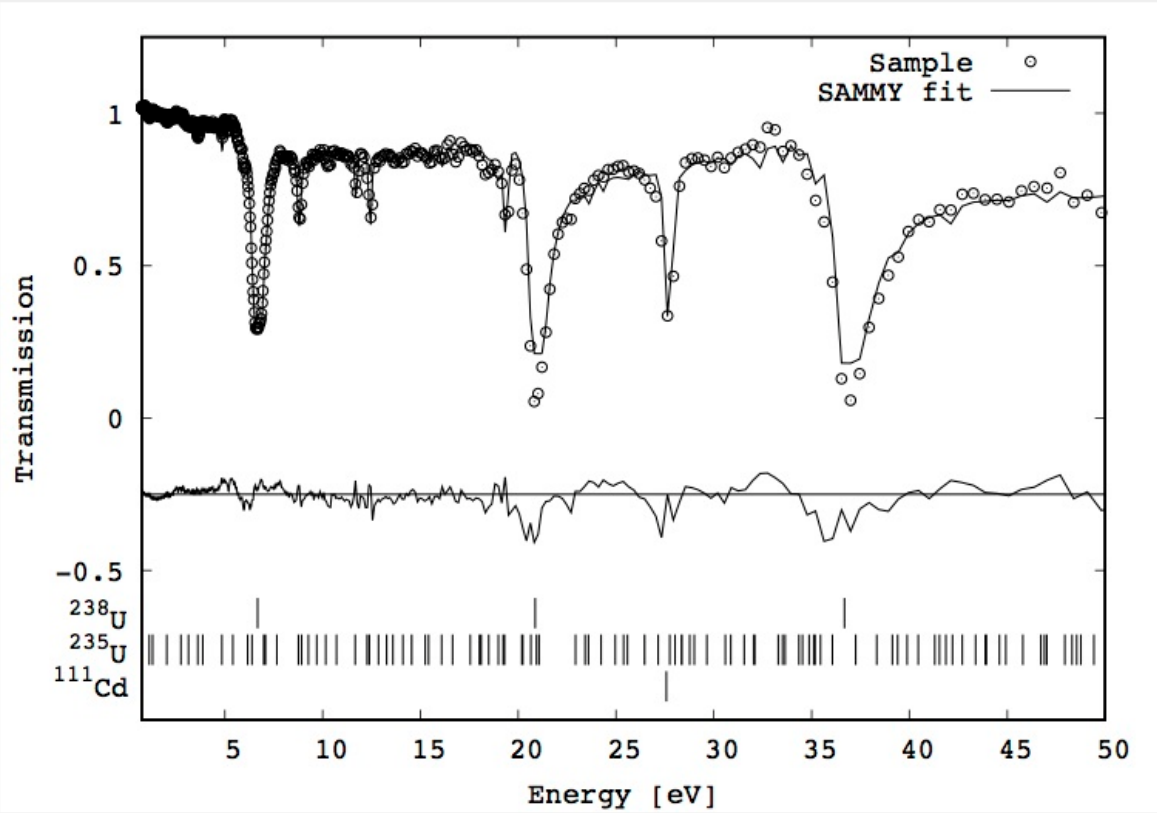

Example fit to normalized experimental data (45min acquisition) of pellet 1. Dots are measured transmission intensities. The curve through the data is the fit. Thedifference curve (experimental data subtracted from fit) shown below. Tick marks indicate positions of ^{238}U, ^{235}U and ^{111}Cd resonances.

Pellet 1 Rodlet 1

Tomographic reconstructions (slicing in 0.6mm steps along cylinder axis):

Thermal reconstruction (1meV-1eV)

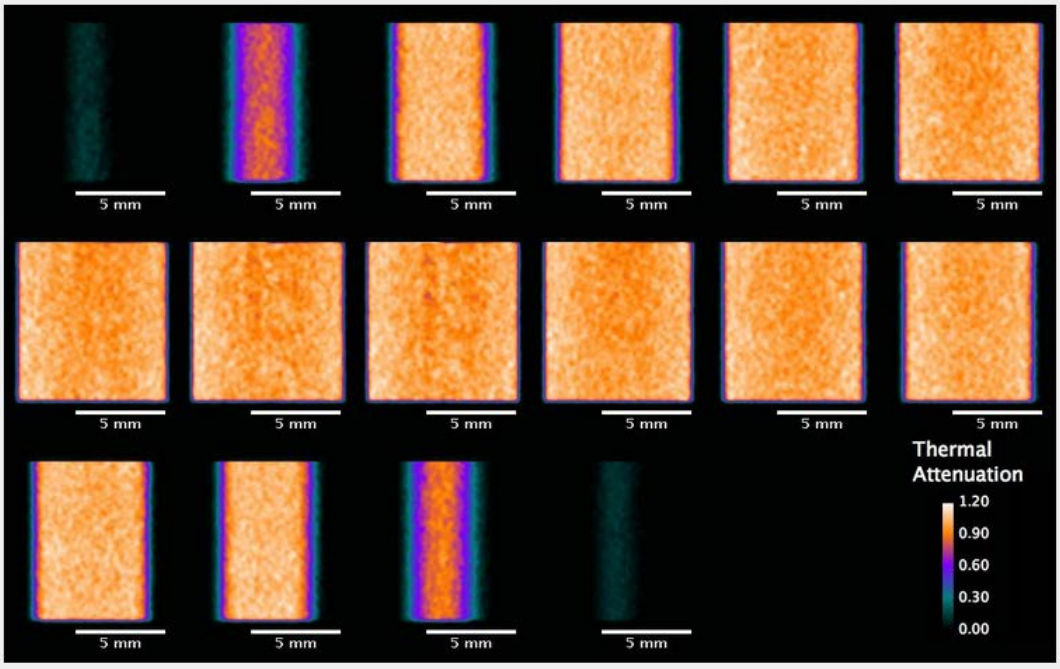

Epithermal reconstruction (1eV-200eV)

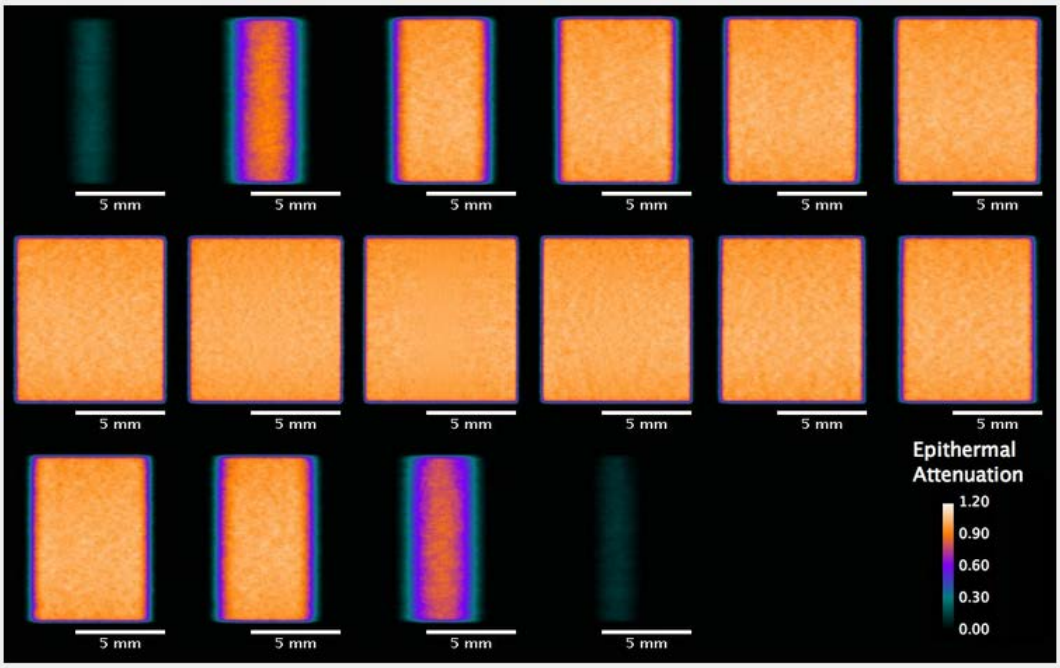

Pellet 1 Rodlet 1

^{238}U reconstruction

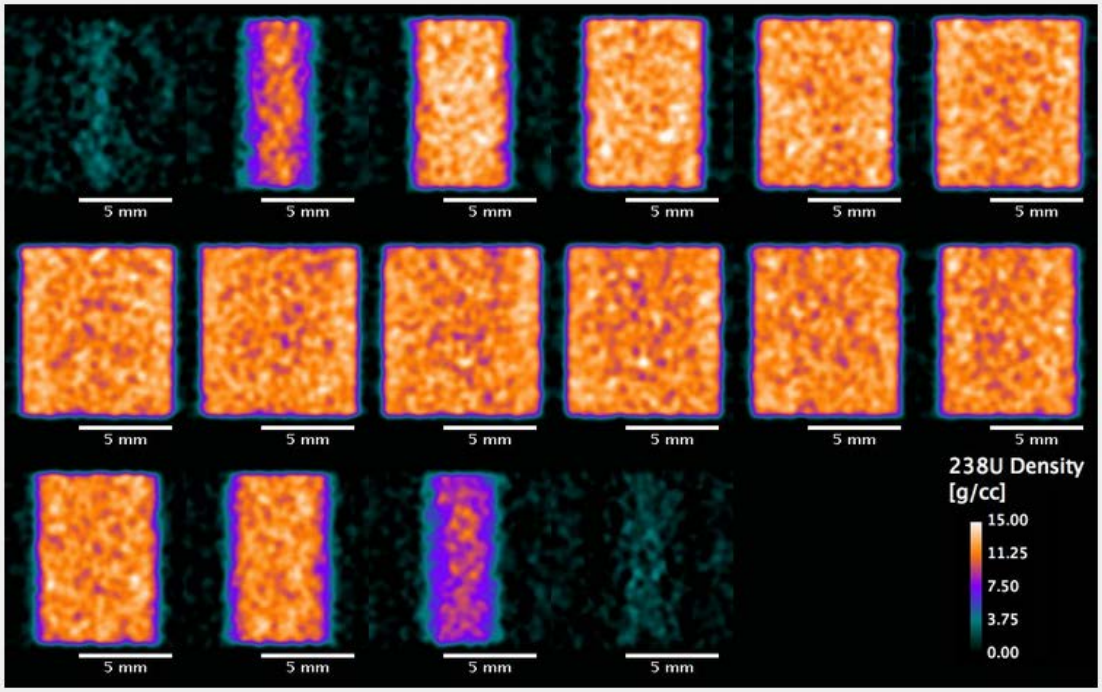

^{235}U reconstruction

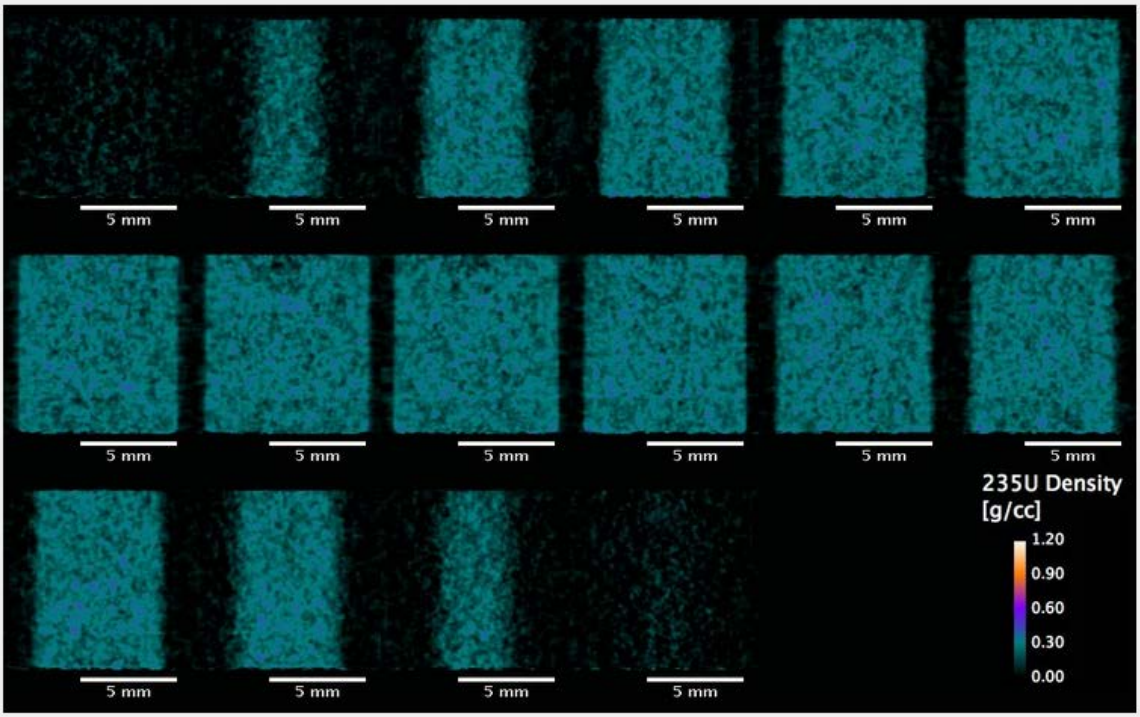

Pellet #2 Rodlet #1

Composition	U3Si5
Enrichment	8.84 wt% ^{235}U in U_3Si_5
Pellet #	2
Rodlet #	1
Epithermal measurement	10/23/2015
Background stabilization	1mm Cd sheet on collimator
Projections #	51
Time/ projection	45 mins
Angular separation	3.6 degrees
L/D	100
Source to detector	8.36 m
Thermal measurement	02/26/2016
Background stabilization	0.1mm Ta (mounted on detector)
Projections #	101
Time/ projection	5 mins
Angular separation	1.8
L/D	100
Source to detector	8.36 m
Summary	No visible features in thermal or epithermal reconstruction of the pellet ^{235}U Density variation along the cylinder axis of the pellet within 6.5% ^{238}U Density variation along the cylinder axis of the pellet within 2.2%

SAMMY Fit

^{235}U enrichment	6.97 wt%
^{238}U density	7.199 g/cc
^{235}U density	0.494 g /cc

ISOTOPE	MOLAR MASS	AREAL DENSITY [ATOMS/BARN]	AREAL DENSITY REL. ERROR
^{238}U	238.051	1.46E-02	0.98%
^{235}U	235.044	1.10E-03	1.20%
^{184}W	183.951	2.69E-05	5.66%
^{186}W	185.954	3.75E-06	3.38%

Pellet #2 Rodlet #1

SAMMY fit

Fitted energy profile of pellet 2 from detector area indicated above:

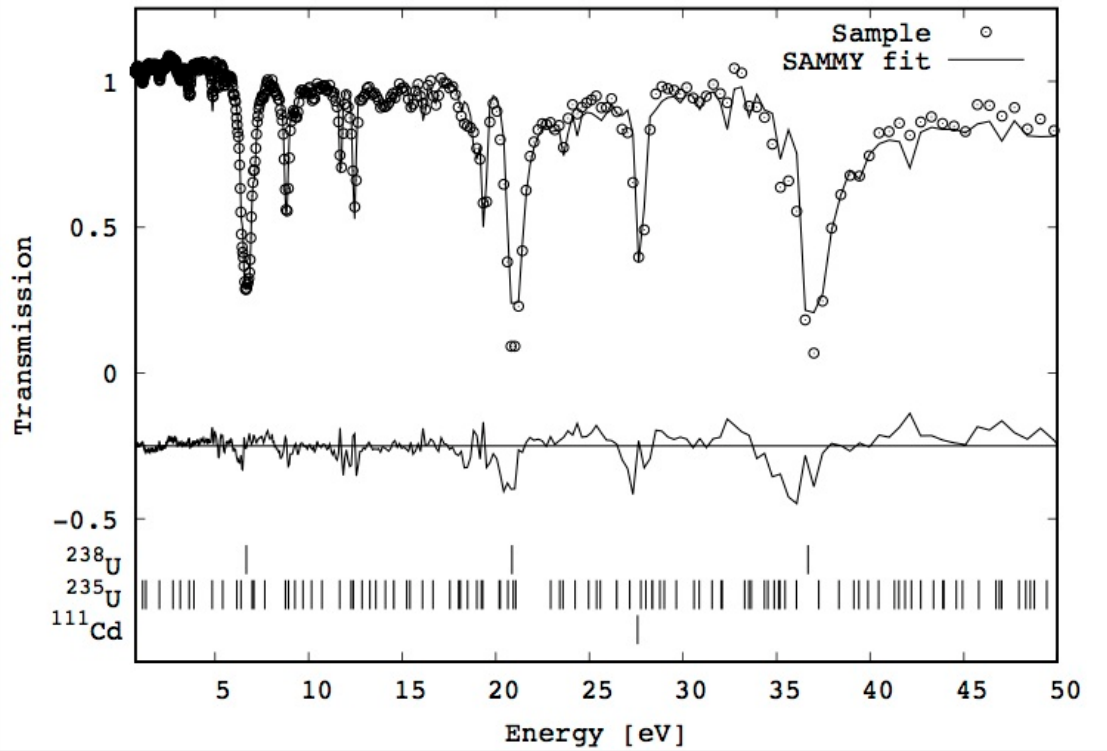

Example fit to normalized experimental data (45min acquisition) of pellet 2. Dots are measured transmission intensities. The curve through the data is the fit. Thedifference curve (experimental data subtracted from fit) shown below. Tick marks indicate positions of ^{238}U, ^{235}U and ^{111}Cd resonances.

Pellet #2 Rodlet #1

Tomographic reconstructions (slicing in 0.6mm steps along cylinder axis):

Thermal reconstruction (1meV-1eV)

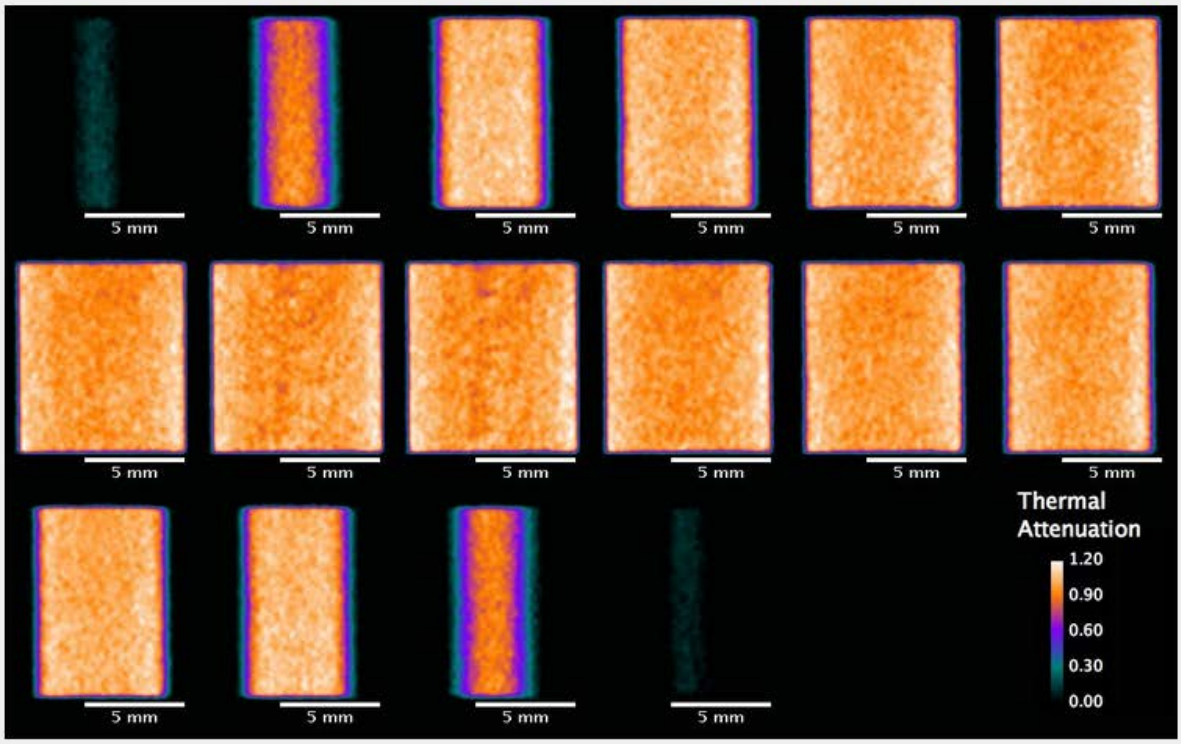

Epithermal reconstruction (1eV-200eV)

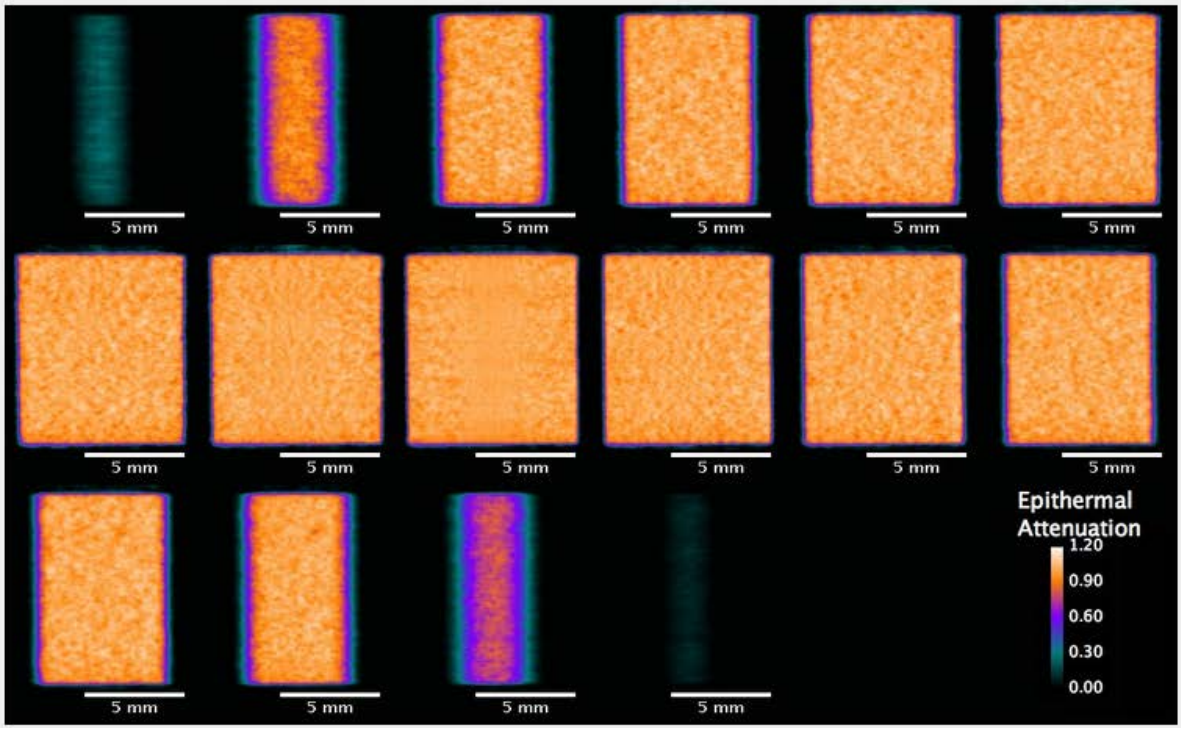

Pellet #2 Rodlet #1

^{238}U reconstruction

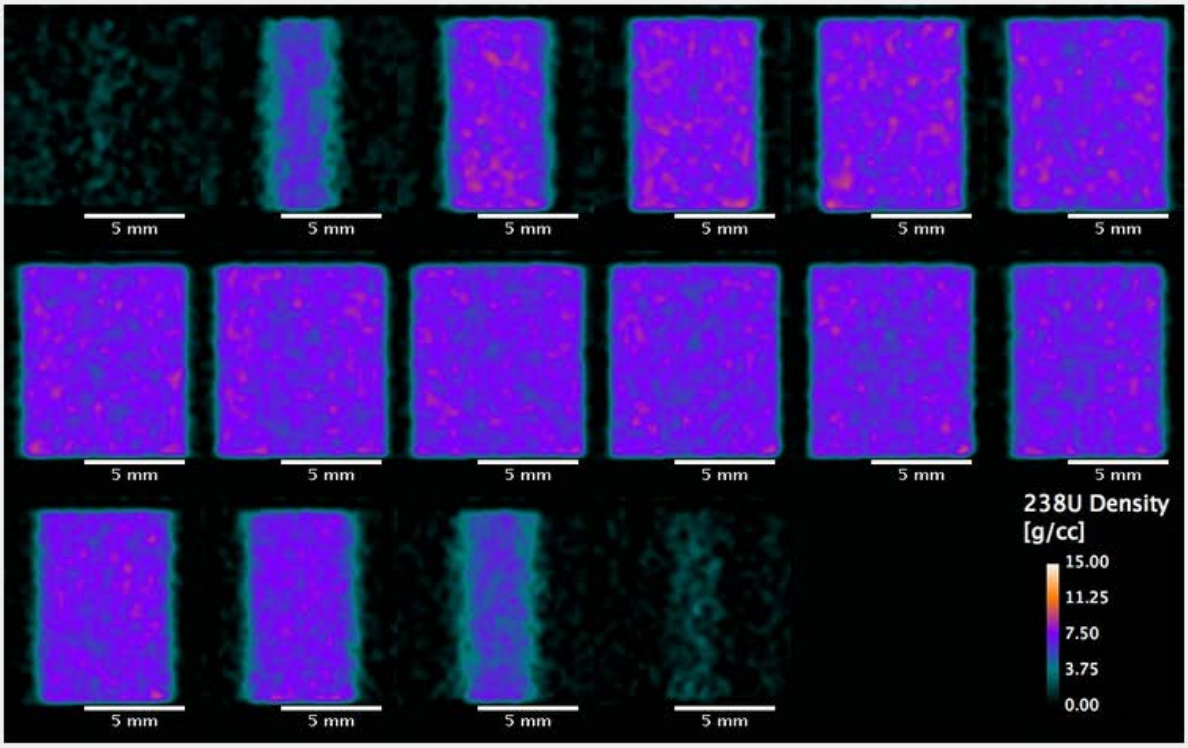

^{235}U reconstruction

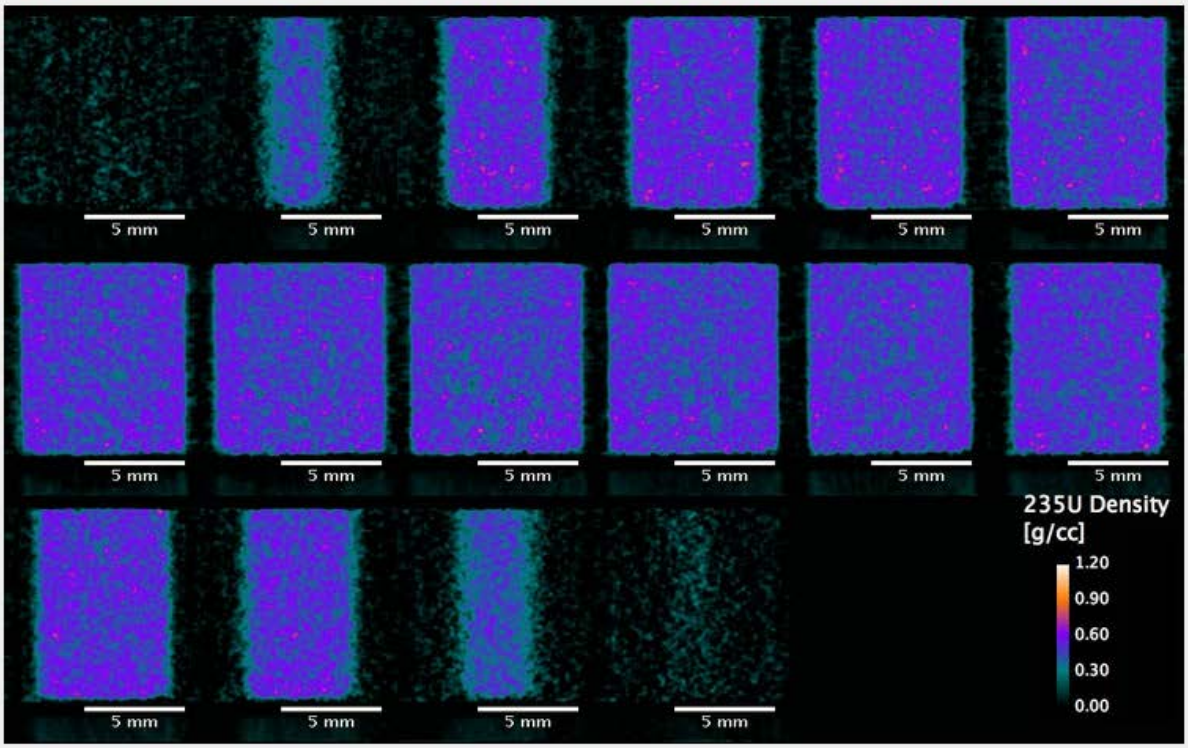

Pellet #3 Rodlet #1

Composition	U3Si5
Enrichment	0.2 wt% ^{235}U in U3Si5
Pellet #	3
Rodlet #	1
Epithermal measurement	10/23/2015 (top 1mm only)
Background stabilization	1mm Cd sheet on collimator
Projections #	51
Time/ projection	45 mins
Angular separation	3.6 degrees
L/D	100
Source to detector	8.36 m
Thermal measurement	02/26/2016
Background stabilization	0.1mm Ta (mounted on detector)
Projections #	101
Time/ projection	5 mins
Angular separation	1.8
L/D	100
Source to detector	8.36 m
Summary	End cap but no other features in thermal or epithermal reconstruction ^{235}U Density variation along the cylinder axis of the pellet within NA% ^{238}U Density variation along the cylinder axis of the pellet within NA%

SAMMY Fit

^{235}U enrichment	0.14 wt%
^{238}U density	7.066 g/cc
^{235}U density	0.058 g/cc

PARAMETER	ISOTOPE	MOLAR MASS	AREAL DENSITY [ATOMS/BARN]	AREAL DENSITY REL. ERROR
1	238U	238.051	1.58E-02	0.95%
3	235U	235.044	2.21E-05	9.58%
9	186W	185.954	1.55E-06	5.79%

Pellet #3 Rodlet #1

SAMMY fit

Fitted energy profile of pellet 3 from detector area indicated above:

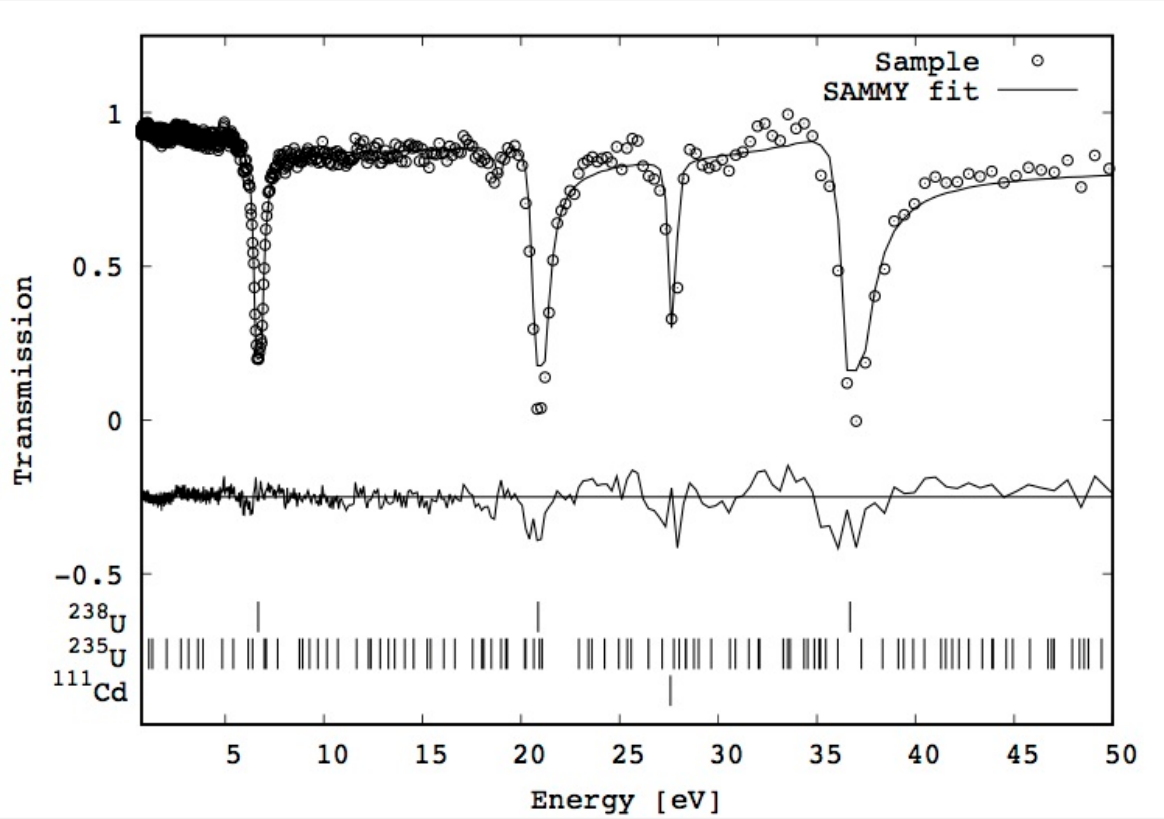

Example fit to normalized experimental data (45min acquisition) of pellet 3. Dots are measured transmission intensities. The curve through the data is the fit. Thedifference curve (experimental data subtracted from fit) shown below. Tick marks indicate positions of ^{238}U, ^{235}U and ^{111}Cd resonances.

Pellet #3 Rodlet #1

Tomographic reconstructions (slicing in 0.6mm steps along cylinder axis):

Thermal reconstruction (1meV-1eV)

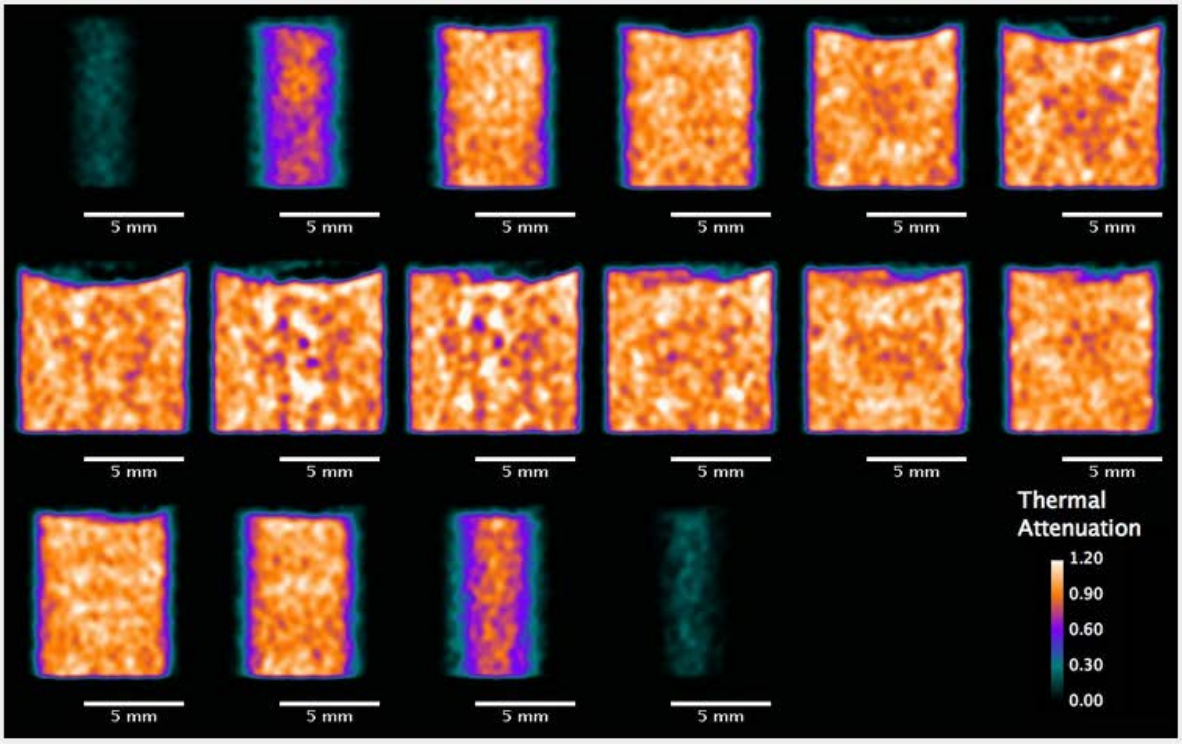

Epithermal reconstruction (1eV-200eV)

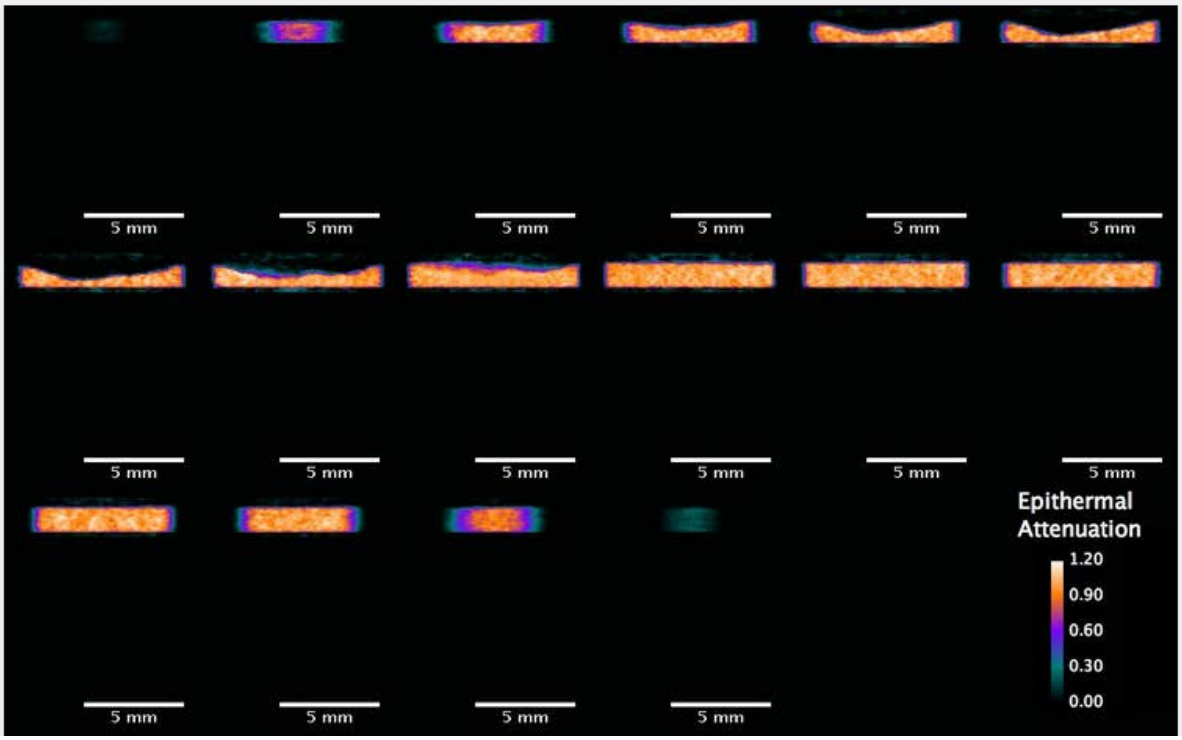

Pellet #3 Rodlet #1

^{238}U reconstruction

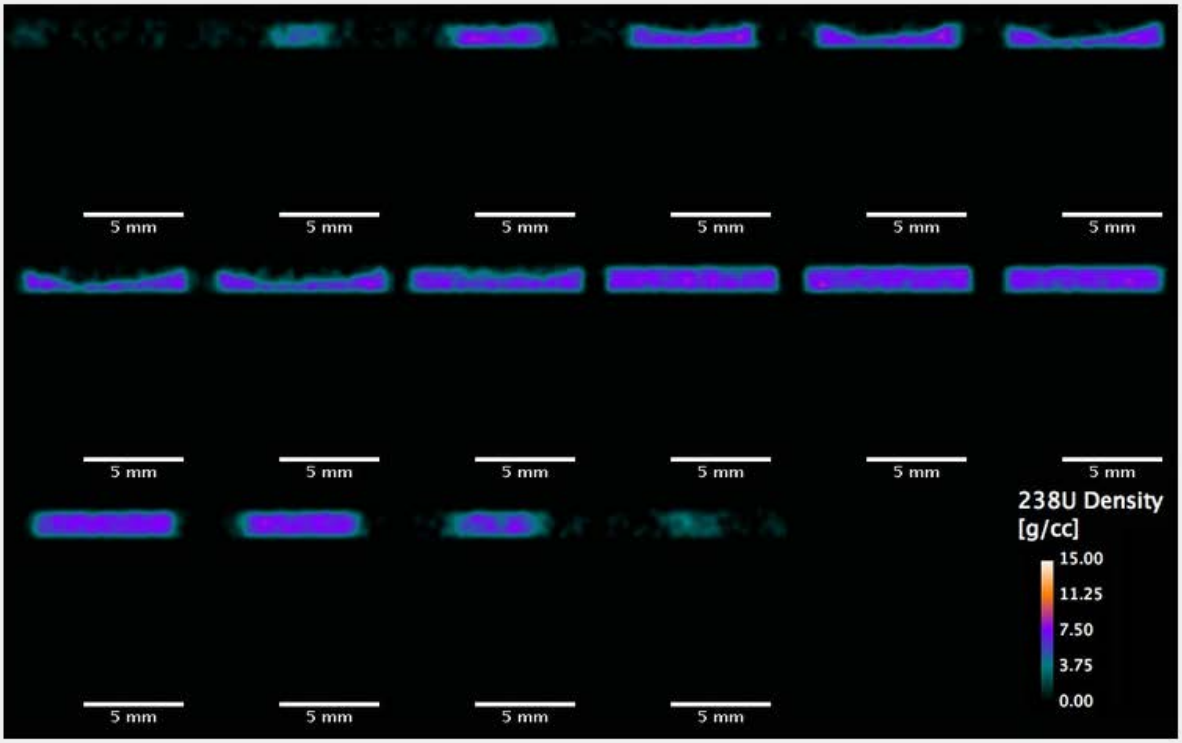

^{235}U reconstruction

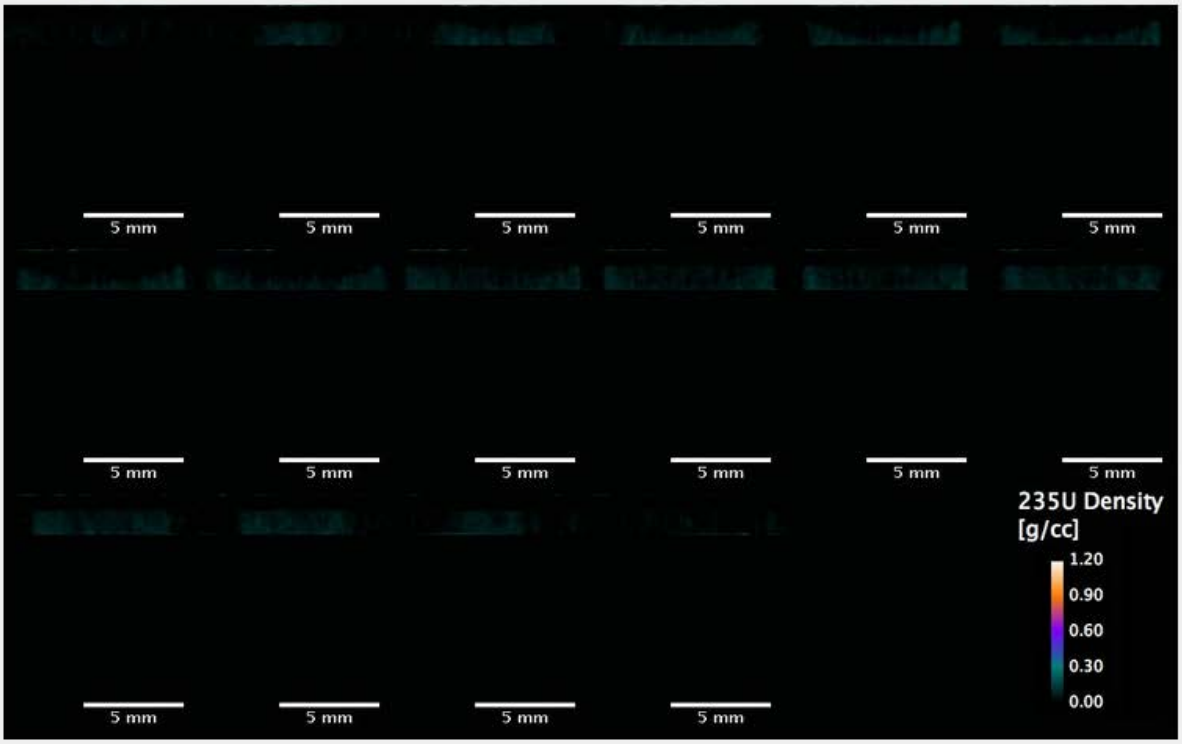

Pellet #4 Rodlet #2

Composition	UN (30 wt% U3Si2)
Enrichment	^{235}U in UN: 4.1 wt%; ^{235}U in U_3Si_2: 4.9 wt%
Pellet #	4
Rodlet #	2
Epithermal measurement	10/23/2015 (top 1mm only)
Background stabilization	1mm Cd sheet on collimator
Projections #	51
Time/ projection	45 mins
Angular separation	3.6 degrees
L/D	100
Source to detector	8.36 m
Thermal measurement	02/26/2016
Background stabilization	0.1mm Ta (mounted on detector)
Projections #	101
Time/ projection	5 mins
Angular separation	1.8
L/D	100
Source to detector	8.36 m
Summary	Visible end-capping and non-visible crack in pellet resolved in all reconstructions ^{235}U Density variation along the cylinder axis of the pellet within 10.25% Increase in ^{235}U density at the bottom of the pellet likely background induced ^{38}U Density variation along the cylinder axis of the pellet within 3.1%

SAMMY Fit

^{235}U enrichment	3.72 wt%
^{238}U density	11.460 g/cc
^{235}U density	0.351 g/cc

ISOTOPE	MOLAR MASS	AREAL DENSITY [ATOMS/BARN]	AREAL DENSITY REL. ERROR
^{238}U	238.051	2.36E-02	0.90%
^{235}U	235.044	9.13E-04	1.27%
^{184}W	183.951	3.61E-05	4.27%
^{186}W	185.954	3.11E-06	3.88%

Pellet #4 Rodlet #2

SAMMY fit

Fitted energy profile of pellet 4 from detector area indicated above:

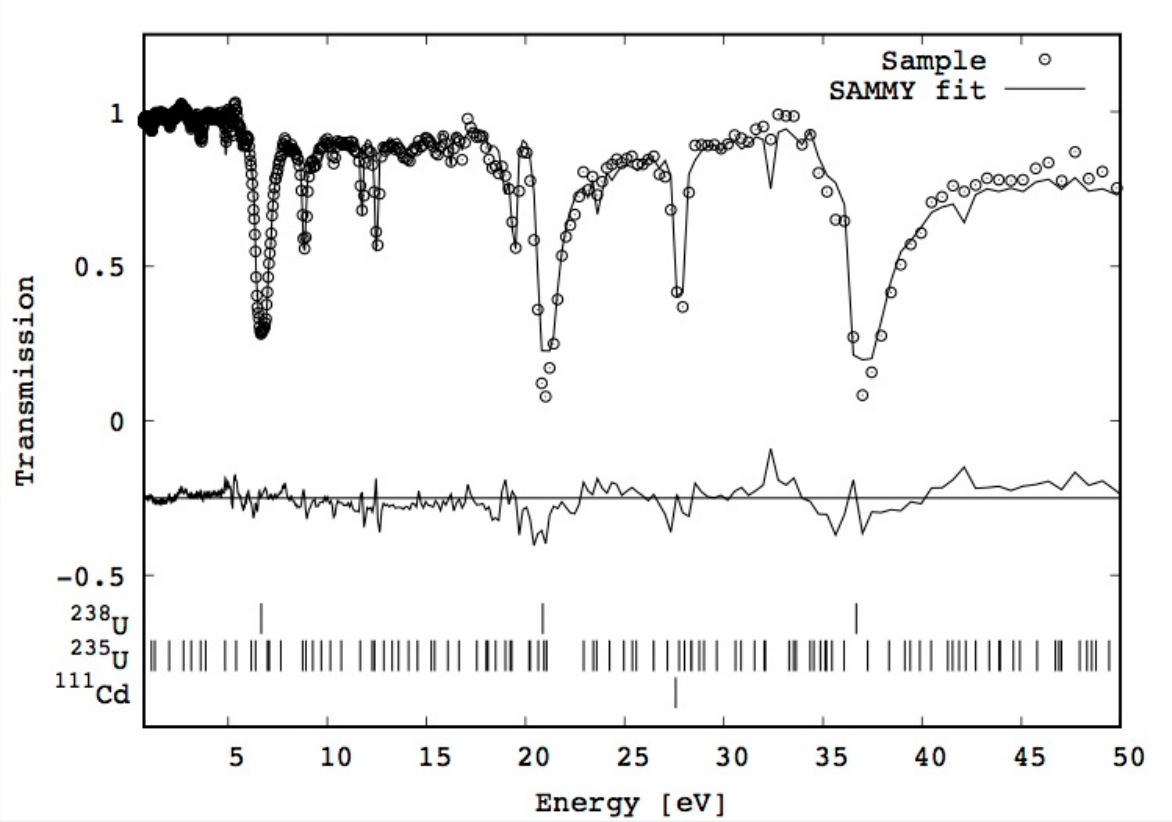

Example fit to normalized experimental data (45min acquisition) of pellet 4. Dots are measured transmission intensities. The curve through the data is the fit. Thedifference curve (experimental data subtracted from fit) shown below. Tick marks indicate positions of ^{238}U, ^{235}U and ^{111}Cd resonances.

Pellet #4 Rodlet #2

Tomographic reconstructions (slicing in 0.6mm steps along cylinder axis):

Thermal reconstruction (1meV-1eV)

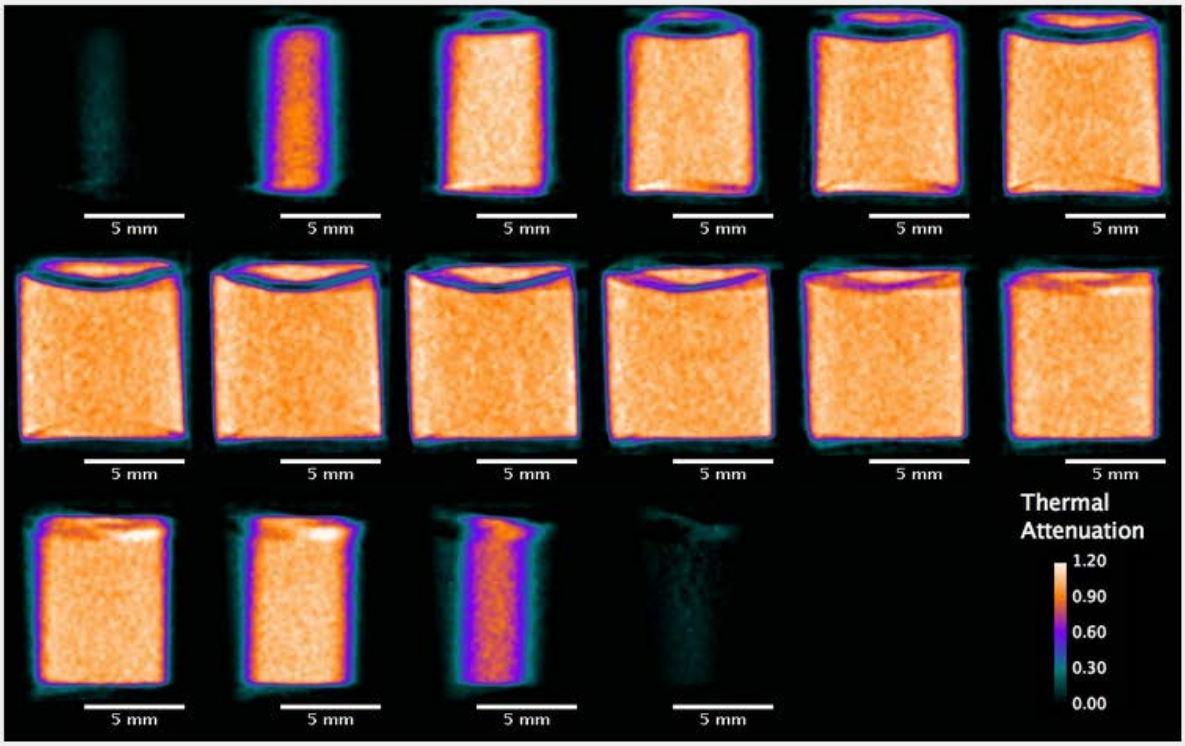

Epithermal reconstruction (1eV-200eV)

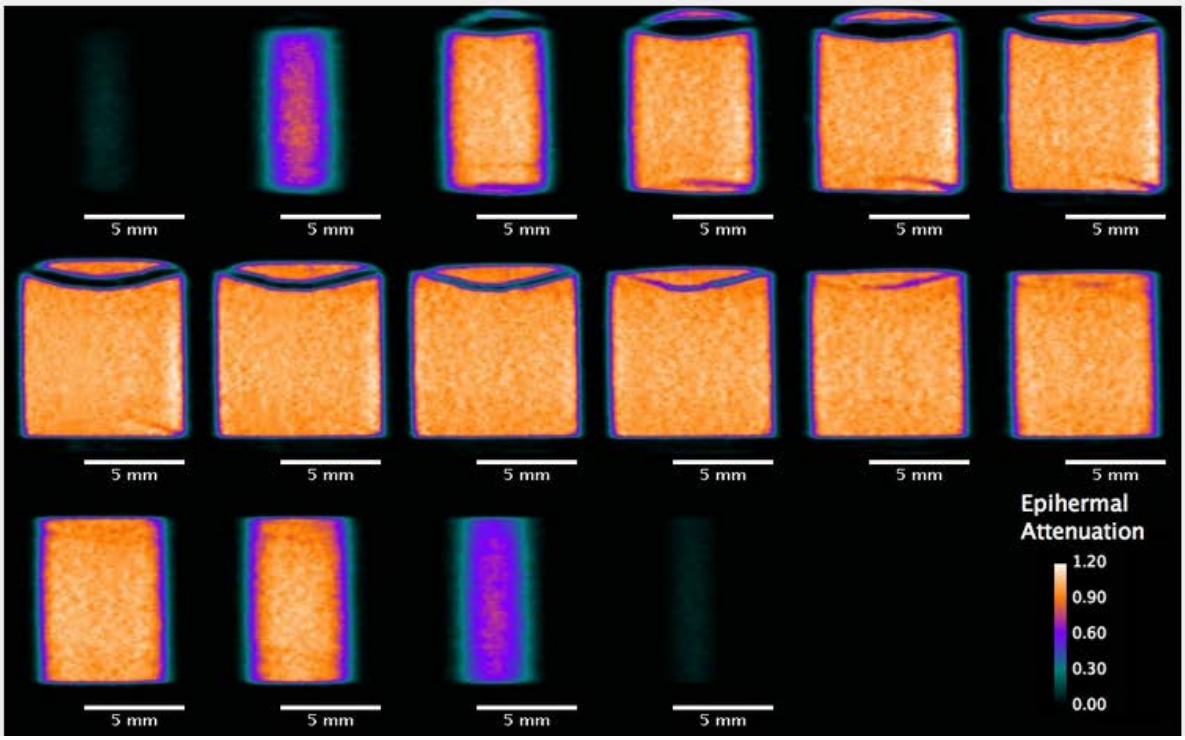

Pellet #4 Rodlet #2

^{238}U reconstruction

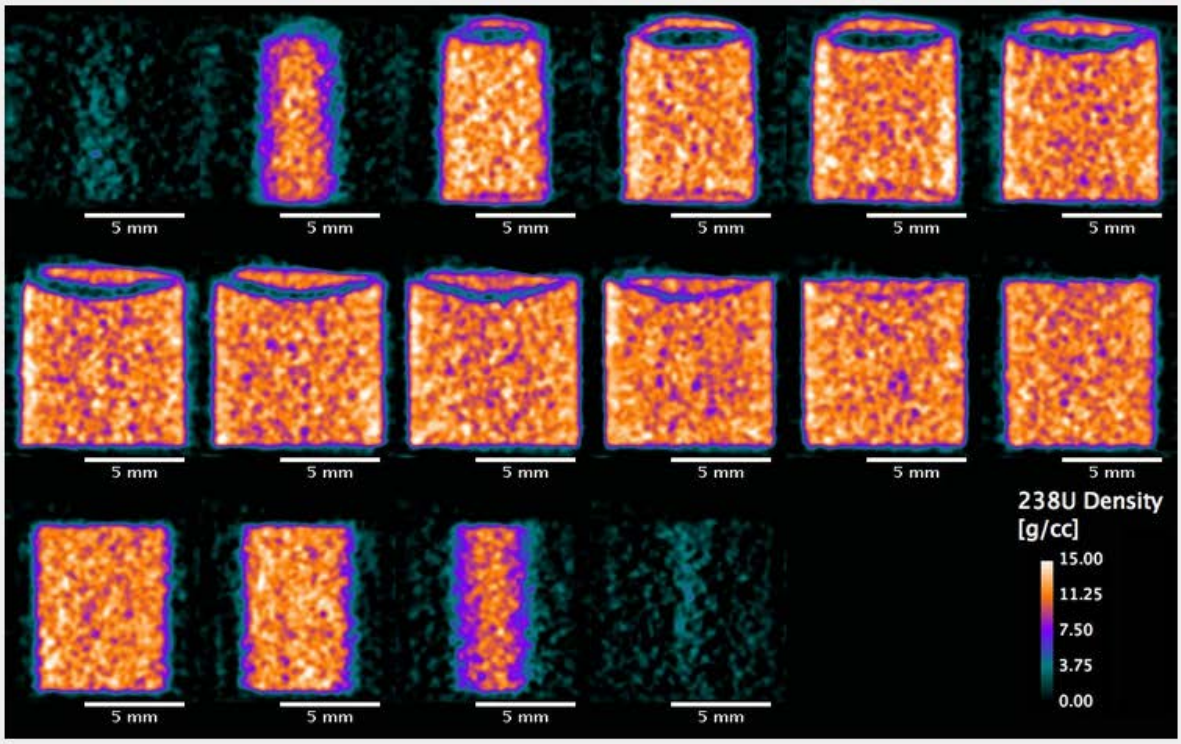

^{235}U reconstruction

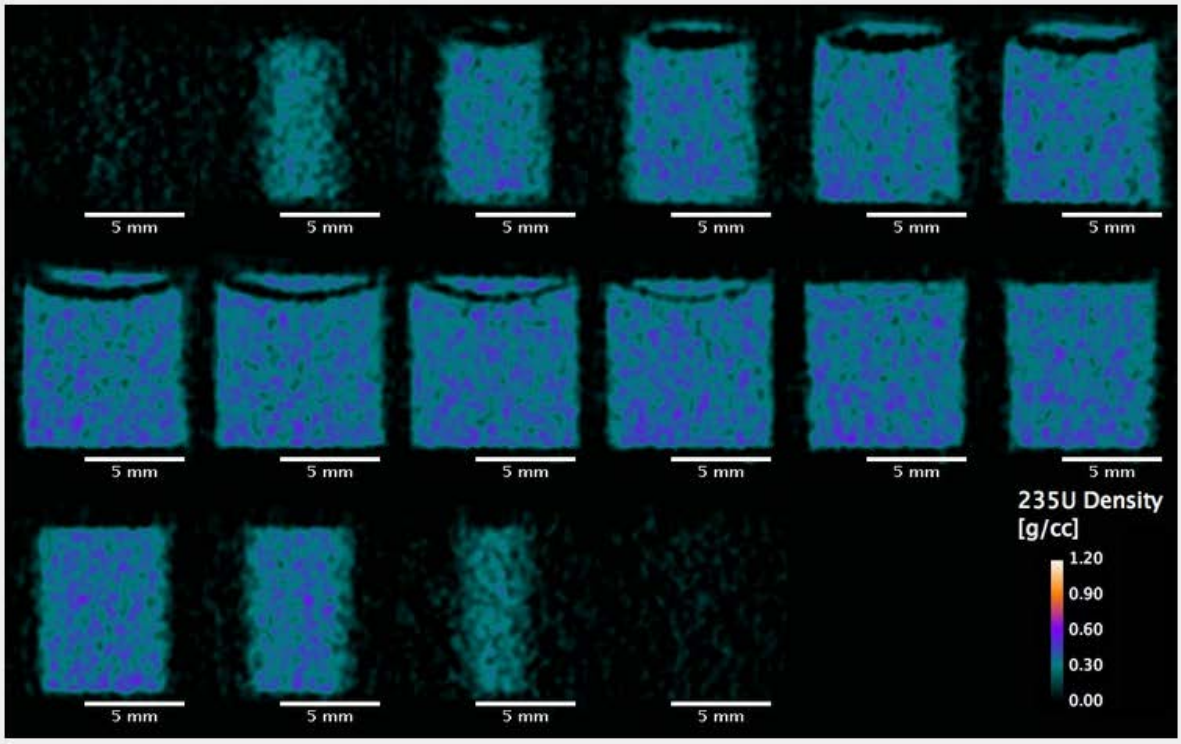

Pellet #5 Rodlet #2

Composition	UN (30 wt% U3Si2)
Enrichment	^{235}U in UN: 4.1 wt%; ^{235}U in U_3Si_2: 4.9 wt%
Pellet #	5
Rodlet #	2
Epithermal measurement	10/23/2015 (top 1mm only)
Background stabilization	1mm Cd sheet on collimator
Projections #	51
Time/ projection	45 mins
Angular separation	3.6 degrees
L/D	100
Source to detector	8.36 m
Thermal measurement	02/26/2016
Background stabilization	0.1mm Ta (mounted on detector)
Projections #	101
Time/ projection	5 mins
Angular separation	1.8
L/D	100
Source to detector	8.36 m
Summary	End-cap ^{235}U Density variation along the cylinder axis of the pellet within 21.9% Increase in ^{235}U density at the bottom of the pellet likely background induced ^{238}U Density variation along the cylinder axis of the pellet within 5.0%

SAMMY Fit

^{235}U enrichment	3.79 wt%
^{238}U density	11.596 g/cc
^{235}U density	0.361 g/cc

ISOTOPE	MOLAR MASS	AREAL DENSITY [ATOMS/BARN]	AREAL DENSITY REL. ERROR
^{238}U	238.051	2.35E-02	0.95%
^{235}U	235.044	9.25E-04	1.34%
^{184}W	183.951	3.32E-05	4.66%
^{186}W	185.954	3.14E-06	4.06%

Pellet #5 Rodlet #2

SAMMY fit

Fitted energy profile of pellet 5 from detector area indicated above:

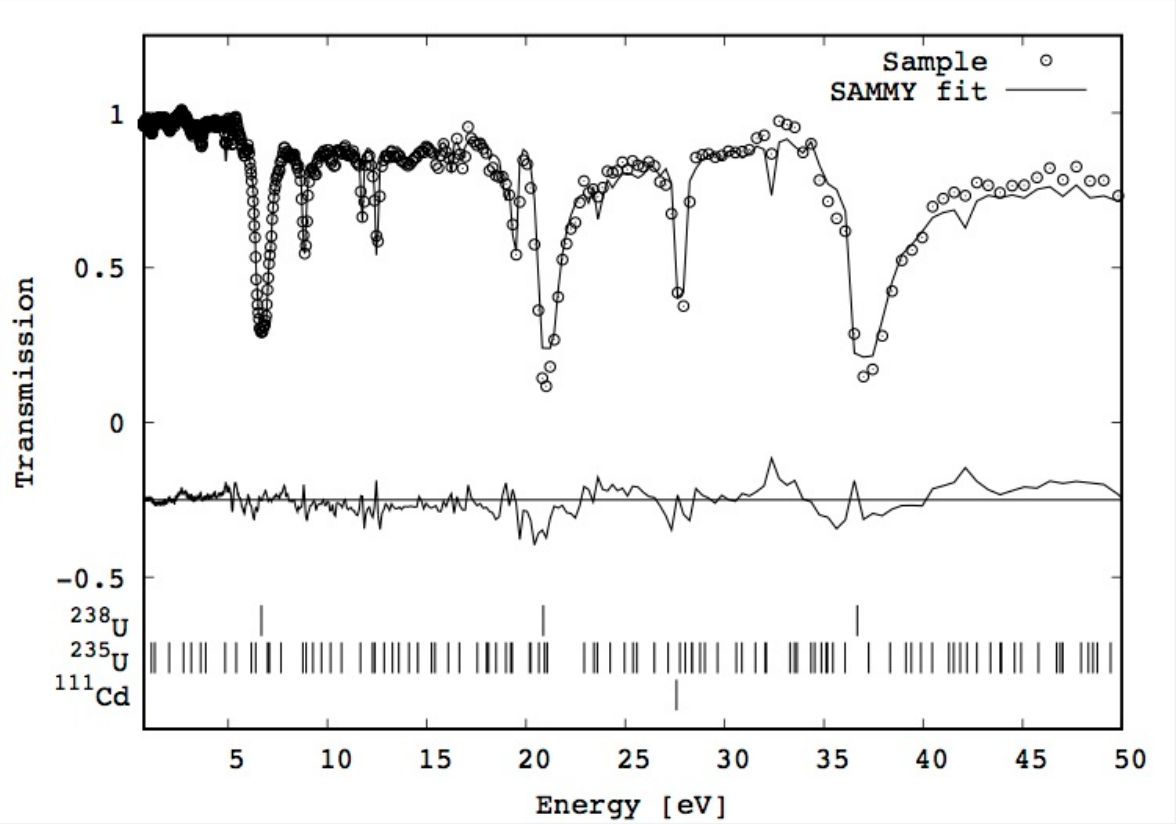

Example fit to normalized experimental data (45min acquisition) of pellet 5. Dots are measured transmission intensities. The curve through the data is the fit. Thedifference curve (experimental data subtracted from fit) shown below. Tick marks indicate positions of ^{238}U, ^{235}U and ^{111}Cd resonances.

Pellet #5 Rodlet #2

Tomographic reconstructions (slicing in 0.6mm steps along cylinder axis):

Thermal reconstruction (1meV-1eV)

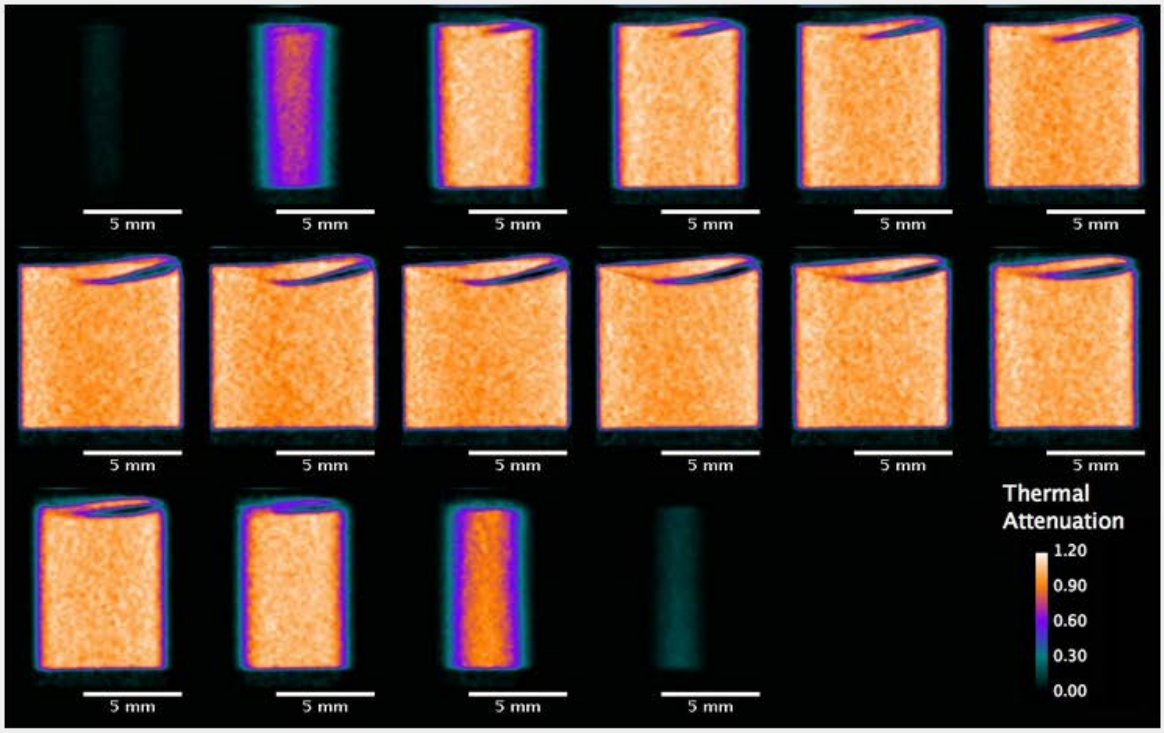

Epithermal reconstruction (1eV-200eV)

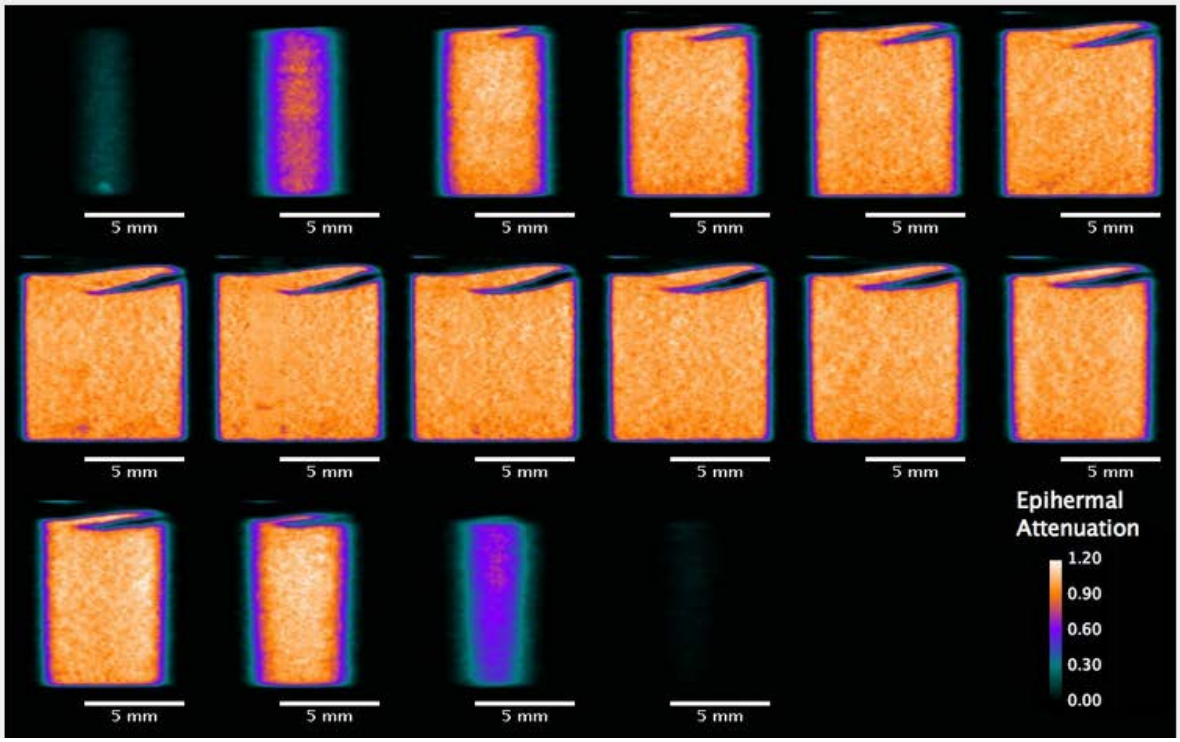

Pellet #5 Rodlet #2

^{238}U reconstruction

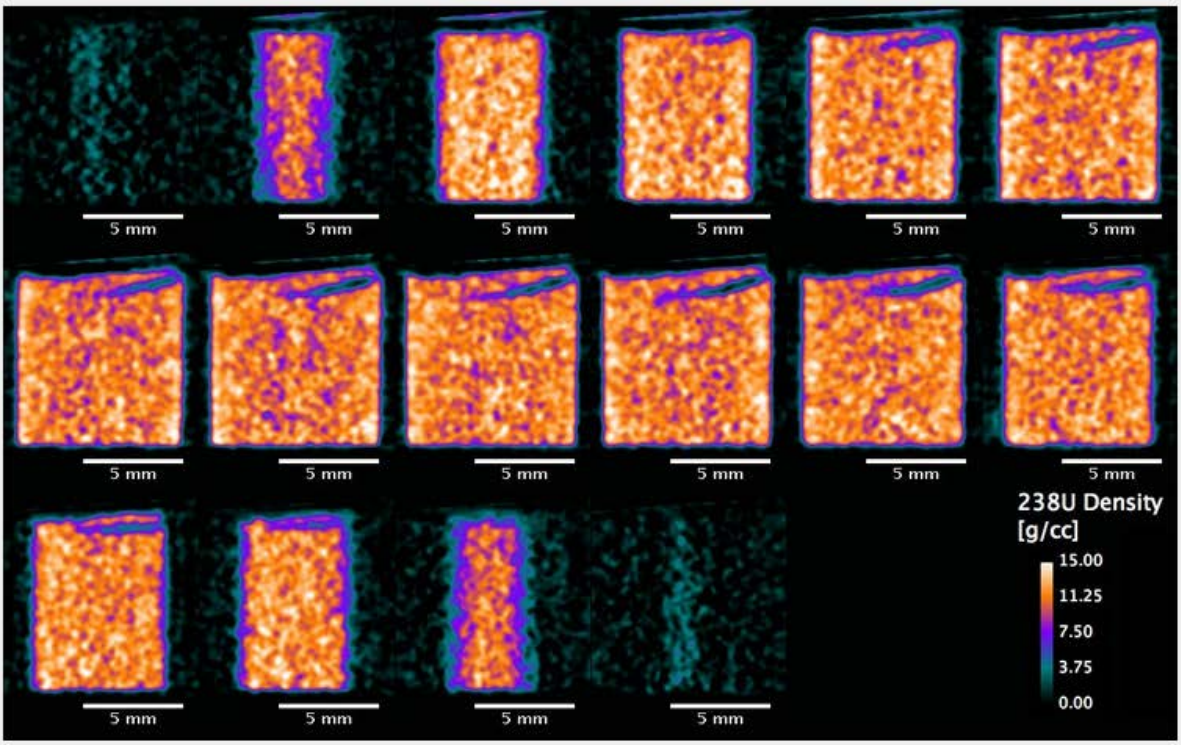

^{235}U reconstruction

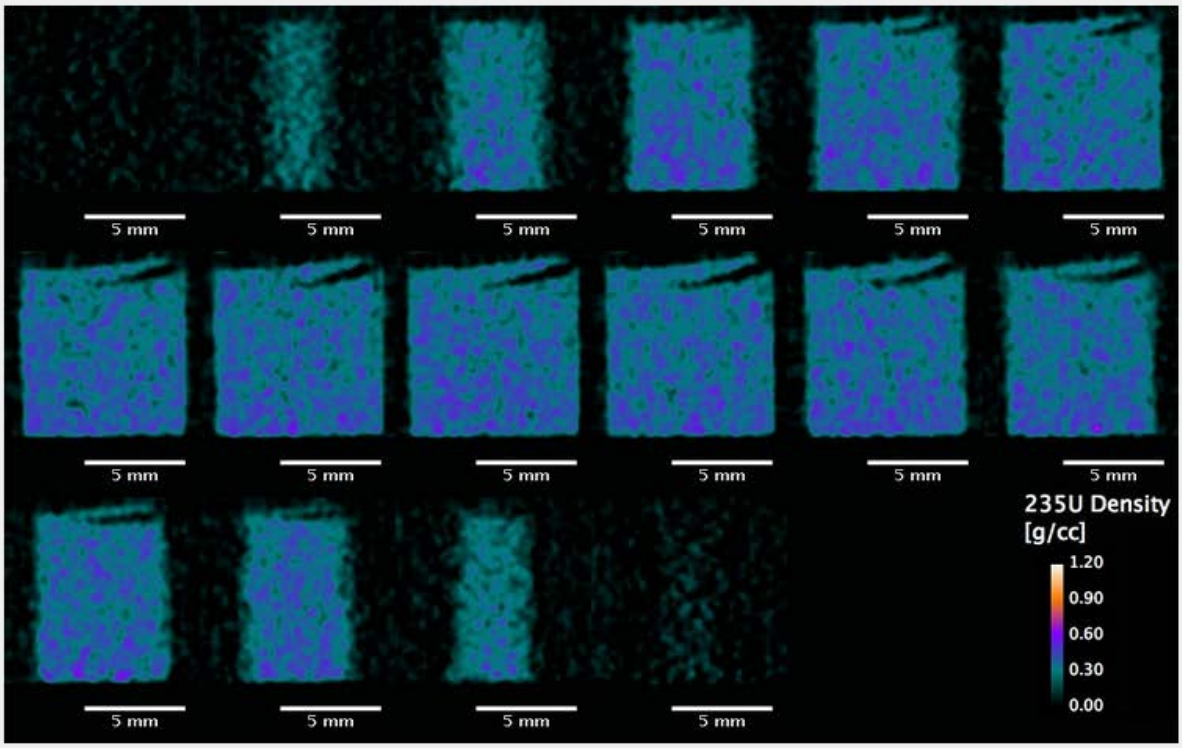

Pellet # 6 Rodlet # 4

Composition	U3Si5
Enrichment	^{235}U in U3Si5 8.84 wt%
Pellet #	6
Rodlet #	4
Epithermal measurement	01/22/2016
Background stabilization	1mm Cd sheet on collimator 0.1mm Ta mounted on detector
Projections #	52
Time/ projection	60
Angular separation	3.6 degrees
L/D	100
Source to detector	8.36 m
Thermal measurement	02/26/2016
Background stabilization	0.1mm Ta (mounted on detector)
Projections #	101
Time/ projection	5 mins
Angular separation	1.8
L/D	100
Source to detector	8.36 m
Summary	Endcap ^{235}U Density variation along the cylinder axis of the pellet within 2% ^{238}U Density variation along the cylinder axis of the pellet within 1%

SAMMY Fit

^{235}U enrichment	8.68 wt%
^{238}U density	7.197 g/cc
^{235}U density	0.625 g/cc

ISOTOPE	MOLAR MASS	AREAL DENSITY [ATOMS/BARN]	AREAL DENSITY REL. ERROR
^{238}U	238.051	1.25E-02	0.44%
^{235}U	235.044	1.19E-03	0.82%
^{234}U	234.041	6.44E-07	9.62%
^{186}W	185.954	1.31E-06	6.42%
^{181}Ta	180.94	3.29E-04	0.64%

Pellet # 6 Rodlet # 4

SAMMY fit

Fitted energy profile of pellet 6 from detector area indicated above:

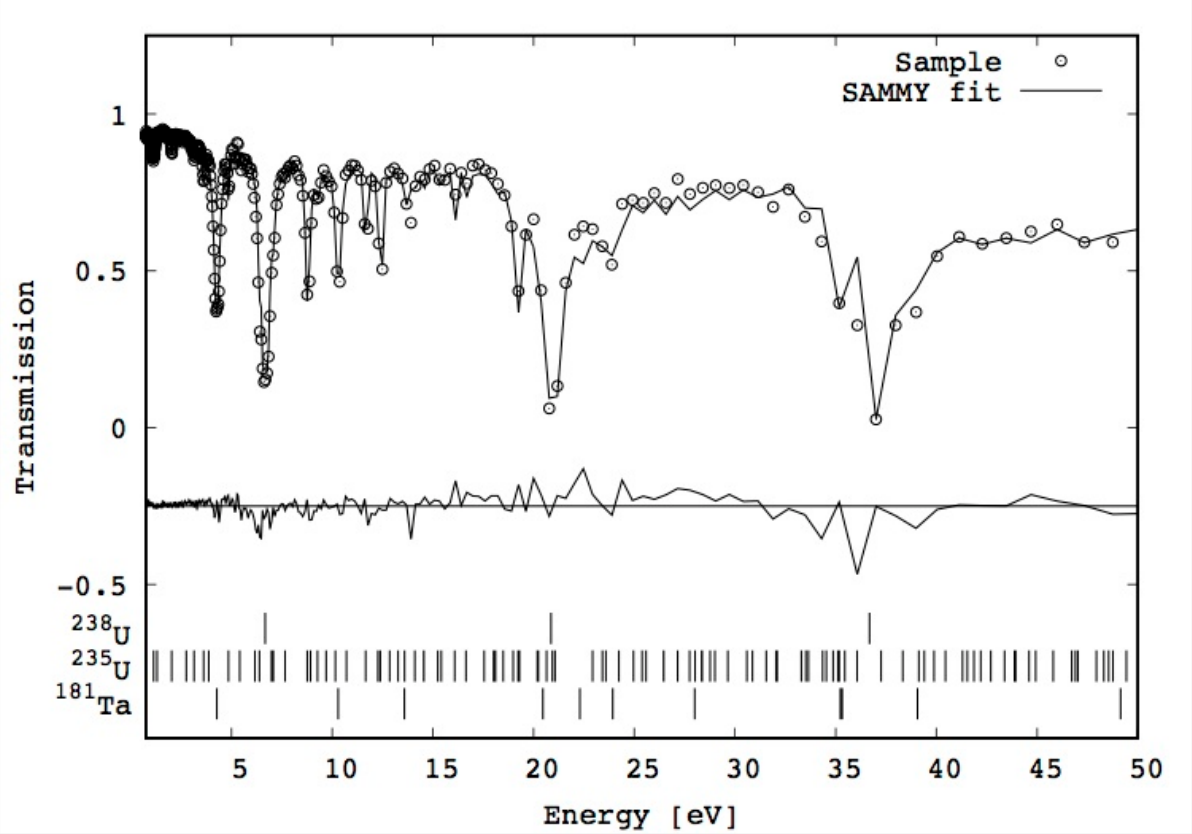

Example fit to normalized experimental data (60min acquisition) of pellet 6. Dots are measured transmission intensities. The curve through the data is the fit. Thedifference curve (experimental data subtracted from fit) shown below. Tick marks indicate positions of ^{238}U, ^{235}U and ^{181}Ta resonances.

Pellet # 6 Rodlet # 4

Tomographic reconstructions (slicing in 0.6mm steps along cylinder axis):

Thermal reconstruction (1meV-1eV)

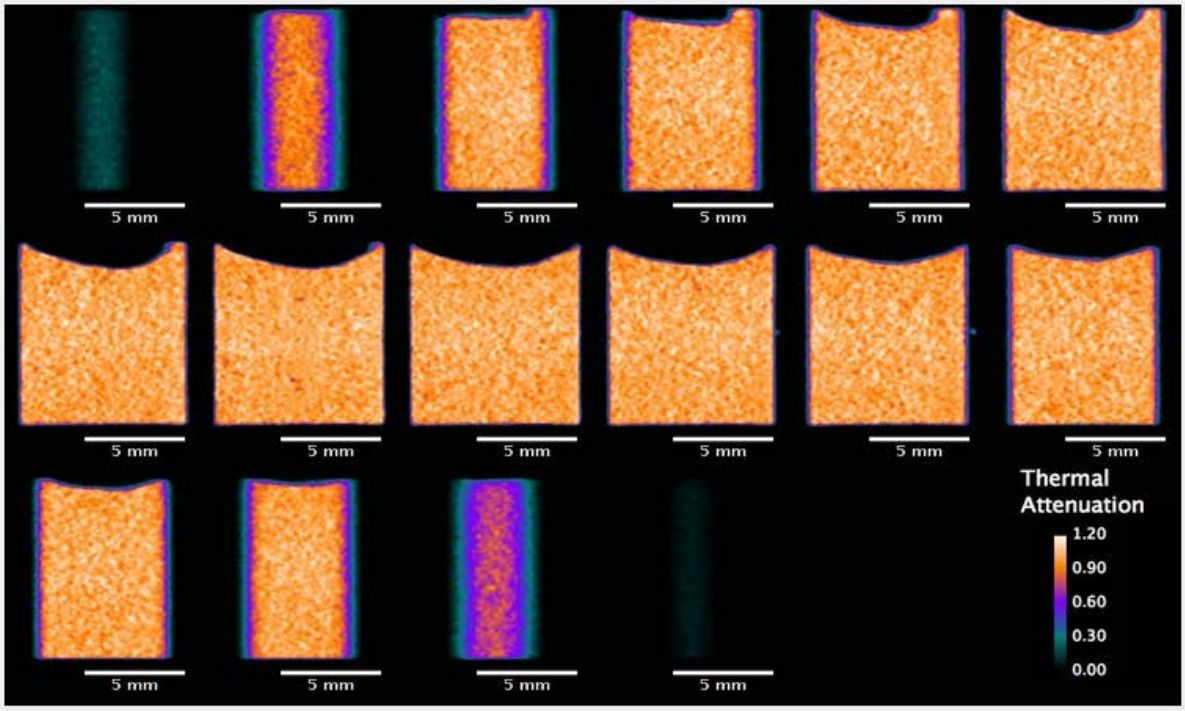

Epithermal reconstruction (1eV-200eV)

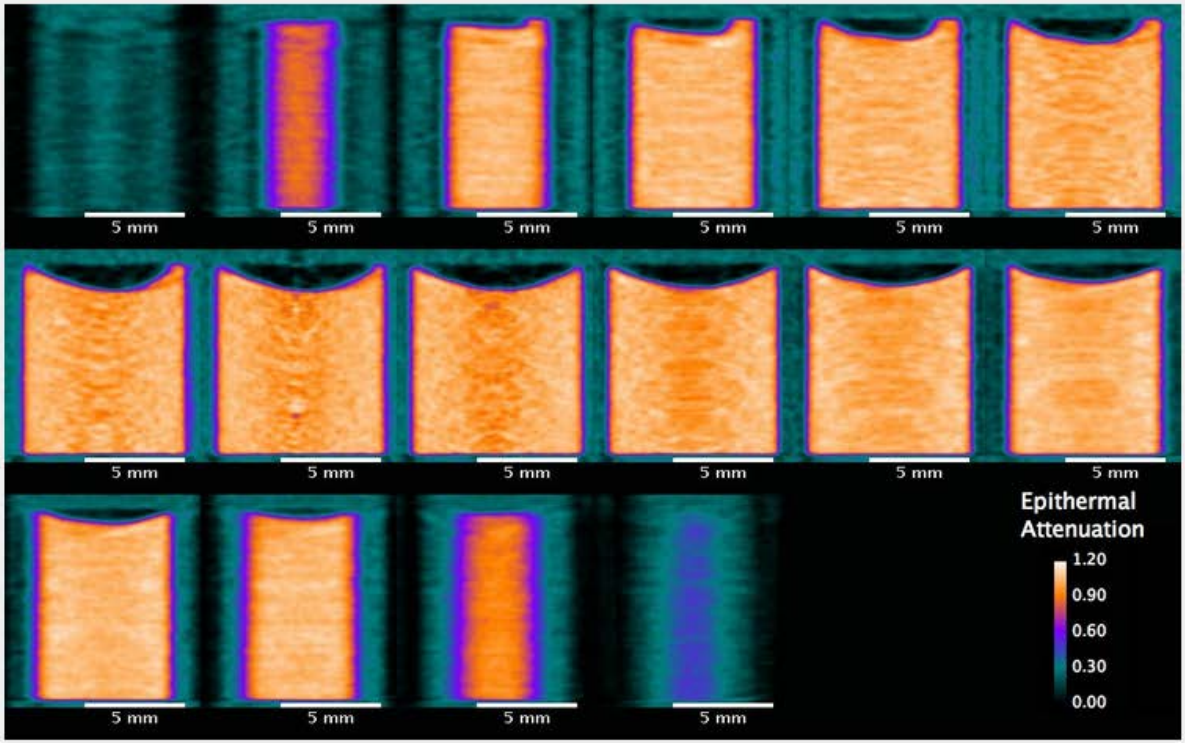

Pellet # 6 Rodlet # 4

^{238}U reconstruction

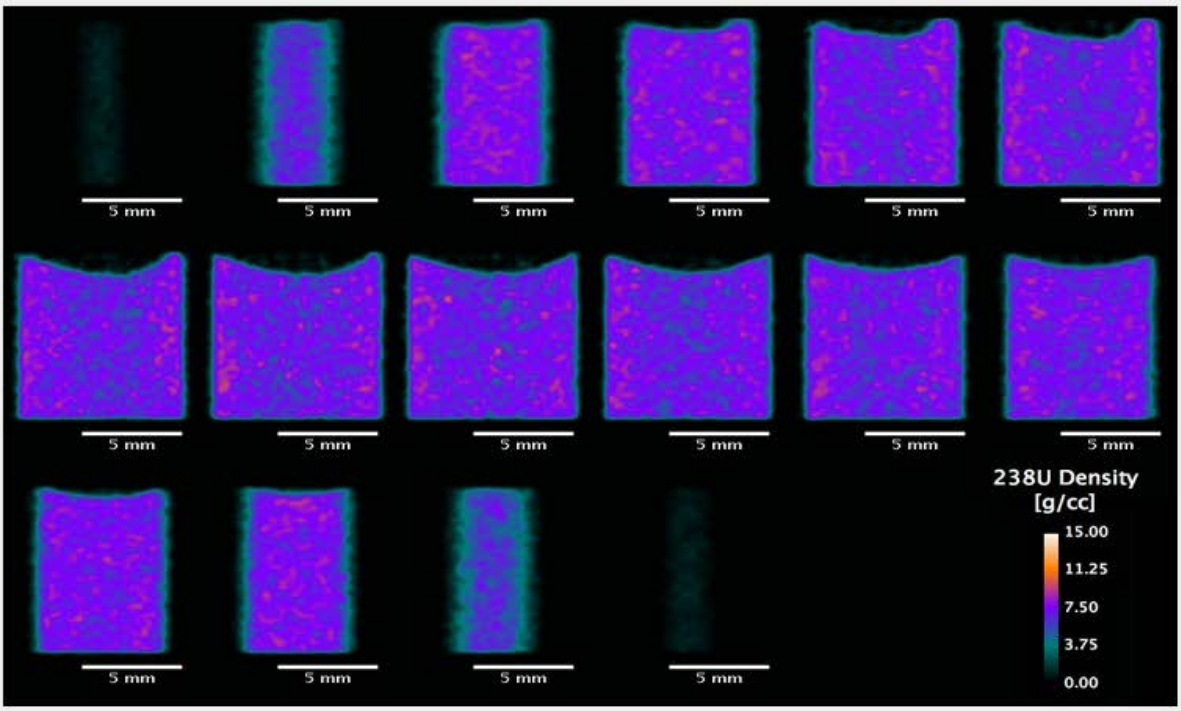

^{235}U reconstruction

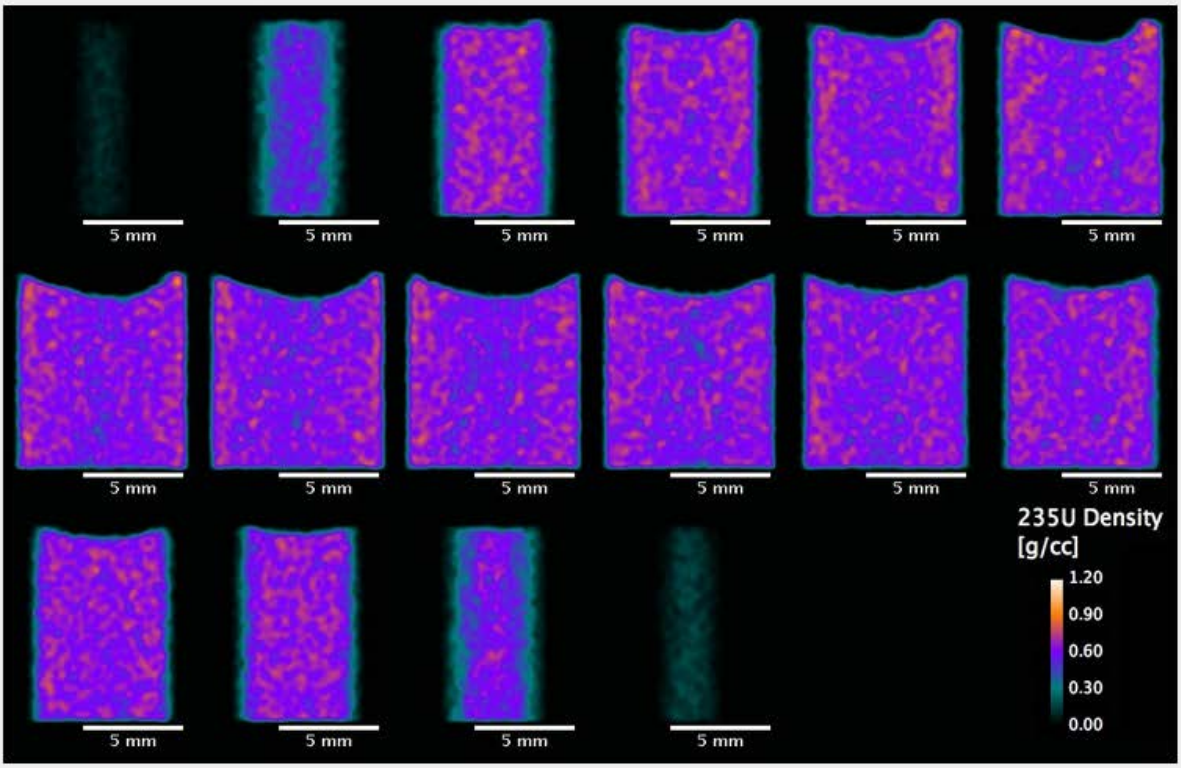

Pellet # 7 Rodlet # 4

Composition	UN (15 vol% U3Si5)
Enrichment	^{235}U in UN: 4.95 wt% ^{235}U in U_3Si_5: 8.84 wt%
Pellet #	7
Rodlet #	4
Epithermal measurement	01/22/2016
Background stabilization	1mm Cd sheet on collimator 0.1mm Ta mounted on detector
Projections #	52
Time/ projection	60
Angular separation	3.6 degrees
L/D	100
Source to detector	8.36 m
Thermal measurement	02/26/2016
Background stabilization	0.1mm Ta (mounted on detector)
Projections #	101
Time/ projection	5 mins
Angular separation	1.8
L/D	100
Source to detector	8.36 m
Summary	No features > 50 microns visible in pellet ^{235}U Density variation along the cylinder axis of the pellet < 4.4% ^{238}U Density variation along the cylinder axis of the pellet < 4.4%

SAMMY Fit

^{235}U enrichment	5.58 wt%
^{238}U density	11.958 g/cc
^{235}U density	0.618 g /cc

ISOTOPE	MOLAR MASS	AREAL DENSITY [ATOMS/BARN]	AREAL DENSITY REL. ERROR
^{238}U	238.051	1.90E-02	0.37%
^{235}U	235.044	1.13E-03	0.80%
^{182}W	181.948	7.29E-06	8.20%
^{186}W	185.954	4.20E-07	9.35%
^{181}Ta	180.94	2.12E-04	0.77%

Pellet # 7 Rodlet # 4

SAMMY fit

Fitted energy profile of pellet 7 from detector area indicated above:

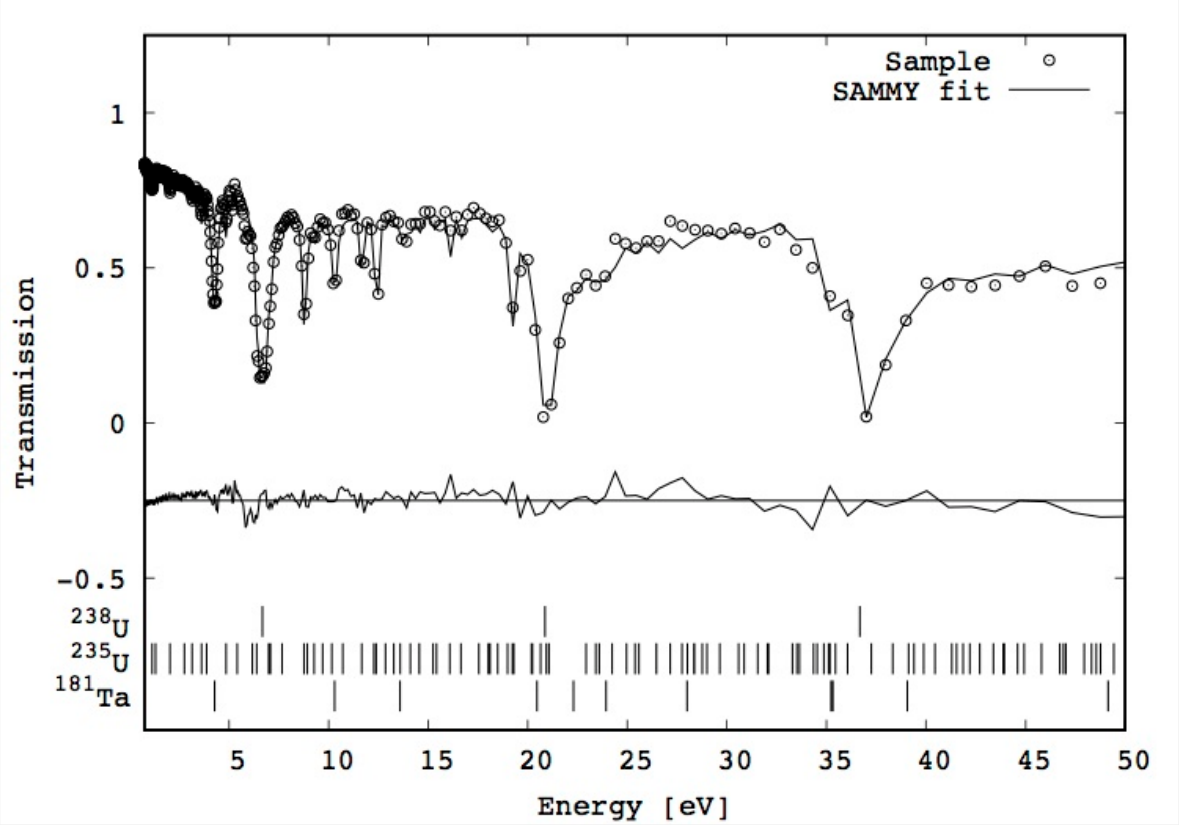

Example fit to normalized experimental data (60min acquisition) of pellet 7. Dots are measured transmission intensities. The curve through the data is the fit. Thedifference curve (experimental data subtracted from fit) shown below. Tick marks indicate positions of ^{238}U, ^{235}U and ^{181}Ta resonances.

Pellet # 7 Rodlet # 4

Tomographic reconstructions (slicing in 0.6mm steps along cylinder axis):

Thermal reconstruction (1meV-1eV)

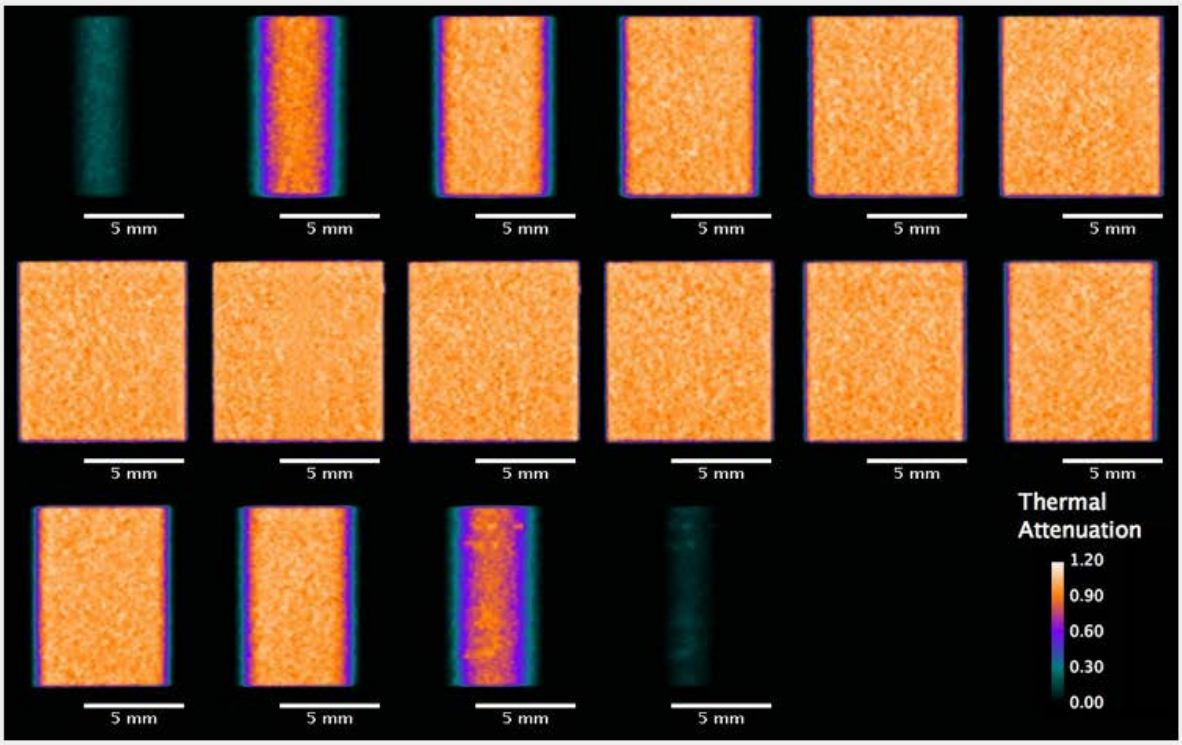

Epithermal reconstruction (1eV-200eV)

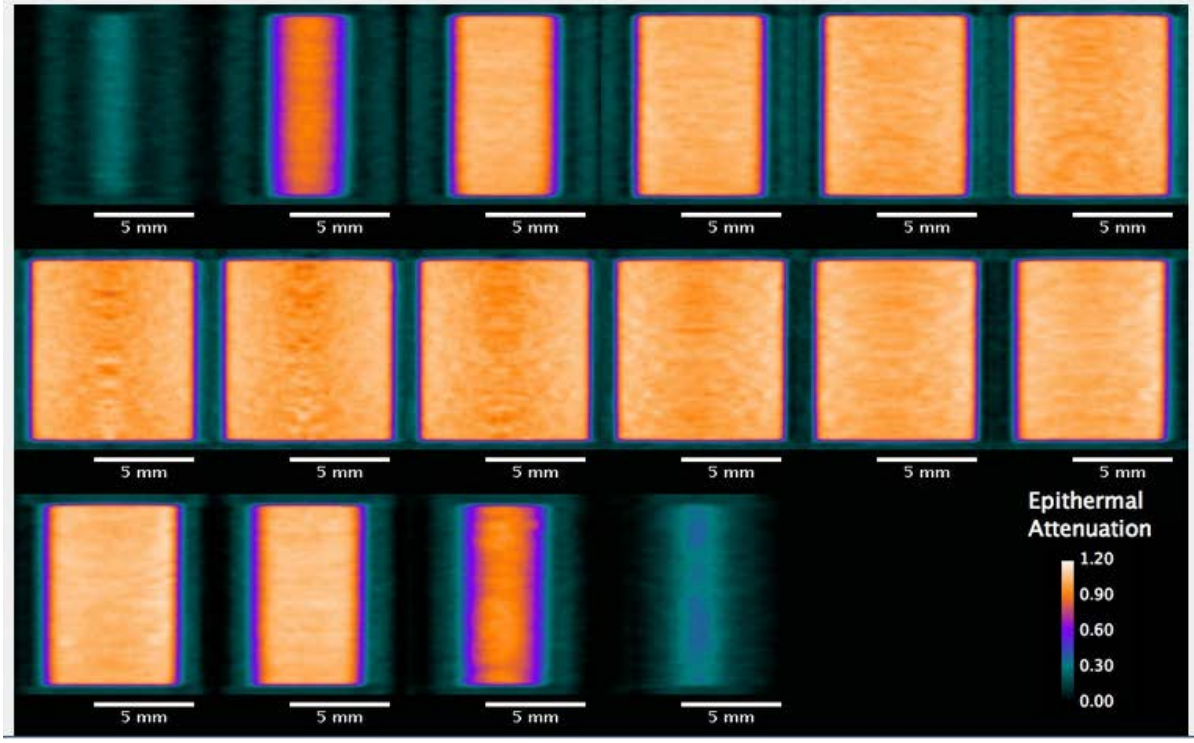

Pellet # 7 Rodlet # 4

^{238}U reconstruction

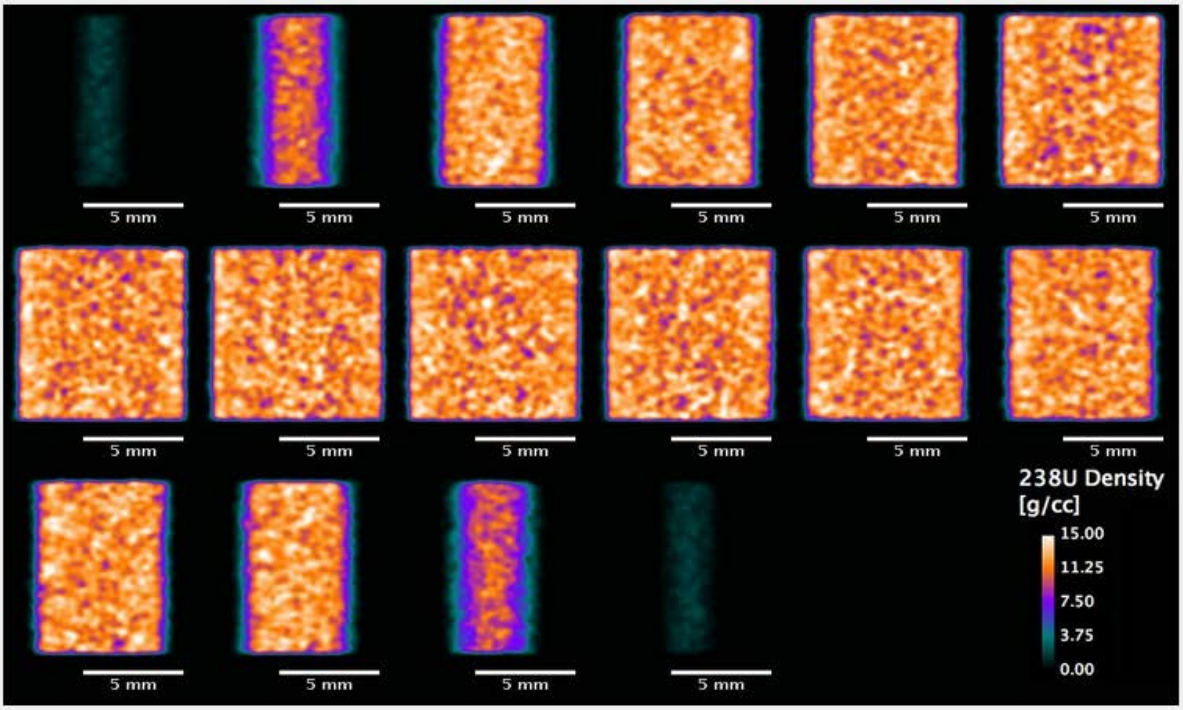

^{235}U reconstruction

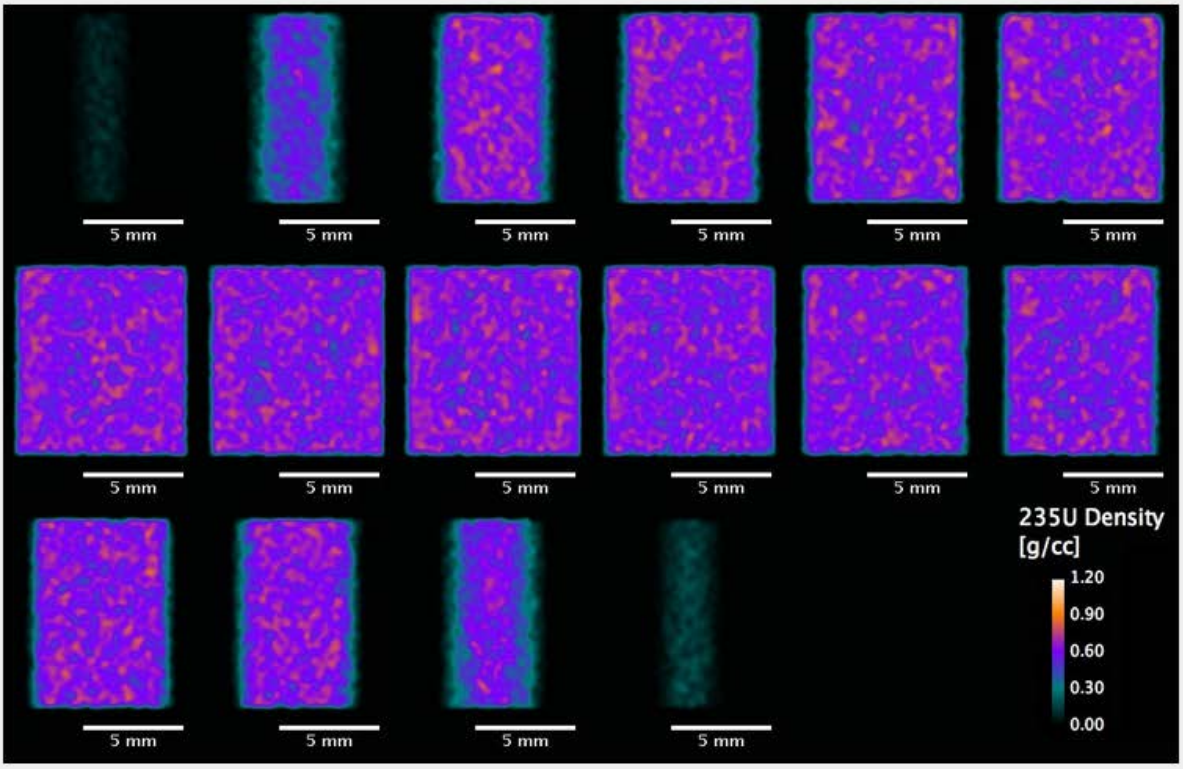

Pellet # 8 Rodlet # 3

Composition	UN (15 vol% U3Si5)
Enrichment	^{235}U in UN: 2.7 wt% ^{235}U in U_3Si_5: 2.7 wt%
Pellet #	8
Rodlet #	3
Epithermal measurement	01/22/2016
Background stabilization	1mm Cd sheet on collimator 0.1mm Ta mounted on detector
Projections #	52
Time/ projection	60
Angular separation	3.6 degrees
L/D	100
Source to detector	8.36 m
Thermal measurement	02/26/2016
Background stabilization	0.1mm Ta (mounted on detector)
Projections #	101
Time/ projection	5 mins
Angular separation	1.8
L/D	100
Source to detector	8.36 m
Summary	No visible features > x microns in pellet ^{235}U Density variation along the cylinder axis of the pellet within 3.4% ^{238}U Density variation along the cylinder axis of the pellet within 1.4%

SAMMY Fit

^{235}U enrichment	2.65 wt%
^{238}U density	12.258 g/cc
^{235}U density	0.351 g /cc

ISOTOPE	MOLAR MASS	AREAL DENSITY [ATOMS/BARN]	AREAL DENSITY REL. ERROR
^{238}U	238.051	2.31E-02	1.54%
^{235}U	235.044	6.27E-04	2.51%
^{182}W	181.948	1.80E-05	8.31%
^{186}W	185.954	3.81E-07	9.81%
^{181}Ta	180.94	2.93E-04	1.78%

Pellet # 8 Rodlet # 3

SAMMY fit

Fitted energy profile of pellet 8 from detector area indicated above:

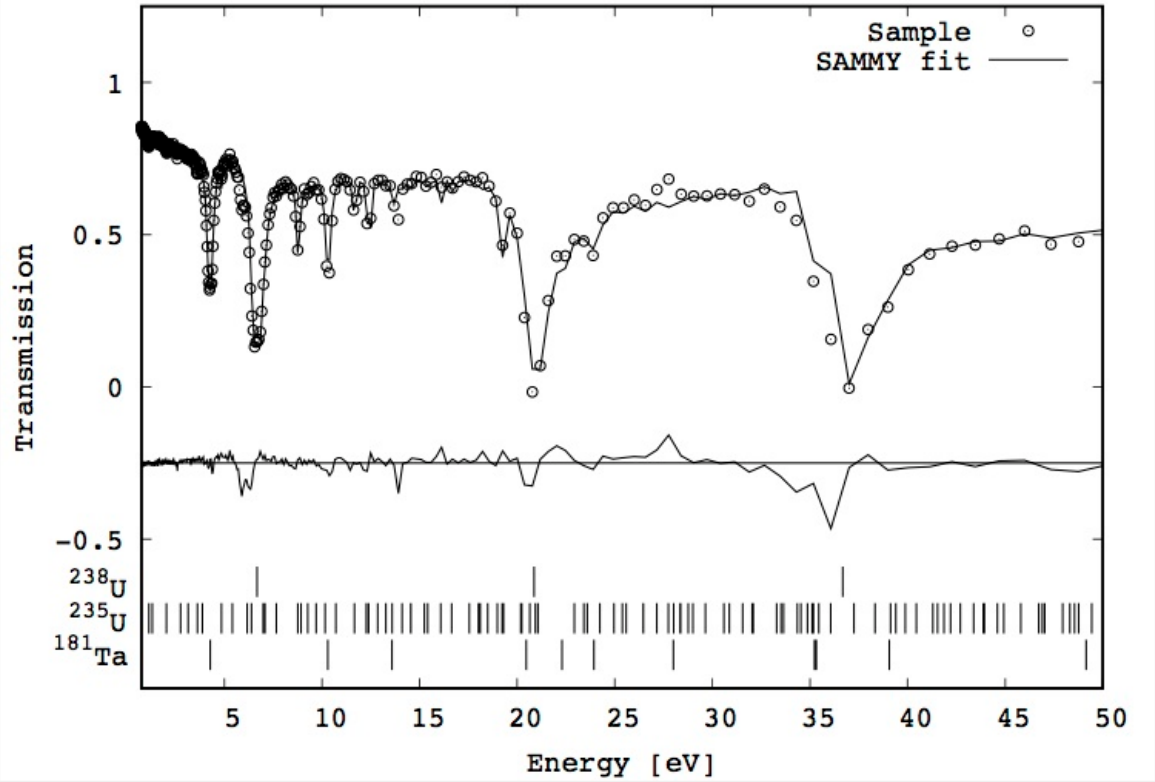

Example fit to normalized experimental data (60min acquisition) of pellet 8. Dots are measured transmission intensities. The curve through the data is the fit. Thedifference curve (experimental data subtracted from fit) shown below. Tick marks indicate positions of ^{238}U, ^{235}U and ^{181}Ta resonances.

Pellet # 8 Rodlet # 3

Tomographic reconstructions (slicing in 0.6mm steps along cylinder axis):

Thermal reconstruction (1meV-1eV)

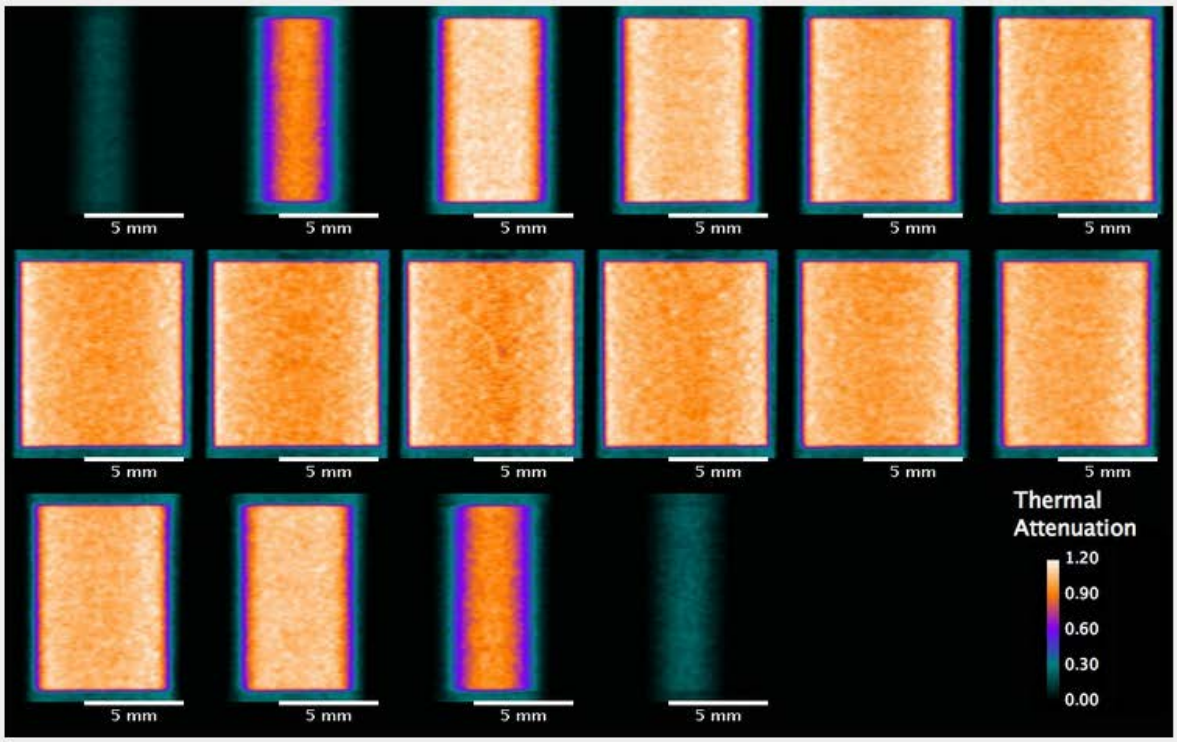

Epithermal reconstruction (1eV-200eV)

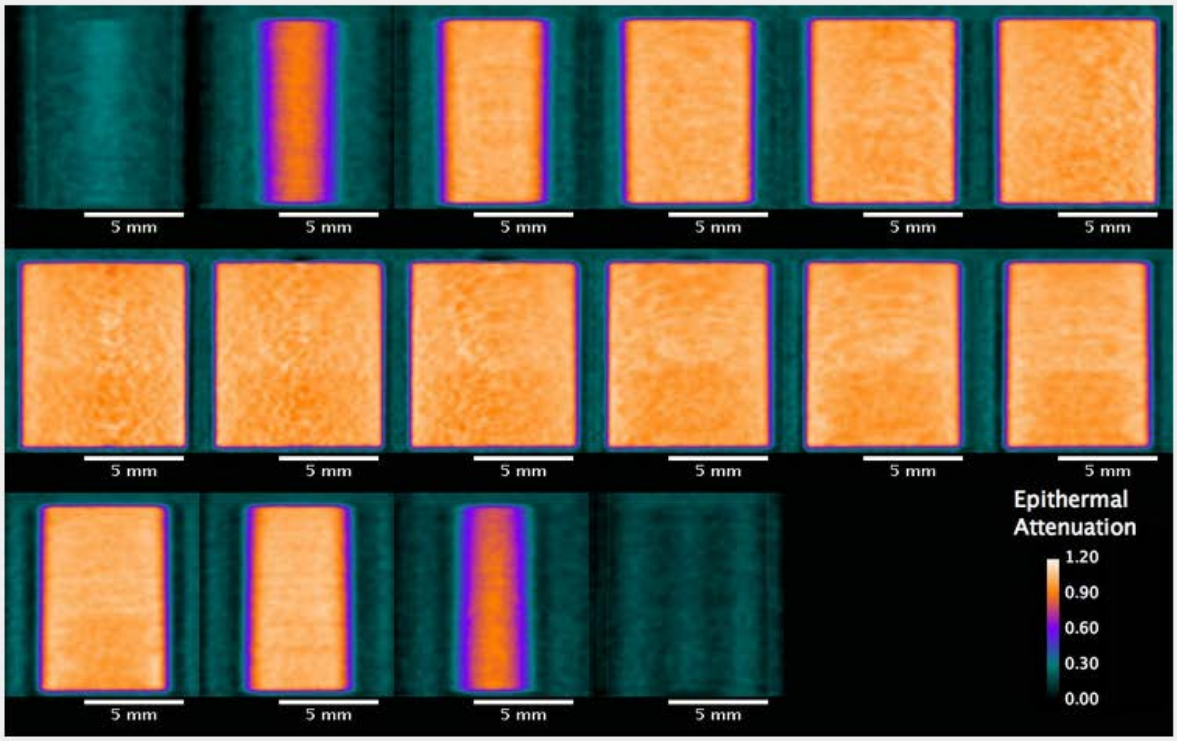

Pellet # 8 Rodlet # 3

^{238}U reconstruction

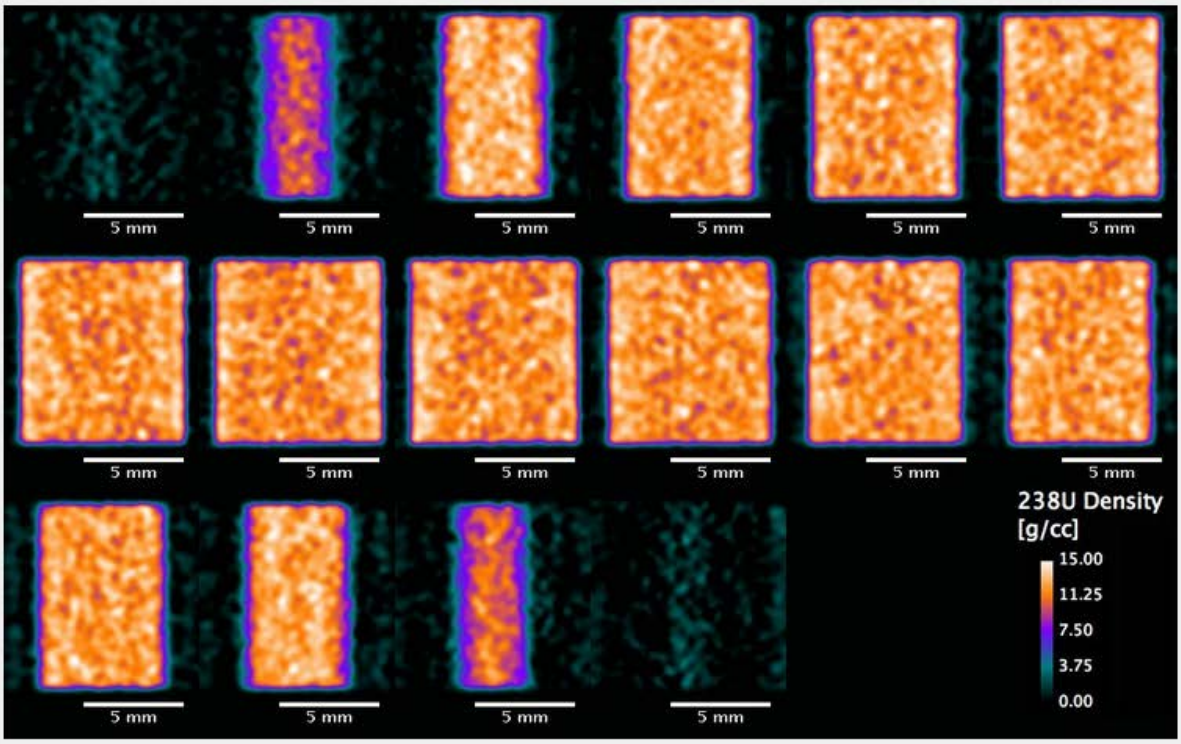

^{235}U reconstruction

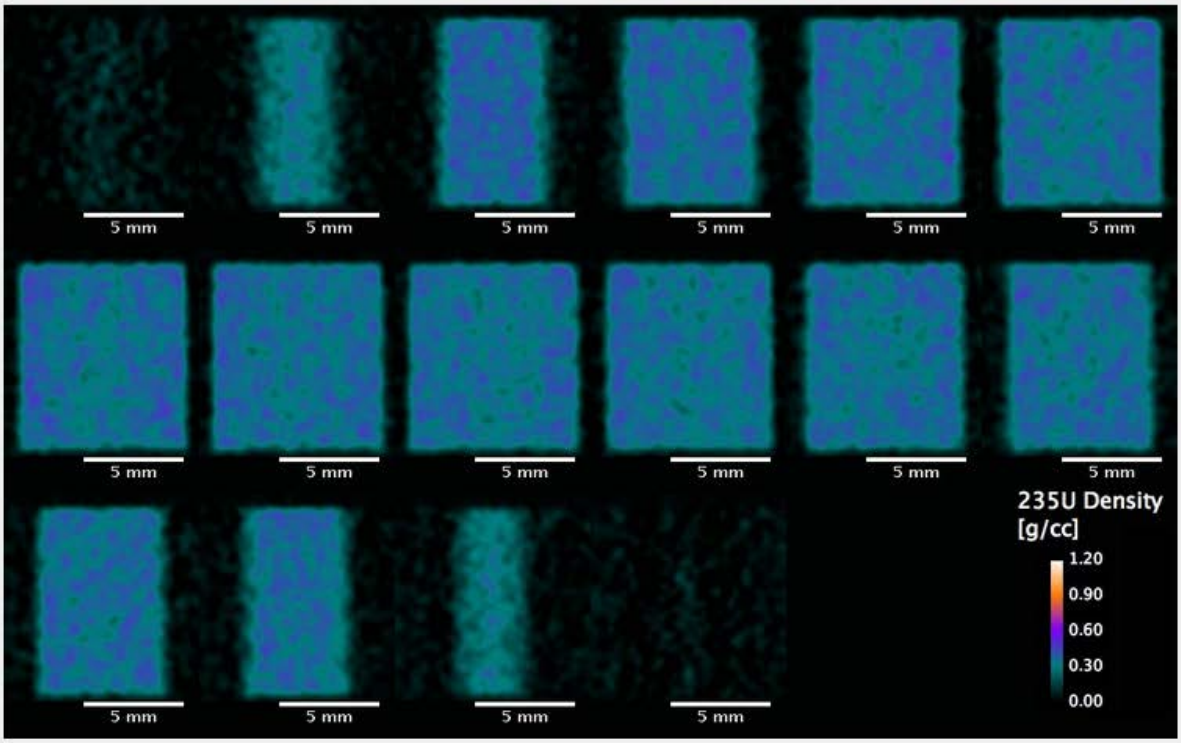

Pellet # 9 Rodlet # 3

Composition	UN (15 vol% U3Si5)
Enrichment	^{235}U in UN: 2.7 wt% ^{235}U in U_3Si_5: 2.7 wt%
Pellet #	9
Rodlet #	3
Epithermal measurement	01/22/2016
Background stabilization	1mm Cd sheet on collimator 0.1mm Ta mounted on detector
Projections #	52
Time/ projection	60
Angular separation	3.6 degrees
L/D	100
Source to detector	8.36 m
Thermal measurement	02/26/2016
Background stabilization	0.1mm Ta (mounted on detector)
Projections #	101
Time/ projection	5 mins
Angular separation	1.8
L/D	100
Source to detector	8.36 m
Summary	Visible feature in thermal and epithermal reconstruction of the pellet. ^{235}U Density variation along the cylinder axis of the pellet within 2.5% ^{238}U Density variation along the cylinder axis of the pellet within 1.3%

SAMMY Fit

^{235}U enrichment	2.65 wt%
^{238}U density	12.057 g/cc
^{235}U density	0.356 g /cc

ISOTOPE	MOLAR MASS	AREAL DENSITY [ATOMS/BARN]	AREAL DENSITY REL. ERROR
^{238}U	238.051	2.20E-02	1.57%
^{235}U	235.044	5.99E-04	2.60%
^{186}W	185.954	5.46E-07	9.48%
^{181}Ta	180.94	2.17E-04	1.97%

Pellet # 9 Rodlet # 3

SAMMY fit

Fitted energy profile of pellet 9 from detector area indicated above:

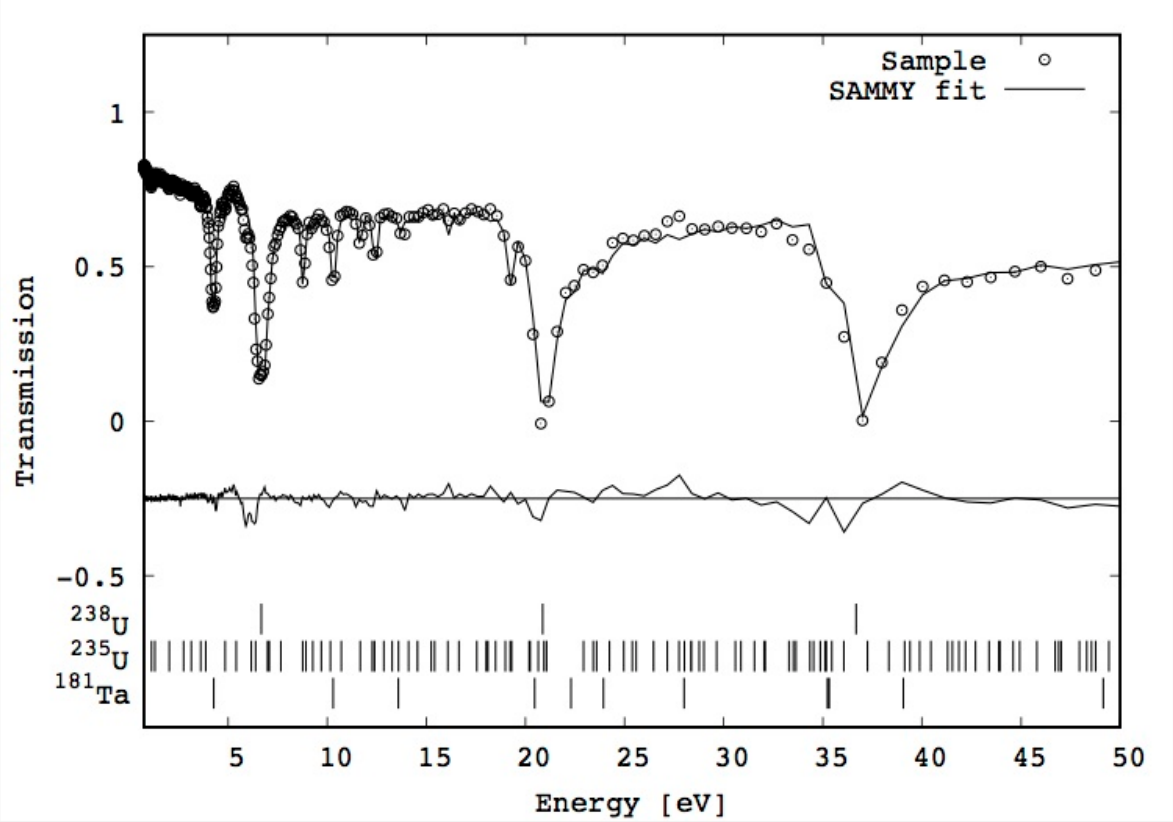

Example fit to normalized experimental data (60min acquisition) of pellet 9. Dots are measured transmission intensities. The curve through the data is the fit. Thedifference curve (experimental data subtracted from fit) shown below. Tick marks indicate positions of ^{238}U, ^{235}U and ^{181}Ta resonances.

Pellet # 9 Rodlet # 3

Tomographic reconstructions (slicing in 0.6mm steps along cylinder axis):

Thermal reconstruction (1meV-1eV)

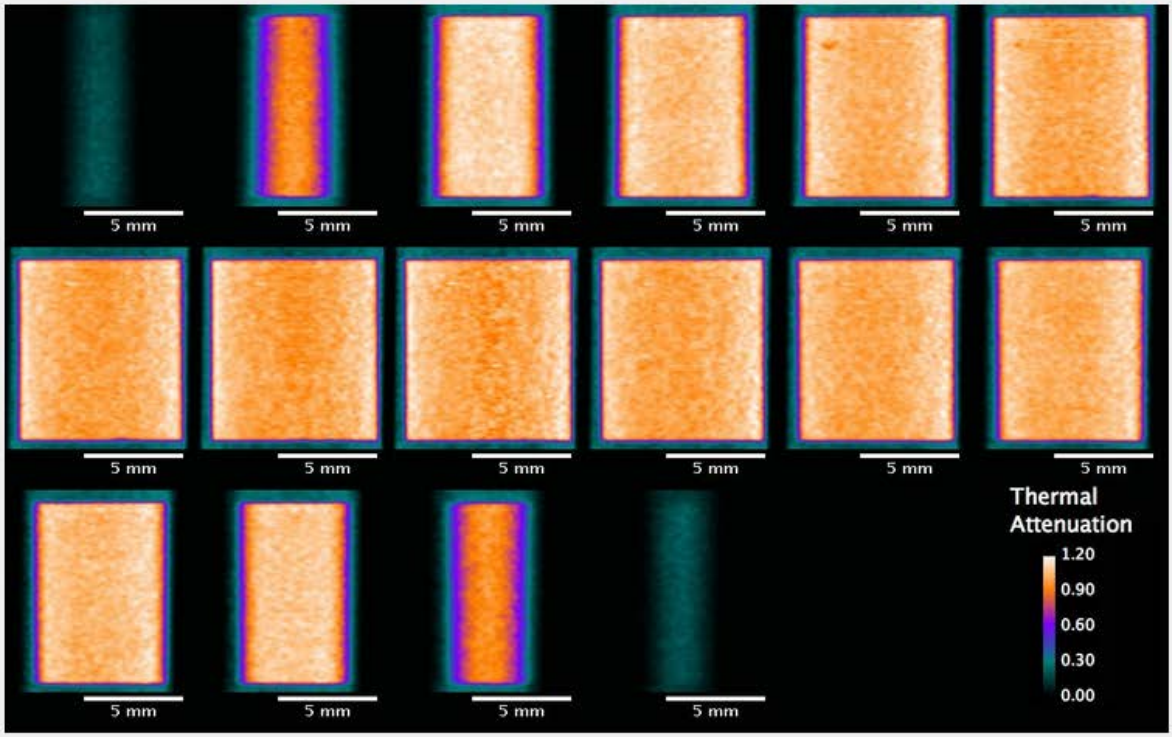

Epithermal reconstruction (1eV-200eV)

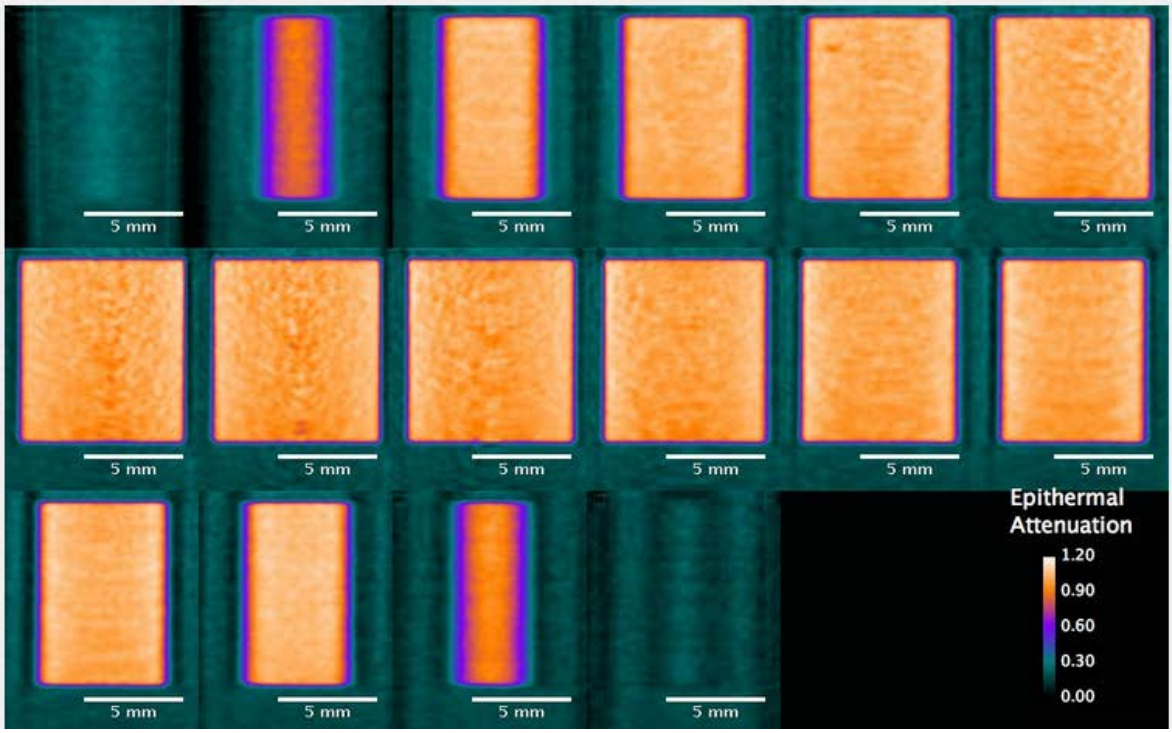

Pellet # 9 Rodlet # 3

^{238}U reconstruction

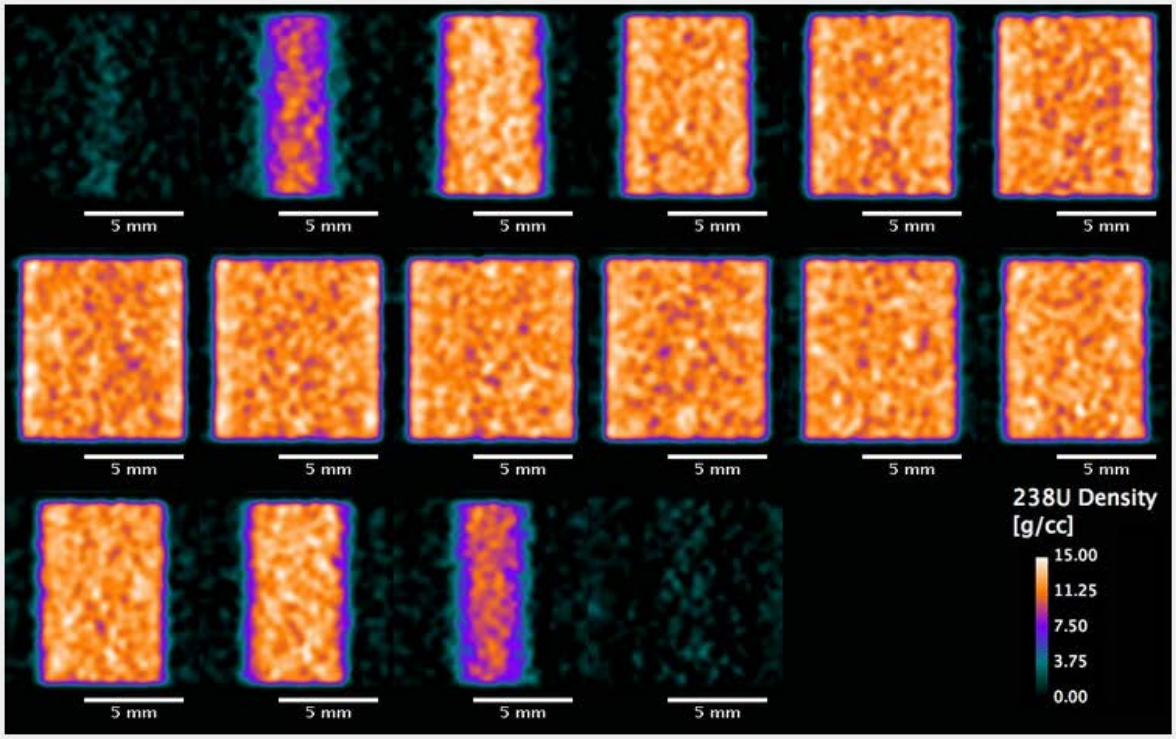

^{235}U reconstruction

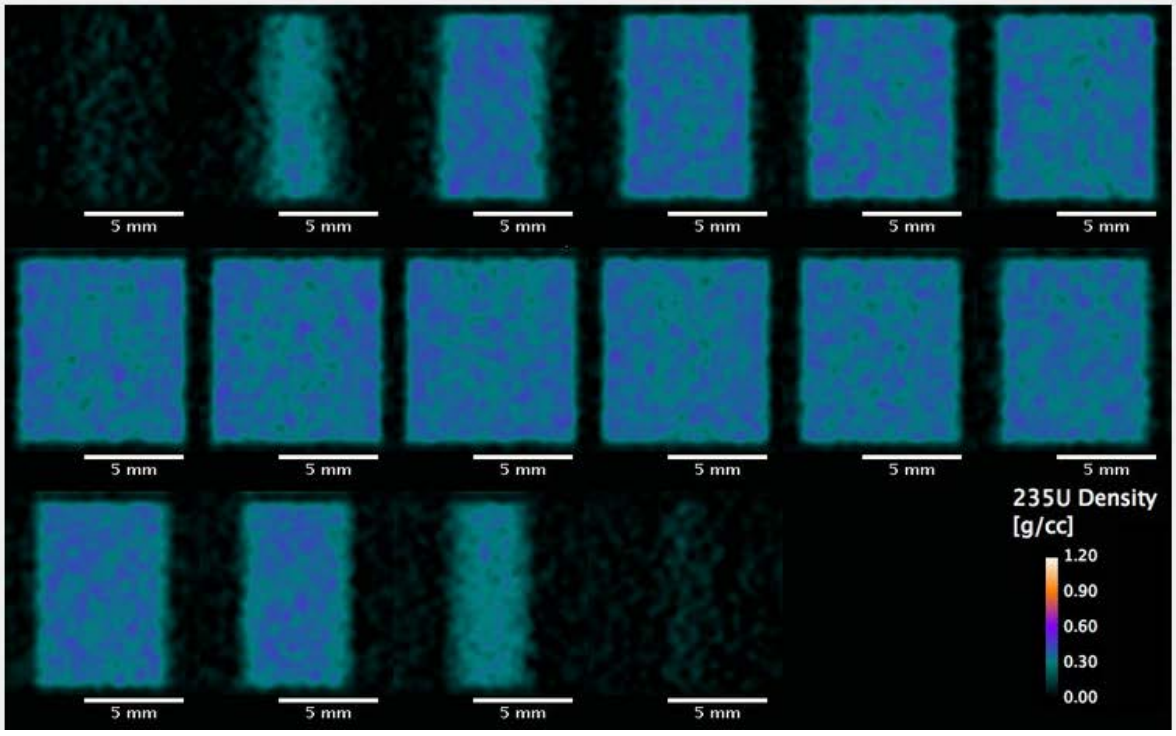

APPENDIX C: RESULTS OF GAMMA SPECTROSCOPY

Rodlet 1 30days after FP5

```
ORTEC g v - i (  15) wan32  G53W2.06  26-JAN-2016 12:55:55 Page    1
Spectrum name: 160121   LUJAN   1  ATF    12 in

 Sample description
      (C) LUJAN   1    ATF        12 inches    1.21.15


- - - - - - - - - - - - - - - - - - - - - - - - - - - - - - - - - - - - - -

 *****   S U M M A R Y   O F   N U C L I D E S   I N   S A M P L E   *****
          Time of Count   Uncertainty  1 Sigma
 Nuclide    Activity        Counting     Total
                Bq
 ____________________________________________________________________________
 NA-24   <    3.2181E+00
 K-40         6.8316E+03    7.830E+00%    8.044E+00%
 CO-56   <    5.4633E+00
 SR-91   C    2.4145E+02    2.293E+01%    2.300E+01%
 SR-92   <    7.4553E+00
 AG-110M      1.1210E+02    1.964E+01%    1.973E+01%
 TE-132  <    2.2273E+01
 I-132   <    1.6112E+01
 I-133        2.0734E+02    2.374E+01%    2.381E+01%
 I-135   C    1.2121E+02    3.198E+01%    3.203E+01%
 XE-135 #     9.9714E+01    2.815E+01%    2.821E+01%
 PA-234M H    1.8662E+05    4.725E+00%    5.070E+00%
 235U        5.4613E+03    2.027E+00%    2.738E+00%
 238U   <    1.5430E+03
 NP-239       6.7918E+02    1.873E+01%    1.876E+01%

   # - All peaks for activity calculation had bad shape.
   * - Activity omitted from total
   & - Activity omitted from total and all peaks had bad shape.
   < - MDA value printed.
   A - Activity printed, but activity < MDA.
   B - Activity < MDA and failed test.
   C - Area < Critical level.
   F - Failed fraction or key line test.
   H - Halflife limit exceeded
 ----------------------------   S U M M A R Y   ----------------------------
 Total Activity (    1.2 to  1751.1 keV) 2.0037753E+05  Bq
```

```
- - - - - - - - - - - - - - - - - - - - - - - - - - - - - - - - - - - - -
Spectrum Filename: C:\Gamma Spec files\2016 Gamma Folder\Bourke 1-21-
                   16\160121   LUJAN   1  ATF    12 inches  900 sec.A

 Acquisition information
        Start time:                21-Jan-2016 10:12:07
        Live time:                852
        Real time:                901
        Dead time:                  5.47 %
        Detector ID:                   10

 Detector system
      HSR-PN1168061 MCB 129


 Calibration
        Filename:                  16Jan25at12inches.Clb
      Energy recalibration on 01/25/16      Efficiency determined on 1
      1/25/15

        Energy Calibration
             Created:              26-Jan-2016 10:51:01
             Zero offset:          0.152 keV
             Gain:                 0.107 keV/channel
             Quadratic:            8.524E-09 keV/channel^2

        Efficiency Calibration
             Created:              26-Jan-2016 10:53:54
             Knee Energy:         110.00 keV
             Above the Knee:       Quadratic        Uncertainty =   2.48 %
             Log(Eff):            -6.757823E+00 + ( 5.745552E-01*Log(E) ) +
                                   ( -1.016668E-01*Log(E)^2 )
             Below the Knee:       Quadratic        Uncertainty =   0.00 %
             Log(Eff):            -1.110210E+01 + ( 1.020891E+00*Log(E) ) +
                                   (  0.000000E+00*Log(E)^2 )

 Library Files
        Main analysis library:     LEU2.LIB
        Library Match Width:       0.500

 Analysis parameters
        Analysis engine:           wan32   G53W2.06
        Start channel:              10 (     1.22keV )
        Stop channel:            16336 (  1751.12keV )
        Peak rejection level:     100.000%
        Peak search sensitivity:    3
        Sample Size:               1.0000E+00
        Activity scaling factor:   1.0000E+00/(  1.0000E+00*  1.0000E+00) =
                                   1.0000E+00
```

```
     ORTEC g v - i (  15) wan32  G53W2.06  26-JAN-2016 12:55:55 Page    2
 LANL                           Spectrum name: 160121   LUJAN   1  ATF    12 in

        Detection limit method:     Traditional ORTEC method
        Random error:               1.0000000E+00
        Systematic error:           1.0000000E+00
        Fraction Limit:             0.000%
        Background width:           best method (based on spectrum).
        Half lives decay limit:    12.000
        Activity range factor:      2.000
        Min. step backg. energy     0.000

 Corrections                          Status          Comments
        Decay correct to date:         NO
        Decay during acquisition:      YES
        Decay during collection:       NO
        True coincidence correction:   NO
        Peaked background correction:  NO
        Absorption (Internal):         NO
        Geometry correction:           NO
        Random summing:                NO


        Energy Calibration
             Normalized diff:       0.2332

Laboratory:  LANL
```

Rodlet 1 30 days after FP5 1 day after SMARTS

```
ORTEC g v - i (  47) wan32  G53W2.06  26-JAN-2016 13:10:12 Page    1
Spectrum name: 160125   LUJAN   1  ATF  12 inch

 Sample description
      LUJAN ATF  1   After SMARTS (3 days)  at 12 inches   1-25-16


- - - - - - - - - - - - - - - - - - - - - - - - - - - - - - - - - - - - -

 *****   S U M M A R Y   O F   N U C L I D E S   I N   S A M P L E   *****
          Time of Count   Uncertainty  1 Sigma
 Nuclide    Activity        Counting     Total
               Bq
 ____________________________________________________________________________
 NA-24  #     1.7632E+02    1.644E+01%    1.654E+01%
 K-40   #     6.4769E+03    9.856E+00%    1.003E+01%
 CO-56        2.8479E+01    3.333E+01%    3.338E+01%
 SR-91        4.6954E+02    1.651E+01%    1.661E+01%
 SR-92   <    1.4018E+01
 AG-110M      4.1602E+02    9.776E+00%    9.948E+00%
 TE-132       2.6930E+02    2.237E+01%    2.244E+01%
 I-132   <    3.2754E+01
 I-133        3.7294E+02    1.099E+01%    1.114E+01%
 I-135        3.9332E+02    2.218E+01%    2.226E+01%
 XE-135       1.3505E+02    3.876E+01%    3.880E+01%
 PA-234M      1.0969E+06    5.774E+00%    6.060E+00%
 235U        5.8610E+03    2.728E+00%    3.291E+00%
 238U   <    2.1468E+03
 NP-239  C    9.0402E+02    1.669E+01%    1.673E+01%

   # - All peaks for activity calculation had bad shape.
   * - Activity omitted from total
   & - Activity omitted from total and all peaks had bad shape.
   < - MDA value printed.
   A - Activity printed, but activity < MDA.
   B - Activity < MDA and failed test.
   C - Area < Critical level.
   F - Failed fraction or key line test.
   H - Halflife limit exceeded
----------------------------   S U M M A R Y   ----------------------------
Total Activity (    1.2 to  1751.1 keV) 1.1123920E+06  Bq


************ U N I D E N T I F I E D     P E A K    S U M M A R Y ************
  Peak Centroid  Background Net Area   Intensity   Uncert   FWHM  Suspected
Channel   Energy   Counts     Counts   Cts/Sec   1 Sigma %  keV   Nuclide
____________________________________________________________________________
   54.86     6.02       400.      3148.     5.483    2.22   0.747  -      s
  232.06    24.99       140.        35.     0.062   52.92   0.139  -      s
  988.33   106.07       313.       200.     0.348   14.37   0.730  -       D
 1098.07   117.82       214.        27.     0.046   80.12   0.743  -       D
 1491.72   159.85       155.        41.     0.071   46.16   0.790  -       D

   s - Peak fails shape tests.
   D - Peak area deconvoluted.
```

```
- - - - - - - - - - - - - - - - - - - - - - - - - - - - - - - - - - - - -
Spectrum Filename: C:\Gamma Spec files\2016 Gamma Folder\Bourke 1-21-
                   16\160125   LUJAN   1  ATF  12 inches post SMARTS.
                   An1

 Acquisition information
        Start time:                25-Jan-2016 13:53:51
        Live time:               574
        Real time:               601
        Dead time:                 4.46 %
        Detector ID:                  10

 Detector system
      HSR-PN1168061 MCB 129


 Calibration
        Filename:                  16Jan25at12inches.Clb
      Energy recalibration on 01/25/16      Efficiency determined on 1
      1/25/15

        Energy Calibration
             Created:              26-Jan-2016 10:51:01
             Zero offset:          0.152 keV
             Gain:                 0.107 keV/channel
             Quadratic:            8.524E-09 keV/channel^2

        Efficiency Calibration
             Created:              26-Jan-2016 10:53:54
             Knee Energy:        110.00 keV
             Above the Knee:       Quadratic        Uncertainty =   2.48 %
             Log(Eff):            -6.757823E+00 + ( 5.745552E-01*Log(E) ) +
                                   ( -1.016668E-01*Log(E)^2 )
             Below the Knee:       Quadratic        Uncertainty =   0.00 %
             Log(Eff):            -1.110210E+01 + ( 1.020891E+00*Log(E) ) +
                                   (  0.000000E+00*Log(E)^2 )

 Library Files
        Main analysis library:     LEU2.LIB
        Library Match Width:       0.500

 Analysis parameters
        Analysis engine:           wan32   G53W2.06
        Start channel:            10 (     1.22keV )
        Stop channel:          16336 (  1751.12keV )
        Peak rejection level:    100.000%
        Peak search sensitivity:   3
        Sample Size:               1.0000E+00
        Activity scaling factor:   1.0000E+00/(  1.0000E+00*  1.0000E+00) =
```

```
     ORTEC g v - i (  47) wan32  G53W2.06  26-JAN-2016 13:10:12 Page    2
LANL                           Spectrum name: 160125   LUJAN   1  ATF  12 inch

                                  1.0000E+00
       Detection limit method:    Traditional ORTEC method
       Random error:              1.0000000E+00
       Systematic error:          1.0000000E+00
       Fraction Limit:            0.000%
       Background width:          best method (based on spectrum).
       Half lives decay limit:   12.000
       Activity range factor:     2.000
       Min. step backg. energy    0.000

 Corrections                        Status          Comments
       Decay correct to date:        NO
       Decay during acquisition:     YES
       Decay during collection:      NO
       True coincidence correction:  NO
       Peaked background correction: NO
       Absorption (Internal):        NO
       Geometry correction:          NO
       Random summing:               NO


       Energy Calibration
            Normalized diff:      0.1231

Laboratory:  LANL
```

Rodlet 2 30 days after FP5

```
ORTEC g v - i (  15) wan32  G53W2.06  26-JAN-2016 13:01:30 Page    1
Spectrum name: 160121   LUJAN   2   WEC    12 i

 Sample description
      (C) LUJAN   2    WEC        12 inches    1.21.15


- - - - - - - - - - - - - - - - - - - - - - - - - - - - - - - - - - - - - -

 *****   S U M M A R Y   O F   N U C L I D E S   I N   S A M P L E   *****
          Time of Count   Uncertainty  1 Sigma
 Nuclide    Activity        Counting     Total
                Bq
 ____________________________________________________________________________
 NA-24         5.6355E+01    2.332E+01%    2.339E+01%
 K-40          7.3617E+03    6.551E+00%    6.805E+00%
 CO-56   <     5.4433E+00
 SR-91   <     1.2270E+01
 SR-92   <     8.2002E+00
 AG-110M       5.1990E+01    2.051E+01%    2.060E+01%
 TE-132  <     2.1285E+01
 I-132   <     1.4615E+01
 I-133         9.5534E+01    2.156E+01%    2.164E+01%
 I-135   <     1.0500E+01
 XE-135        2.8984E+02    2.781E+01%    2.787E+01%
 PA-234M H     1.4195E+05    5.392E+00%    5.697E+00%
 235U         3.6182E+03    2.983E+00%    3.505E+00%
 238U         4.6729E+03    4.182E+01%    4.183E+01%
 NP-239  <     2.5447E+02
   < - MDA value printed.
   A - Activity printed, but activity < MDA.
   B - Activity < MDA and failed test.
   C - Area < Critical level.
   F - Failed fraction or key line test.
   H - Halflife limit exceeded

----------------------------   S U M M A R Y   ----------------------------
 Total Activity (    1.2 to  1751.1 keV) 1.5809766E+05  Bq


 The library has energies which are not separable.
```

```
- - - - - - - - - - - - - - - - - - - - - - - - - - - - - - - - - - - - -

Spectrum Filename: C:\Gamma Spec files\2016 Gamma Folder\Bourke 1-21-
                   16\160121   LUJAN   2   WEC    12 inches   900sec.
                   An1

 Acquisition information
        Start time:                21-Jan-2016 10:31:54
        Live time:               855
        Real time:               902
        Dead time:                 5.18 %
        Detector ID:                  10

 Detector system
      HSR-PN1168061 MCB 129


 Calibration
        Filename:                  16Jan25at12inches.Clb
      Energy recalibration on 01/25/16      Efficiency determined on 1
      1/25/15

        Energy Calibration
             Created:              26-Jan-2016 10:51:01
             Zero offset:          0.152 keV
             Gain:                 0.107 keV/channel
             Quadratic:            8.524E-09 keV/channel^2

        Efficiency Calibration
             Created:              26-Jan-2016 10:53:54
             Knee Energy:        110.00 keV
             Above the Knee:       Quadratic        Uncertainty =   2.48 %
             Log(Eff):            -6.757823E+00 + ( 5.745552E-01*Log(E) ) +
                                  ( -1.016668E-01*Log(E)^2 )
             Below the Knee:       Quadratic        Uncertainty =   0.00 %
             Log(Eff):            -1.110210E+01 + ( 1.020891E+00*Log(E) ) +
                                  (  0.000000E+00*Log(E)^2 )

 Library Files
        Main analysis library:     LEU2.LIB
        Library Match Width:       0.500

 Analysis parameters
        Analysis engine:           wan32   G53W2.06
        Start channel:            10 (     1.22keV )
        Stop channel:          16336 (  1751.12keV )
        Peak rejection level:    100.000%
        Peak search sensitivity:   3
        Sample Size:               1.0000E+00
        Activity scaling factor:   1.0000E+00/(  1.0000E+00*  1.0000E+00) =
```

```
     ORTEC g v - i (  15) wan32  G53W2.06  26-JAN-2016 13:01:30 Page    2
LANL                           Spectrum name: 160121   LUJAN   2   WEC    12 i

                                  1.0000E+00
       Detection limit method:    Traditional ORTEC method
       Random error:              1.0000000E+00
       Systematic error:          1.0000000E+00
       Fraction Limit:            0.000%
       Background width:          best method (based on spectrum).
       Half lives decay limit:   12.000
       Activity range factor:     2.000
       Min. step backg. energy    0.000

 Corrections                        Status          Comments
       Decay correct to date:        NO
       Decay during acquisition:     YES
       Decay during collection:      NO
       True coincidence correction:  NO
       Peaked background correction: NO
       Absorption (Internal):        NO
       Geometry correction:          NO
       Random summing:               NO


       Energy Calibration
            Normalized diff:      0.1243

Laboratory:  LANL
```

Rodlet 3 As received

```
ORTEC g v - i (  47) wan32  G53W2.06  26-JAN-2016 13:03:47 Page    1
Spectrum name: 160121   LUJAN   3  ATF MT32

Sample description
     LUJAN3 ATF MT32       12 inches    1.21.15

- - - - - - - - - - - - - - - - - - - - - - - - - - - - - - - - - - - - -

*****   S U M M A R Y   O F   N U C L I D E S   I N   S A M P L E   *****
         Time of Count   Uncertainty  1 Sigma
Nuclide    Activity        Counting     Total
              Bq
_____________________________________________________________________________
NA-24  #C    4.6859E+01    3.395E+01%    3.400E+01%
K-40         7.7314E+03    6.555E+00%    6.809E+00%
CO-56  #     2.5568E+01    4.082E+01%    4.087E+01%
SR-91        2.0794E+02    2.244E+01%    2.251E+01%
SR-92   <    3.7239E+00
AG-110M#     4.4227E+01    2.862E+01%    2.868E+01%
TE-132       1.7531E+02    2.428E+01%    2.435E+01%
I-132   C    9.1884E+01    1.926E+01%    1.935E+01%
I-133   <    1.5687E+01
I-135   <    2.1055E+01
XE-135  <    9.0589E+00
PA-234M H    1.6260E+05    5.044E+00%    5.369E+00%
235U        2.5025E+03    4.206E+00%    4.590E+00%
238U   <    1.3523E+03
NP-239       6.9130E+02    2.035E+01%    2.038E+01%

  # - All peaks for activity calculation had bad shape.
  * - Activity omitted from total
  & - Activity omitted from total and all peaks had bad shape.
  < - MDA value printed.
  A - Activity printed, but activity < MDA.
  B - Activity < MDA and failed test.
  C - Area < Critical level.
  F - Failed fraction or key line test.
  H - Halflife limit exceeded
----------------------------   S U M M A R Y   ----------------------------
Total Activity (    1.2 to  1751.1 keV) 1.7411761E+05  Bq


************ U N I D E N T I F I E D     P E A K    S U M M A R Y ************
   Peak Centroid  Background Net Area   Intensity   Uncert   FWHM  Suspected
Channel   Energy   Counts     Counts   Cts/Sec   1 Sigma %  keV   Nuclide
_____________________________________________________________________________
   54.02     5.93       479.      4287.     5.026    1.85   0.533  -      s
 1505.27   161.39       253.        46.     0.054   50.55   0.791  -       D
 2832.72   303.45       119.        59.     0.069   47.56   0.252  -      s

  s - Peak fails shape tests.
  D - Peak area deconvoluted.
```

```
- - - - - - - - - - - - - - - - - - - - - - - - - - - - - - - - - - - - -

Spectrum Filename: C:\Gamma Spec files\2016 Gamma Folder\Bourke 1-21-
                   16\160121   LUJAN   3  ATF MT32    12 inches  900s
                   ec.An1

 Acquisition information
        Start time:                21-Jan-2016 09:29:56
        Live time:               853
        Real time:               901
        Dead time:                 5.32 %
        Detector ID:                  10

 Detector system
      HSR-PN1168061 MCB 129


 Calibration
        Filename:                  16Jan25at12inches.Clb
      Energy recalibration on 01/25/16      Efficiency determined on 1
      1/25/15

        Energy Calibration
             Created:              26-Jan-2016 10:51:01
             Zero offset:          0.152 keV
             Gain:                 0.107 keV/channel
             Quadratic:            8.524E-09 keV/channel^2

        Efficiency Calibration
             Created:              26-Jan-2016 10:53:54
             Knee Energy:        110.00 keV
             Above the Knee:       Quadratic        Uncertainty =   2.48 %
             Log(Eff):            -6.757823E+00 + ( 5.745552E-01*Log(E) ) +
                                  ( -1.016668E-01*Log(E)^2 )
             Below the Knee:       Quadratic        Uncertainty =   0.00 %
             Log(Eff):            -1.110210E+01 + ( 1.020891E+00*Log(E) ) +
                                  (  0.000000E+00*Log(E)^2 )

 Library Files
        Main analysis library:     LEU2.LIB
        Library Match Width:       0.500

 Analysis parameters
        Analysis engine:           wan32   G53W2.06
        Start channel:            10 (     1.22keV )
        Stop channel:          16336 (  1751.12keV )
        Peak rejection level:    100.000%
        Peak search sensitivity:   3
        Sample Size:               1.0000E+00
        Activity scaling factor:   1.0000E+00/(  1.0000E+00*  1.0000E+00) =
```

```
     ORTEC g v - i (  47) wan32  G53W2.06  26-JAN-2016 13:03:47 Page    2
LANL                           Spectrum name: 160121   LUJAN   3  ATF MT32

                                  1.0000E+00
       Detection limit method:    Traditional ORTEC method
       Random error:              1.0000000E+00
       Systematic error:          1.0000000E+00
       Fraction Limit:            0.000%
       Background width:          best method (based on spectrum).
       Half lives decay limit:   12.000
       Activity range factor:     2.000
       Min. step backg. energy    0.000

Corrections                         Status          Comments
       Decay correct to date:        NO
       Decay during acquisition:     YES
       Decay during collection:      NO
       True coincidence correction:  NO
       Peaked background correction: NO
       Absorption (Internal):        NO
       Geometry correction:          NO
       Random summing:               NO


       Energy Calibration
            Normalized diff:      0.2764
```

Rodlet 3 1 day post FP5

```
ORTEC g v - i (  47) wan32  G53W2.06  26-JAN-2016 13:13:21 Page    1
Spectrum name: 160125   LUJAN   3  ATF   12 inc

 Sample description
      LUJAN ATF  3   After FP-5 (3 days)  at 12 inches   1-25-16

- - - - - - - - - - - - - - - - - - - - - - - - - - - - - - - - - - - - -

 *****   S U M M A R Y   O F   N U C L I D E S   I N   S A M P L E   *****
          Time of Count   Uncertainty  1 Sigma
 Nuclide    Activity        Counting     Total
                Bq
 ____________________________________________________________________________
 NA-24         2.4638E+03    4.415E+00%    4.783E+00%
 K-40    <     7.6041E+02
 CO-56         1.3607E+03    7.506E+00%    7.728E+00%
 SR-91         2.2623E+03    7.982E+00%    8.192E+00%
 SR-92         1.1645E+03    1.155E+01%    1.170E+01%
 AG-110M       2.6279E+03    4.062E+00%    4.460E+00%
 TE-132        3.8924E+03    3.820E+00%    4.240E+00%
 I-132         1.3090E+03    4.475E+00%    4.838E+00%
 I-133         2.2631E+03    4.270E+00%    4.649E+00%
 I-135         3.3478E+03    6.852E+00%    7.095E+00%
 XE-135        1.1027E+03    9.252E+00%    9.433E+00%
 PA-234M       1.2300E+06    7.285E+00%    7.514E+00%
 235U         2.8522E+03    5.361E+00%    5.668E+00%
 238U    <    4.0526E+03
 NP-239  <    5.7695E+02
   < - MDA value printed.
   A - Activity printed, but activity < MDA.
   B - Activity < MDA and failed test.
   C - Area < Critical level.
   F - Failed fraction or key line test.
   H - Halflife limit exceeded
 ----------------------------   S U M M A R Y   ---------------------------
 Total Activity (    1.2 to  1751.1 keV) 1.2546671E+06  Bq


 ************ U N I D E N T I F I E D     P E A K     S U M M A R Y ************
   Peak Centroid  Background Net Area   Intensity   Uncert   FWHM  Suspected
 Channel   Energy   Counts     Counts   Cts/Sec   1 Sigma %  keV   Nuclide
 ____________________________________________________________________________
    55.67     6.11       765.      2817.     4.944    2.79   0.782  -       s
   351.45    37.70       315.        68.     0.119   38.80   0.653  -       D
   764.59    82.00       309.        66.     0.116   43.87   0.375  -       s
  1547.76   165.86       556.        64.     0.112   53.89   0.796  -       D
  1687.28   180.79       475.        83.     0.146   50.12   0.189  -       s
  2735.67   293.06       357.       308.     0.541   14.53   0.288  -       s
  3206.30   343.50       185.        29.     0.051   68.73   0.987  -       D

   s - Peak fails shape tests.
   D - Peak area deconvoluted.
```

```
- - - - - - - - - - - - - - - - - - - - - - - - - - - - - - - - - - - - -

Spectrum Filename: C:\Gamma Spec files\2016 Gamma Folder\Bourke 1-21-
                   16\160125   LUJAN   3  ATF   12 inches  600 sec po
                   st FP5.An1

 Acquisition information
        Start time:                25-Jan-2016 13:01:05
        Live time:               570
        Real time:               604
        Dead time:                 5.60 %
        Detector ID:                  10

 Detector system
      HSR-PN1168061 MCB 129


 Calibration
        Filename:                  16Jan25at12inches.Clb
      Energy recalibration on 01/25/16      Efficiency determined on 1
      1/25/15

        Energy Calibration
             Created:              26-Jan-2016 10:51:01
             Zero offset:          0.152 keV
             Gain:                 0.107 keV/channel
             Quadratic:            8.524E-09 keV/channel^2

        Efficiency Calibration
             Created:              26-Jan-2016 10:53:54
             Knee Energy:        110.00 keV
             Above the Knee:       Quadratic        Uncertainty =   2.48 %
             Log(Eff):            -6.757823E+00 + ( 5.745552E-01*Log(E) ) +
                                   ( -1.016668E-01*Log(E)^2 )
             Below the Knee:       Quadratic        Uncertainty =   0.00 %
             Log(Eff):            -1.110210E+01 + ( 1.020891E+00*Log(E) ) +
                                   (  0.000000E+00*Log(E)^2 )

 Library Files
        Main analysis library:     LEU2.LIB
        Library Match Width:       0.500

 Analysis parameters
        Analysis engine:           wan32   G53W2.06
        Start channel:            10 (     1.22keV )
        Stop channel:          16336 (  1751.12keV )
        Peak rejection level:    100.000%
        Peak search sensitivity:   3
        Sample Size:               1.0000E+00
        Activity scaling factor:   1.0000E+00/(  1.0000E+00*  1.0000E+00) =
```

```
     ORTEC g v - i (  47) wan32  G53W2.06  26-JAN-2016 13:13:21 Page    2
LANL                           Spectrum name: 160125   LUJAN   3  ATF   12 inc

                                  1.0000E+00
       Detection limit method:    Traditional ORTEC method
       Random error:              1.0000000E+00
       Systematic error:          1.0000000E+00
       Fraction Limit:            0.000%
       Background width:          best method (based on spectrum).
       Half lives decay limit:   12.000
       Activity range factor:     2.000
       Min. step backg. energy    0.000

Corrections                         Status          Comments
       Decay correct to date:        NO
       Decay during acquisition:     YES
       Decay during collection:      NO
       True coincidence correction:  NO
       Peaked background correction: NO
       Absorption (Internal):        NO
       Geometry correction:          NO
       Random summing:               NO


       Energy Calibration
            Normalized diff:      0.2174
```

Rodlet 4 As received

```
ORTEC g v - i (  47) wan32  G53W2.06  26-JAN-2016 13:06:57 Page    1
 Spectrum name: 160121 LUJAN   4  ATF  MT26 32 3
 Sample description
      LUJAN4 ATF MT26+32 = 31       12 inches    1.21.15

- - - - - - - - - - - - - - - - - - - - - - - - - - - - - - - - - - - - -

 *****   S U M M A R Y   O F   N U C L I D E S   I N   S A M P L E   *****
          Time of Count   Uncertainty  1 Sigma
 Nuclide    Activity        Counting     Total
                Bq
 ____________________________________________________________________________
 NA-24   <    3.2159E+00
 K-40    #    8.1336E+02    6.750E+01%    6.752E+01%
 CO-56   #    5.1152E+01    2.041E+01%    2.050E+01%
 SR-91   <    1.8828E+01
 SR-92   <    3.7251E+00
 AG-110M <    9.6600E+00
 TE-132  <    6.4133E+00
 I-132        8.2350E+01    2.098E+01%    2.106E+01%
 I-133   C    1.3683E+02    2.499E+01%    2.506E+01%
 I-135   <    1.0531E+01
 XE-135 #     6.0836E+01    3.468E+01%    3.472E+01%
 PA-234M H    1.1780E+05    5.944E+00%    6.223E+00%
 235U        6.3916E+03    1.842E+00%    2.604E+00%
 238U    <   1.6295E+03
 NP-239  <    2.6836E+02

   # - All peaks for activity calculation had bad shape.
   * - Activity omitted from total
   & - Activity omitted from total and all peaks had bad shape.
   < - MDA value printed.
   A - Activity printed, but activity < MDA.
   B - Activity < MDA and failed test.
   C - Area < Critical level.
   F - Failed fraction or key line test.
   H - Halflife limit exceeded


 ----------------------------   S U M M A R Y   ----------------------------
 Total Activity (    1.2 to  1751.1 keV) 1.2533771E+05  Bq


************ U N I D E N T I F I E D     P E A K    S U M M A R Y ************
   Peak Centroid  Background Net Area   Intensity   Uncert   FWHM  Suspected
 Channel   Energy   Counts     Counts   Cts/Sec   1 Sigma %  keV   Nuclide
 ____________________________________________________________________________
    54.72     6.01       338.      4808.     5.639    1.69   0.591  -      s
   861.50    92.52       727.       400.     0.470   10.76   0.715  -       D
  2946.88   315.68        17.        16.     0.019   44.19   0.134  -      sM

   s - Peak fails shape tests.
   D - Peak area deconvoluted.
   M - Peak is close to a library peak.
```

```
Spectrum Filename: C:\Gamma Spec files\2016 Gamma Folder\Bourke 1-21-
                   16\160121 LUJAN   4  ATF  MT26 32 31   12 inches
                   900 sec.An1

 Acquisition information
        Start time:                21-Jan-2016 09:51:19
        Live time:                853
        Real time:                901
        Dead time:                  5.37 %
        Detector ID:                   10

 Detector system
      HSR-PN1168061 MCB 129


 Calibration
        Filename:                  16Jan25at12inches.Clb
      Energy recalibration on 01/25/16      Efficiency determined on 1
      1/25/15

        Energy Calibration
             Created:              26-Jan-2016 10:51:01
             Zero offset:          0.152 keV
             Gain:                 0.107 keV/channel
             Quadratic:            8.524E-09 keV/channel^2

        Efficiency Calibration
             Created:              26-Jan-2016 10:53:54
             Knee Energy:         110.00 keV
             Above the Knee:       Quadratic        Uncertainty =   2.48 %
             Log(Eff):            -6.757823E+00 + ( 5.745552E-01*Log(E) ) +
                                   ( -1.016668E-01*Log(E)^2 )
             Below the Knee:       Quadratic        Uncertainty =   0.00 %
             Log(Eff):            -1.110210E+01 + ( 1.020891E+00*Log(E) ) +
                                   (  0.000000E+00*Log(E)^2 )

 Library Files
        Main analysis library:     LEU2.LIB
        Library Match Width:       0.500

 Analysis parameters
        Analysis engine:           wan32   G53W2.06
        Start channel:            10 (     1.22keV )
        Stop channel:          16336 (  1751.12keV )
        Peak rejection level:    100.000%
        Peak search sensitivity:   3
        Sample Size:               1.0000E+00
        Activity scaling factor:   1.0000E+00/(  1.0000E+00*  1.0000E+00) =
```

```
     ORTEC g v - i (  47) wan32  G53W2.06  26-JAN-2016 13:06:57 Page    2
LANL                           Spectrum name: 160121 LUJAN   4  ATF  MT26 32 3

                                  1.0000E+00
       Detection limit method:    Traditional ORTEC method
       Random error:              1.0000000E+00
       Systematic error:          1.0000000E+00
       Fraction Limit:            0.000%
       Background width:          best method (based on spectrum).
       Half lives decay limit:   12.000
       Activity range factor:     2.000
       Min. step backg. energy    0.000

Corrections                         Status          Comments
       Decay correct to date:        NO
       Decay during acquisition:     YES
       Decay during collection:      NO
       True coincidence correction:  NO
       Peaked background correction: NO
       Absorption (Internal):        NO
       Geometry correction:          NO
       Random summing:               NO


       Energy Calibration
            Normalized diff:      0.1663
```

Rodlet 4 1 day post FP5

```
ORTEC g v - i (  47) wan32  G53W2.06  26-JAN-2016 13:15:45 Page    1
 Spectrum name: 160125   LUJAN   4   12 inches p
 Sample description
      LUJAN ATF  4   After FP-5 (3 days)  at 12 inches   1-25-16

- - - - - - - - - - - - - - - - - - - - - - - - - - - - - - - - - - - - -

 *****   S U M M A R Y   O F   N U C L I D E S   I N   S A M P L E   *****
          Time of Count   Uncertainty  1 Sigma
 Nuclide    Activity        Counting     Total
                Bq
 ____________________________________________________________________________
 NA-24        2.3228E+03    5.284E+00%    5.595E+00%
 K-40         8.8213E+03    9.989E+00%    1.016E+01%
 CO-56        1.5333E+03    6.653E+00%    6.902E+00%
 SR-91        3.1963E+03    5.818E+00%    6.102E+00%
 SR-92        1.1240E+03    1.361E+01%    1.373E+01%
 AG-110M      4.2472E+03    3.490E+00%    3.945E+00%
 TE-132       3.9774E+03    3.281E+00%    3.762E+00%
 I-132        1.4467E+03    6.103E+00%    6.374E+00%
 I-133        3.6005E+03    3.180E+00%    3.674E+00%
 I-135        5.0204E+03    5.698E+00%    5.988E+00%
 XE-135       2.1275E+03    6.184E+00%    6.452E+00%
 PA-234M      9.7532E+05    8.244E+00%    8.447E+00%
 235U        7.3253E+03    3.999E+00%    4.402E+00%
 238U   <    3.1918E+03
 NP-239       1.1127E+04    2.100E+00%    2.396E+00%

   < - MDA value printed.
   A - Activity printed, but activity < MDA.
   B - Activity < MDA and failed test.
   C - Area < Critical level.
   F - Failed fraction or key line test.
   H - Halflife limit exceeded
 ----------------------------   S U M M A R Y   ---------------------------
 Total Activity (    1.2 to  1751.1 keV) 1.0311942E+06  Bq


 ************ U N I D E N T I F I E D     P E A K    S U M M A R Y ************
   Peak Centroid  Background Net Area   Intensity   Uncert   FWHM  Suspected
 Channel   Energy   Counts     Counts   Cts/Sec   1 Sigma %  keV   Nuclide
 ____________________________________________________________________________
    54.84     6.02       896.      2832.     5.002    2.90   0.710  -       s
   343.54    36.93       493.        61.     0.108   53.04   0.652  -        D
  2225.11   238.38       480.        63.     0.111   50.67   0.875  -        D
  2789.82   298.86        84.        32.     0.057   50.68   0.189  -       s
  3591.66   384.73       230.        61.     0.108   56.14   0.205  -       s
  4651.85   498.30        24.        20.     0.036   41.84   0.298  -       s
  8718.82   934.21        60.       180.     0.317    9.65   1.558  -        D

   s - Peak fails shape tests.
   D - Peak area deconvoluted.
```

```
Spectrum Filename: C:\Gamma Spec files\2016 Gamma Folder\Bourke 1-21-
                   16\160125   LUJAN   4   12 inches post FP5.An1

 Acquisition information
        Start time:                25-Jan-2016 13:29:00
        Live time:                566
        Real time:                602
        Dead time:                  5.92 %
        Detector ID:                   10

 Detector system
      HSR-PN1168061 MCB 129


 Calibration
        Filename:                  16Jan25at12inches.Clb
      Energy recalibration on 01/25/16      Efficiency determined on 1
      1/25/15

        Energy Calibration
             Created:              26-Jan-2016 10:51:01
             Zero offset:          0.152 keV
             Gain:                 0.107 keV/channel
             Quadratic:            8.524E-09 keV/channel^2

        Efficiency Calibration
             Created:              26-Jan-2016 10:53:54
             Knee Energy:         110.00 keV
             Above the Knee:       Quadratic        Uncertainty =   2.48 %
             Log(Eff):            -6.757823E+00 + ( 5.745552E-01*Log(E) ) +
                                   ( -1.016668E-01*Log(E)^2 )
             Below the Knee:       Quadratic        Uncertainty =   0.00 %
             Log(Eff):            -1.110210E+01 + ( 1.020891E+00*Log(E) ) +
                                   (  0.000000E+00*Log(E)^2 )

 Library Files
        Main analysis library:     LEU2.LIB
        Library Match Width:       0.500

 Analysis parameters
        Analysis engine:           wan32   G53W2.06
        Start channel:              10 (     1.22keV )
        Stop channel:            16336 (  1751.12keV )
        Peak rejection level:     100.000%
        Peak search sensitivity:   3
        Sample Size:               1.0000E+00
        Activity scaling factor:   1.0000E+00/(  1.0000E+00*  1.0000E+00) =
                                   1.0000E+00
```

```
     ORTEC g v - i (  47) wan32  G53W2.06  26-JAN-2016 13:15:45 Page    2
LANL                           Spectrum name: 160125   LUJAN   4   12 inches p

       Detection limit method:     Traditional ORTEC method
       Random error:               1.0000000E+00
       Systematic error:           1.0000000E+00
       Fraction Limit:             0.000%
       Background width:           best method (based on spectrum).
       Half lives decay limit:    12.000
       Activity range factor:      2.000
       Min. step backg. energy     0.000

Corrections                          Status          Comments
       Decay correct to date:         NO
       Decay during acquisition:      YES
       Decay during collection:       NO
       True coincidence correction:   NO
       Peaked background correction:  NO
       Absorption (Internal):         NO
       Geometry correction:           NO
       Random summing:                NO


       Energy Calibration
            Normalized diff:       0.1393
```